Faculdade de Engenharia da Universidade do Porto

Improving Stability of Reduced Inertia Transmission Systems

Margarida Inês de Almeida Borges Pereira

Master in Electric and Computer Engineering
Energy Major

Supervisor: Professor Doctor Carlos Coelho Leal Monteiro Moreira

30th June, 2023

Resumo

Para atingir a neutralidade carbónica em 2050, a Comissão Europeia definiu várias estratégias que conferem grande importância à produção de energia de origem renovável. Assim, as tecnologias de geração convencionais associadas a combustíveis fósseis e utilizadas em centrais térmicas estão a ser progressivamente substituídas por tecnologias mais ecológicas, maduras e com custos competitivos, como é o caso da geração eólica e solar. No entanto, apenas instalar parques eólicos e centrais fotovoltaicas é somente uma solução parcial para se garantir a existência de sistemas de energia sustentáveis.

A progressiva remoção da tecnologia térmica convencional tem como consequência a redução da componente síncrona do sistema. Além disso, o aumento da importância das fontes renováveis no sistema e o facto de estas tecnologias não terem inércia diretamente ligada à rede são também fatores que contribuem para a redução da inércia do sistema. Perante perturbações que afetem o equilíbrio geração/consumo, um sistema com inércia reduzida apresenta maiores e mais rápidos desvios de frequência. Estes fenómenos podem levar a que unidades de produção saiam de serviço e ao corte de carga, provocando eventos em cascata que podem causar cortes de energia severos.

Por estas razões, esta dissertação procura analisar os impactos resultantes da integração das fontes renováveis e ligadas à rede por interfaces eletrónicos na estabilidade de frequência, considerando perturbações críticas que envolvem a ocorrência de curto-circuitos em diferentes localizações. Para simular o comportamento dinâmico de uma rede com forte integração de fontes renováveis, as máquinas síncronas do Sistema de 39 Barramentos do IEEE são progressivamente substituídas por fontes renováveis, usando, para isso, modelos presentes nas bibliotecas do PSS/E. Após a obtenção de um cenário com componente síncrona reduzida, a resposta em frequência do sistema é avaliada, tendo sido testadas e comparadas diferentes soluções de controlo para a diminuição dos problemas de tensão e frequência. As soluções para melhorar os indicadores de frequência usadas neste trabalho são a inclusão de reservas de potência ativa/frequência nas fontes renováveis, a utilização de baterias e de compensadores síncronos. Assim, a eficácia de cada uma destas soluções é testada, assim como é averiguada a influência da localização e da potência aparente dos compensadores síncronos e das baterias nos indicadores de frequência.

Palavras-Chave: inércia reduzida, estabilidade de frequência, energia eólica e solar, geração síncrona, PSS/E, códigos de rede, compensação síncrona, sistemas de armazenamento de energia.

Abstract

To achieve net-zero carbon emissions by 2050, the European Commission envisioned several strategies placing great importance in renewable energy generation. Therefore, the conventional synchronous generators associated to fossil fuels existing in thermal power plants are progressively being replaced by more environmentally friendly and mature technologies with competitive costs: this is the case of wind and solar generation. However, just installing wind farms and solar power plants is only a partial solution for achieving sustainable energy systems.

The progressive replacement of thermal power plants reduces the synchronous component available in the system. Additionally, the increase of renewable energy sources and the fact that they do not directly provide inertia to the grid is also contributing for the inertia reduction in the power systems. When facing perturbations affecting the balance between generation and demand, a reduced inertia system exhibits higher and faster frequency deviations and dynamics. This can result in the disconnection of production units and load shedding, provoking a cascading effect that can compel severe power outages.

This dissertation examines the impacts of the integration of converter-interfaced renewable energy sources in the frequency stability, considering critical perturbations involving short-circuits in different locations. To simulate the dynamic behaviour of a network containing high shares of renewable energy integration, the IEEE 39-Bus System is used while resorting to the PSS/E simulation package. After obtaining a scenario with reduced synchronous generation, the network's stability is assessed in face of key frequency indicators (frequency nadir and Rate of Change of Frequency). Regarding the critical disturbances applied in a low inertia scenario, different control solutions for the mitigation of frequency stability problems are tested and their performance is assessed comparatively. This involves the investigation of the performance of the active power-frequency control in the renewable energy sources, of synchronous condensers, or fast active power-frequency regulation services from stationary energy storage. Moreover, the influence of the location and apparent power of synchronous condensers and Battery Energy Storage Systems on the frequency indicators is also evaluated.

Keywords: reduced inertia, frequency stability, wind and solar energy, synchronous generation, PSS/E, grid codes, synchronous condensers, energy storage systems.

Acknowledgements

I would like to thank my supervisor, professor Carlos Moreira, who has agreed to guide, help, and teach me during this dissertation, while always encouraging me to pursue my professional ambitions and to follow my interests. I am thankful for his time, patience, flexibility, and always clear explanations of what needed to be done, both during this dissertation and during other classes. I should also thank Eng. Rui Sousa (INESC-TEC) for his time, encouragement, reassurance, and help with PSS/E.

This dissertation is not only a product of our work, but also of previous experiences. Therefore, it is dedicated to my family, who has encouraged me to follow my dream of studying sustainable power systems and become an electric engineer. Without their support, none of that would have been possible. A big thank you to them all, with a special credit to my mother, father, and brother, Francisco, who lightens up the mood wherever he goes and is always there for a good laugh. Thank you for your free spirit and for putting up with me since you were born!

I would also like to give a special thanks to Raquel Lucas, for brightening my days at FEUP and for showing me the right path towards happiness. Another honourable mention is Pedro Guimarães, for putting up with me during all the college assignments, for his sense of humour, unique wisdom, for his teachings, and unconditional help. The three of us did make the best study team I could possibly ask for.

This dissertation is also dedicated to Catarina Brandão (Cathy), for being my oldest friend, for her amusing ways, for her courage to be herself in every circumstance, for always having my back, and for accompanying my evolution as a person. I also thank Francisco Santos for his uniqueness, support, for listening to my crazy ideas, for his immense generosity, and for the encouragement he gives me all the time. Thank you for being always there for me and for knowing me so well. To my friend Inês Martins, I would like to show appreciation for her patience with me after exams and for all the funny moments we shared. This work is dedicated to her, to Sérgio Silva, Francisco Santos, and Diogo Isaías, for all the amazing lunch breaks.

To my fellow friends from the Energy Major classes, Inês Santos, Ricardo Terrinha, Bruno Oliveira, Helena Gonçalves, Francisco Lobo and José Castro, thank you for your friendship and for all the fun you offered me. To Clarisse Lannier and Ivane Bélloir, thank you for allowing me to guide you through the streets of Porto and for our study sessions on Electricity Markets.

To all my colleagues and friends at Vestas, a big thank you from my part: if it wasn't for your patience, if you hadn't believed in me and if you hadn't been so understanding with me during the completion of this work, I would not be where I am today. Thank you for your teachings, for treating me as one of yours, and for allowing me to make a difference.

To all of you and others who are not mentioned here and who have crossed their path with mine during these 22 years, thank you for making me who I am.

Margarida Pereira

“Who has seen the wind?
Neither I nor you:
But when the leaves hang trembling,
The wind is passing through.

Who has seen the wind?
Neither you nor I:
But when the trees bow down their heads,
The wind is passing by.”

- Christina Rossetti

“There is another sky,
Ever serene and fair,
And there is another sunshine,
Though it be darkness there;
Never mind faded forests, Austin,
Never mind silent fields -
Here is a little forest,
Whose leaf is ever green;
Here is a brighter garden,
Where not a frost has been;
In its unfading flowers
I hear the bright bee hum:
Prithee, my brother,
Into my garden come!”

- Emily Dickinson

Index

List of Figures

List of Tables

Abbreviations and Symbols

List of Abbreviations

AC	Alternating Current
AGC	Automatic Generation Control
ASE	Aggregated Swing Equation
BESS	Battery Energy Storage Systems
CIG	Converter Interfaced Generation
DC	Direct Current
DFIG	Doubly Fed Induction Generator
DG	Distributed Generation
DSO	Distribution System operator
EU CR	European Commission Regulation
ENTSO-E	European Network of Transmission System Operators for Electricity
ESS	Energy Storage Systems
FCR	Frequency Containment Reserve
FFCI	Fast Fault Current Injection Capability
FFR	Fast Frequency Response
FRT	Fault Ride-Through
FSM	Frequency Sensitive Modes
GENROU	Round Rotor Generator Model
HV	High Voltage
HVDC	High Voltage Direct Current
LFSM-O	Limited Frequency Sensitive Modes- Over-frequency
LFSM-U	Limited Frequency Sensitive Modes- Under-frequency
LV	Low Voltage
LVRT	Low Voltage Ride-Through

MPP	Maximum Power Point
MPPT	Maximum Power Point Tracking
MV	Medium Voltage
NC	Network Codes
PFR	Primary Frequency Reserve
PI	Proportional-Integral Controller
PLL	Phase Locked Loop
PMSG	Permanent Magnet Synchronous Generators
PPM	Power Park Modules
PV	Photovoltaic
PWM	Pulse Width Modulation
REECA1	Renewable Energy Electrical Model A1
REECCU1	Electrical Control Model for Utility Scale Battery Energy Storage
REGCA1	Renewable Energy Generator Model A1
REPCA1	Renewable Energy Auxiliary Control Model A1
REE	Red Eléctrica de España
RES	Renewable Energy Sources
RfG	Requirements for Generators
RoCoF	Rate of Change of Frequency
RSC	Rotor Speed Control
SC	Synchronous Condenser
SEXS	Simplified Excitation System
SG	Synchronous Generation
SM	Synchronous Machine
SoC	State of Charge
SPGM	Synchronous Power Generation Modules
STATCOM	Static Synchronous Compensator
SVC	Static Var Compensator
TGOV1	Turbine-Governor Model 1
TSO	Transmission System Operator
VSG	Virtual Synchronous Generator
WECC	Western Electricity Coordination Council
WTG	Wind Turbine Generators

List of Symbols

ω	Angular Frequency
θ	Rotor Angular Position
$\boldsymbol{\delta}$	Rotor Angular Position (electrical angles)
P_m	Mechanical Power
P_e	Electrical Power
T_m	Mechanical Torque
T_e	Electromagnetic Torque
D	Damping Coefficient
J	Moment of Inertia
C_p	Power Coefficient
λ	Tip-Speed Ratio
β	Pitch Angle
ω_r	Rotor speed
η	Converter's efficiency

Chapter 1

The Context – Large-scale integration of Renewables in Power Systems

1.1 - Introduction

To achieve the net-zero carbon emissions target by 2050, the European Commission has been developing strategies for a low carbon economy where renewable energy generation has a major relevance, as well as electric power systems in face of the electrification of the economy. This paradigm change implies that conventional synchronous generation existing in conventional thermal power plants is progressively discarded, especially the ones associated to fossil-fuelled power stations (for example, in Portugal, coal-fired power plants were recently decommissioned).

The European policies regarding energy generation enhance the significant increase of renewable energy in the power system (Figures 1.1 and 1.2). However, this will introduce higher and faster frequency dynamics, therefore impacting the frequency stability. Some solutions for mitigating frequency problems are the revision of the grid codes, the introduction of new system services, energy storage systems, and solutions for increasing the grid's flexibility and the use of new technologies for increasing flexibility in hydro power plants. For example, in Alqueva (Southern Portugal), the hydraulic short-circuit technique is already being implemented to improve the grid's flexibility, both in terms of frequency services and voltage support [1]. Another example is Volgengrun (France), where a battery will be added to one of the hydro units for enhancing the contribution to frequency response with high dynamic response, significantly reducing the turbine's wear [1].

These strategies combined with the high shares of converter-interfaced renewable energy generation and the current uncertainties in the supply of natural gas are creating an energy mix mostly composed by hydro power, biomass, a percentage of combined cycle (based on gas turbine plants for regulating the renewable production), on-shore and off-shore wind energy, and solar power. Figure 1.1 illustrates the evolution of renewable energy generation mix and the electricity capacity mix in Europe for 2025, 2030, and 2040.

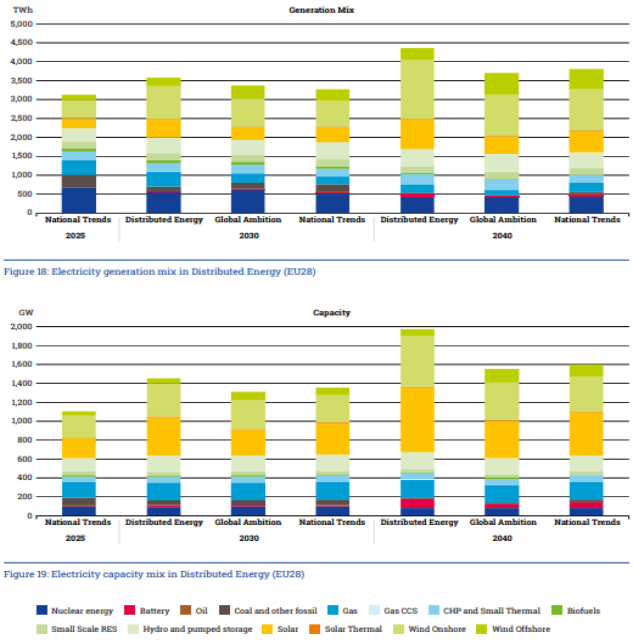

Figure 1.1 – A comparison between the electricity generation mix and the electricity capacity mix in Distributed Energy for future scenarios (EU28) (source: [2]).

In Figure 1.1, it is noted that the renewable energy generation mix (in TWh) will be higher than the renewable energy capacity mix (in GWh), which shows the need for the development of strategies to avoid renewable energy spillage.

In fact, periods in which Renewable Energy Sources (RES) supply all or almost all demand are already a reality in numerous countries, including Portugal. Notably, in March 2018, the renewable energy generation (4812 GWh) surpassed Continental Portugal's consumption (4647 GWh) [3]. Another example is Ireland, where 65% of its demand is already being supplied with wind power, having an installed capacity of 4 GW and expecting to install 10 GW of wind power until 2030 [4].

Since renewable generation is generally interfaced with the electric power grid through power electronic converters, such situations create various scarcities (i.e., shortage of something that the power system once had in good supply [5]) due to the displacement of synchronous generation and the faster time constants of power electronic converters. Indeed, such scarcities are currently being studied in large-scale projects (i.e., the EUSysFlex project [5]), where transmission system operators (TSOs), research and development centres and universities are involved. These scarcities include shortage of inertia, frequency stability, rotor-angle stability, congestion, low short-circuit currents, and limited capacity for restoration [5]. Other problems include the reduction of transient stability margins, power electronic controller interactions with each other and passive AC components, lack of reactive power, loss of devices in the context of Fault Ride Through Capability (FRT), the introduction of new power oscillations and/or reduced damping of existing power oscillations, missing or wrong participation of power electronic connected generators and loads in frequency containment, altered static and dynamic voltage dependence on loads and resonances due to cables and power electronics [4].

Although the problems being faced are of multiple natures, this dissertation will essentially focus on frequency stability problems, resulting from the progressive decrease of system's inertia levels and by the reduced power-frequency control capabilities in the systems, which were traditionally provided by synchronous machines from conventional power plants. In fact, frequency and inertia-related issues will be largely affecting the European synchronous area in the future, since, as seen in Figure 1.2, by 2030 the inertia will be unevenly distributed because of large-scale renewable energy integration.

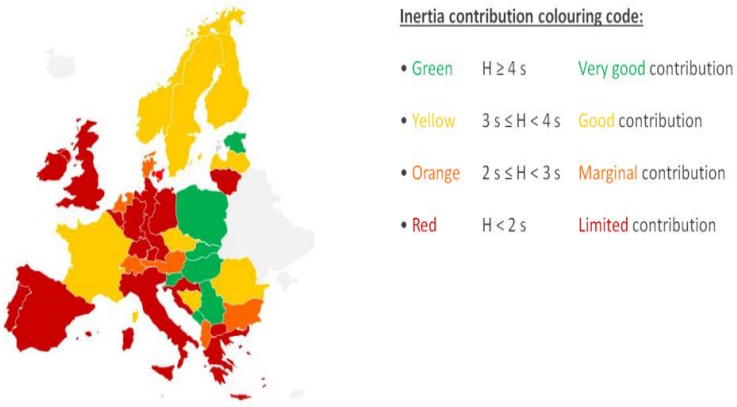

Figure 1.2 – Indicating contribution of each country to the Inertia Constants in 2030 [4].

If no action is taken to counteract the lack of inertia in the power system, the probability of having faster frequency dynamics will continue rising, which can provoke under-frequency load-shedding, since the limit for the tripping of under-frequency relays is 49.2 Hz within the European synchronous area [5]. This can even induce cascading events, further jeopardizing the frequency stability. In fact, periods of low demand and with high renewable energy generation are the source of this problem.

Another extreme situation also occurring at high penetration levels of renewable generation is the system split, which is currently happening once in decades. A system split is a grid extreme contingency leading to the separation of the system into asynchronous zones [4]. It is more likely to occur with highly loaded weak transmission corridors, which is why the European Electricity Markets are gradually allowing more volatile and progressively increasing power flows in the interconnections [4]. After a system split, the imbalance is presently expected to increase, which puts the system closer to its balancing capability physical limits. In these circumstances, the Frequency Containment Reserves (i.e., the limitation of frequency within the permitted ranges defined by the Grid Codes) may not provide enough active power to support the system after such event [4].

As the Iberian Peninsula has few interconnections to Central Europe, it is one of the most affected areas because of RES integration and inherent inertia decrease, along with Central Europe itself, Ireland, the UK, the Nordic Countries, and most islands. It has also been seen that European interconnections themselves can contribute to frequency drops, as the import capacity displaces conventional generation and reduces the systems' inertia [5]. This problem exists due to the power system's nature and can be treated as a two-control area model, being one area the Iberian Peninsula and the other Central Europe [6], where each area is described by its swing equation, stating the equivalent inertia of the control area, as well as its equivalent Frequency Containment Reserve (FCR). A possible solution for the frequency containment is the limitation of the instantaneous penetration of RES [5], which is being implemented especially in islands. Given the direct impact of renewable energy spillage, improved control strategies must be prepared.

When developing improved control strategies, considering conventional deterministic modelling of the network is no longer possible given the uncertain nature of several aspects, such as the weather, the network topology and network observability [7] (since most distributed generation is installed at low and medium voltage levels [4]), the size, the types, locations, and the parameters of the generator and network controllers [7]. To counteract the uncertainties in the active power produced by the RES, energy storage systems are being employed, but these technologies lack operational experience [7]. Moreover, the nature and behaviour of the load has changed from passive to controllable, and insufficiently understood transmission components are being added to the system, increasing its complexity, vulnerability, and time dependence [7].

Within the Iberian Peninsula and the European synchronous area, the foreseen shares of solar and wind integration in mid-term will create a system where the lack of inertia is a major shortcoming, demanding specific control strategies and investigations. Therefore, the developments to be drawn from this work are expected to provide contributions towards the identification of solutions for the stable operation of systems with low rotational inertia. The envisioned solutions involve the use of systems for the fast provision of power-frequency regulation services, either alone or in coordination with the installation of synchronous condensers in the system.

1.2 - Objectives of this work

The present dissertation not only assesses the main operational challenges related to the high integration of renewable energy but also evaluates the performance of different strategies to weaken the consequences of the reduction of synchronous inertia in the power system, using synchronous condensers and fast active power-frequency regulation systems based on batteries, or the availability of synthetic inertia in the power-electronic interfaces.

For these reasons, this work starts by revising the currently available Grid Codes, both in Continental Europe and in Portugal, to understand the technical rules applicable to the generators to be connected to a network and how the balance between the European Interconnections and the system's security are maintained given the evolution of the energy generation. Additionally, this work revises some control strategies applicable to renewable energy generation attempting to solve the problems caused by the reduction of synchronous inertia.

This dissertation identifies a case study and performs dynamic simulations in face of different perturbations to determine the impacts of the inertia reduction in the key frequency indicators (Nadir and RoCoF – Rate of Change of Frequency). After defining a low inertia scenario, potential solutions are selected, and their dynamic models are detailed. The relevance and sensitivity of such solutions are analysed in different situations, aiming to establish the main conclusions and recommendations about their use.

1.3 - Outline

This document is composed by 6 chapters:

- In Chapter 1, the introduction to the theme and the context of this work are detailed.
- In Chapter 2, the theme introduced in Chapter 1 is described and the literature review is conducted. Some implemented solutions for mitigating the frequency problems are discussed and a revision of the Grid Codes for both Continental Europe and Portugal is performed. It also briefly covers some of the solutions for their implementation, focusing on some control solutions used mainly in wind and solar systems.

- In Chapter 3, the test system, the simulation models of synchronous generation, of renewable energy generation and battery energy storage systems are presented.
- In Chapter 4, the dynamic simulations for line faults are performed for the base case containing only synchronous generation.
- In Chapter 5, renewable energy integration scenarios are built, and the key frequency indicators are calculated for a low inertia scenario.
- In Chapter 6, the solutions for the stable operation of the system with reduced inertia are integrated in the power system. This chapter assesses and compares their effectiveness and performs a sensitivity analysis to understand the influence of the location and the apparent power of both BESS and synchronous condensers in the key frequency indicators.

Chapter 2

Low Inertia Systems – A Review

As previously stated, conventional synchronous units are the main sources of inertia in the power system, and some complementary solutions providing inertia contribution are synchronous condensers, virtual inertia provision, energy storage systems, fast frequency reserves and Grid-Forming converters.

The following sections in this chapter aim to explain the impact of renewable energy sources (RES) on the system's inertia and to expose the currently available Grid Codes, as they provide guidance with respect to synthetic inertia. This chapter will also address the theoretical concepts of the novel control strategies and solutions for the operation of a system with low synchronous inertia.

2.1 The impact of RES on the system inertia

Traditional power systems can arrest the frequency changes by providing inertia following an event. However, given the increase of renewable energy sources (RES) and loads connected to the power system through power electronic converters, the inertia is reduced in comparison to traditional power systems [8]. This explains why converter interfaced generation's low inertia creates higher RoCoF (Rate of Change of Frequency), leading to nadirs (minimum frequency values) lower than 49 Hz that can severely impact the power system [5]. If the frequency deviations surpass a given threshold value, this can lead to the tripping of generation units, which can further increase the RoCoF and lead to a cascade failure of the power system [8]. For clarification, the effects of lower inertia on the frequency behaviour are illustrated in Figures 2.1 and 2.2:

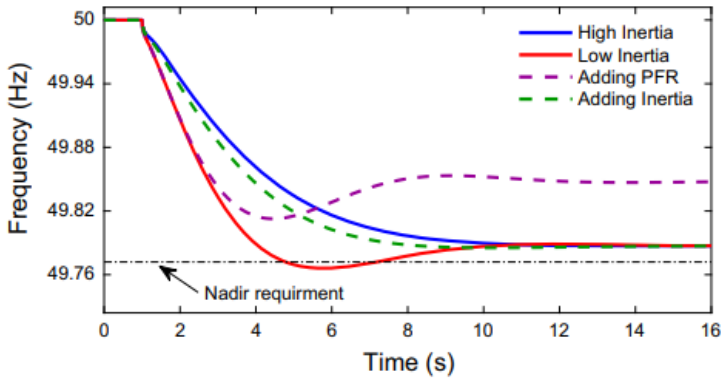

Figure 2.1- The effects of lower inertia on the frequency behaviour (source: [8]).

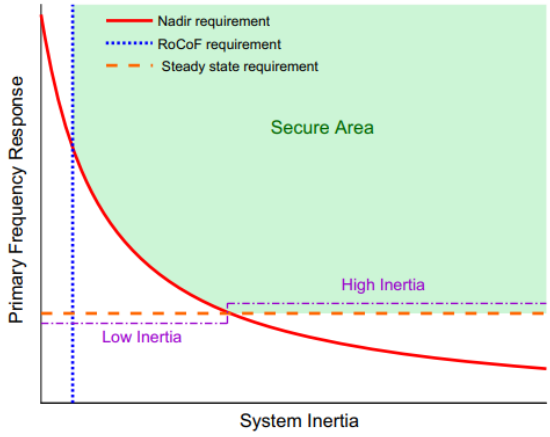

Figure 2.2- Frequency response requirements (source: [8]).

Figure 2.1 shows that, in a low inertia system, the frequency nadir requirement can be respected by adding primary frequency reserve (PFR) to the system or by increasing the system's inertia [8].

The system's inertia is very important to ensure the network's inertial response, which consists of the synchronous machines connected to the grid limiting the frequency drop because of their inertia [9]. This typically happens within milliseconds to tens of seconds after the imbalance started [9]. In PFR, the governor of the synchronous machines participating in the frequency response changes their active power output depending on the local frequency variations [9]. This is done to reduce the frequency deviations and to stabilize the frequency and occurs from 10 to 30 seconds after the fault, being this the first reserve to be automatically activated [9].

As illustrated in Figure 2.2 [8], the secure operation area is obtained by combining the PFR and the inertia requirements. The secure area is limited by the maximum RoCoF allowed (vertical line), the steady-state frequency requirement (horizontal line) and the frequency nadir (red curve) [8]. The frequency nadir constraint is determined by the swing equation (which is detailed in Section 2.2), which depends on PFR and the system inertia [8].

Both these figures explain that, when the inertia is high, the frequency declines at a slower rate, which allows the activation of PFR before the nadir limit is reached [8]. However, the lower the inertia, the faster will be the frequency decline after an event, such as the loss of a generator or the tripping of a transmission line. Therefore, a faster primary reserve response is required, being the slower-acting primary reserves no longer adequate [8].

From the perspective of the TSO, the reduction of the system's inertia leads to larger RoCoF (which can lead to the possible tripping of grid components, especially embedded renewable generation), and to higher frequency deviations (which can cause potential load shedding and, in an extreme case, system collapse). Additionally, the decrease of the system's inertia puts conventional synchronous generators (SGs) at higher risk of instability because they accelerate faster, reaching the maximum rotor angle earlier [8]. If the maximum rotor angle is exceeded, pole slipping of the SGs is very likely to happen, which causes protection to set the generator out of service [8]. This will put the power system in a stress situation, which may lead to a cascade tripping [8]. Then, mechanisms for inertia provision are very important to arrest these fast frequency deviations causing unacceptable frequency drops.

2.2 Equation of Motion of a Synchronous Machine

Conventional synchronous generation is the main contributor of inertia to the power system, where primary energy sources (such as water in hydro power plants, and fossil fuels in thermal power plants), are converted using a mechanical link: the turbine [10]. The inertia is the resistance of a physical object to a change in its state of motion, including speed and direction changes [10], and is defined by the moment of inertia of the rotating mass [8]. In power systems, it defines the time in seconds that a generator can provide power only by using all the kinetic energy stored in their rotating masses [8], which is represented in Equation 2.1.

$$H = \frac{\frac{1}{2} * J * (\omega_{m,0})^2}{S_b} = \frac{\frac{1}{2} * J * (2\pi f_{m,0})^2}{S_b} \tag{2.1}$$

Where J (in kg.m^2) defines the moment of inertia, being $\omega_{m,0}$ and $f_{m,0}$ the rated mechanical angular velocity (in rad/s) and the rated rotational frequency (in Hz) of the generator, respectively, and S_b the system's base apparent power (in MW).

The total inertia of a power system is determined by the large rotating masses of conventional power plants, i.e., the generator and turbine connected to the same shaft [8]. Due to the synchronous coupling of the machines with the grid, their rotational speed, ω_m, is linked with the angular velocity of the electromagnetic field, ω_e [8]. During a disturbance, which causes an imbalance between mechanical and electromagnetic torque (T_m and T_e, respectively), the net torque on the rotor is different from zero, which leads to an acceleration or deceleration according to Equation 2.2 [8]:

$$J\frac{d\omega_m}{dt} = T_m - T_e = T_a \tag{2.2}$$

Where J is the combined moment of inertia of the generator and the turbine (kg.m^2), T_m is the mechanical torque (N.m), T_e is the electrical torque (N.m), and T_a is the acceleration/deceleration torque (N.m) [8].

Given that ω_e=pω_m, where p is the number of pole pairs, and, if p=1 and considering that the power (in W) can be defined as P=ω*T, the Equations 2.1 and 2.2 can be written as:

$$P_m - P_e = \omega_m \frac{2HS_b}{\omega_{m,0}^2}\frac{d\omega_m}{dt} \tag{2.3}$$

Equation 2.3 considers power instead of torque, which is a preferrable quantity in electrical power system's studies [11]. In Equation 2.3, P_m is the mechanical power (in W), P_e is the electrical power (in W), and ω_e is the angular velocity of the electromagnetic field (in rad/s) [8]. Assuming that there are limited angular speed variations [8], it is possible to write that $\omega_m = \omega_{m,0}$. Hence, Equation 2.3 can be rewritten as Equation 2.4:

$$P_m - P_e = \frac{2HS_b}{\omega_{m,0}}\frac{d\omega_m}{dt} \tag{2.4}$$

Noting that the derivative of the rotor's angular velocity is equal to the rotor angular position, Equation 2.5 can be arranged as:

$$P_m - P_e = \frac{2HS_b}{\omega_{m,0}}\frac{d^2\delta}{dt^2} \tag{2.5}$$

With

$$\frac{d\delta}{dt} = \Delta\omega \tag{2.6}$$

Where $\Delta\omega$ is the machine's speed deviation in rad/s and δ is the rotor angular position with respect to a stationary axis, in radians (rad). Considering now the damping constant and that all the variables are expressed in p.u (per unit)., it is possible to write the Swing Equation for one generator as in Equation 2.7:

$$\frac{H}{\pi f}\frac{\partial^2\delta}{\partial t^2} + D\frac{\partial\delta}{\partial t} = P_m - P_e = P_a \tag{2.7}$$

Where H is the inertia constant, and f is the frequency (in Hz). In Equation 2.7, δ is the angular position of the rotor (in radians), D is the damping constant (in pu.MW/pu.Hz), P_m is the mechanical power (in pu.MW in the system's base), and P_{el} is the electrical power (in pu.MW in the system's base; according to [9], it can also be represented as the load, P_L).

The Swing Equation represented by Equation 2.7 can describe not only the behaviour of one synchronous generator, but also the aggregated model of the whole network [9]. According to [9], considering a system with *n* generators, *j* loads, and *l* connecting tie-lines, the Aggregated Swing Equation (ASE) can be written as in Equation 2.8:

$$\frac{d\Delta\omega}{dt} = \frac{\Delta P_m - \Delta P_L - \Delta P_{Loss}}{2H_{sys}} - \frac{D_{sys}.\Delta\omega}{2H_{sys}} \quad (2.8)$$

With

$$\omega = \frac{\sum_{i=1}^{n} H_i \omega_i}{\sum_{i=1}^{n} H_i} \quad (2.9)$$

$$S = \sum_{i=1}^{n} S_i \quad (2.10)$$

$$H_{sys} = \frac{\sum_{i=1}^{n} H_i S_i}{S} \quad (2.11)$$

$$D_{sys} = \frac{\sum_{i=1}^{n} D_i S_i}{S} \quad (2.12)$$

$$P_{m,o} = \sum_{i=1}^{n} P_{m,i} \quad (2.13)$$

$$P_L = \sum_{i=1}^{j} P_{L,i} \quad (2.14)$$

$$P_{Loss} = \sum_{i=1}^{l} P_{Loss,i} \quad (2.15)$$

Equation 2.9 implements the speed of the centre of inertia. Equation 2.11 calculates the system inertia, which is dependent on the number of generators in the power system and their inertia. Equation 2.12 is the system load-damping factor [9]. Therefore, the higher the number of generators connected to the network, the lower the frequency deviations after an event.

From the point of view of the electric power system, there is a close relationship between the speed of the electrical machines connected to the grid and the grid frequency, which is what quantifies the balance between the active power generated and the active power consumed on the system [5]. Indeed, frequency control is achieved by maintaining the frequency in its nominal values (50 Hz in Europe and 60 Hz in the USA).

Prior to a fault, the machines rotate at the same speed and the electrical power matches the mechanical power. Thus, the rotor speed deviation from synchronism is null. Depending on the disturbance, the rotor speed can increase or decrease to balance generation and demand. If the energy that is stored in the rotating masses is provided to the system, the rotor speed decreases; otherwise, if there is shortage of energy in the power system, the rotor speed increases [5]. Since the frequency is proportional to the rotational speed of the synchronous machines, frequency deviations create problems for the stable operation of power systems. As a result of frequency drops, high magnetization currents appear in induction motors and transformers [11]. Moreover, the speed changes affect the auxiliary drives of the generators (which are associated to fuel, feedwater, and combustion air supply systems) [11]. Therefore, the frequency must be as constant as possible.

2.3 The Equal Area Criterion

One important criterion for assessing transient stability of a power system is the Equal Area Criterion, which allows the analysis of the first oscillation of a synchronous machine connected to an infinite bus [12]. If the damping constant, D, is not considered, it is possible to write the Swing Equation for one synchronous machine using Equation 2.5. Equation 2.5 allows one to understand the behaviour of the rotor angle: therefore, when analysing the first oscillation, the frequency remains stable if:

$$\frac{\partial \delta}{\partial t} = 0 \tag{2.16}$$

By multiplying each side of Equation 2.5 by $\frac{\partial \delta}{\partial t}$, it is possible to write Equation 2.17:

$$\frac{HS_b}{2\pi f_{m,0}} \frac{d^2\delta}{dt^2} \frac{d\delta}{dt} = (P_m - P_e) \frac{d\delta}{dt} \tag{2.17}$$

By integrating and performing a few simplifications, Equation 2.17 can be written as:

$$\frac{d\delta}{dt} = \sqrt{\frac{\pi f_{m,0}}{HS_b} \int_{\delta_0}^{\delta} (P_m - P_e) d\delta} \tag{2.18}$$

Where δ_0 is the initial rotor angle before a given perturbation. To achieve stability, Equation 2.18 should be equal to zero. Therefore, Equation 2.19 can be written as:

$$\int_{\delta_0}^{\delta_T} (P_m - P_e) d\delta = \int_{\delta_0}^{\delta_1} P_m d\delta + \int_{\delta_1}^{\delta_T} (P_m - P_{max} sen\delta) d\delta \tag{2.19}$$

Simplifying, it is possible to write Equation 2.20 assuming that P_{max} is given by Equation 2.21:

$$\int_{\delta_0}^{\delta_T} P_m \, d\delta = - \int_{\delta_T}^{\delta_1} (P_m - P_{max} sen\delta) d\delta \tag{2.20}$$

$$P_{max} = \frac{EV}{X_d} \tag{2.21}$$

Being E the electromotive force of the synchronous generator, V the voltage in the machine and X_d the direct-axis reactance of the synchronous machine. The first side of Equation 2.20 refers to area A_1, the acceleration area, and the second side refers to area A_2, corresponding to the deacceleration area, which are present in Figure 2.3, being δ_T the angle when the fault is cleared.

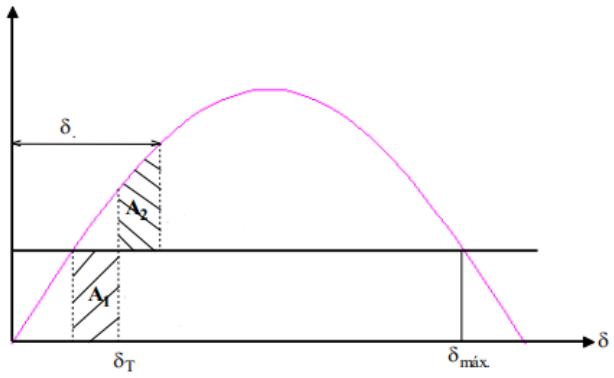

Figure 2.3 – Application of the Equal Area Criterion (source: [12]).

In A_1, the synchronous machine does not provide electrical power, providing instead mechanical power, whereas in A_2, the synchronous machine is providing more electrical than mechanical power. In A_1, the synchronous machine increases the kinetic energy provided by the acceleration until the fault clearance. In A_2, the fault has been cleared and the machine provides again electrical power to the system. The kinetic energy then decreases, and the rotor deaccelerates until reaching the angle δ_1, which corresponds to the moment when the machine returns to its initial speed [12]. For the system to remain stable, A_1 should be equal to A_2.

2.4 RoCoF and Measurement Window Definition

Events such as the loss of the largest generation unit or the loss of transmission lines create frequency changes. Therefore, an important indicator for assessing frequency stability is the RoCoF ("Rate-of-Change-of-Frequency"). The RoCoF indicates how rapidly the frequency changes after a sudden imbalance between generation and demand, being expressed in Hertz per second (Hz/s) [13]. The RoCoF is defined as the rate at which the frequency changes over time, which is described in Equation 2.22 [13]:

$$\frac{\partial \mathrm{f}}{\partial \mathrm{t}}\Big|_{\max} = \Delta \mathrm{P}_{Imbalance} * \frac{\mathrm{f}}{2\mathrm{H}} \tag{2.22}$$

Where $\Delta \mathrm{P}_{Imbalance}$ corresponds to the power imbalance due to the disturbance, and *H* is the system inertia defined in Equation 2.11.

Since the inertia constant is inversely proportional to the RoCoF, Equation 2.22 explains why systems with reduced inertia have larger frequency deviations and have faster dynamics [9]. The highest RoCoF theoretically corresponds to the highest frequency deviation after a disturbance [9]. If the RoCoF is too high, the tripping of the protection relays of the synchronous machines occurs, as they have mechanical limitations [9].

In a low inertia system, high RoCoF can trigger the RoCoF relays and lead to cascading disconnection of distributed generation, enhancing and damaging equipment [9]. Indeed, one of the most important functions of the RoCoF relays is the detection of islanding and disconnection of a generation unit [13]. For example, according to [13], Ireland has increased the RoCoF threshold from 0.5 Hz/s to 1 Hz/s to meet the new renewable generation integration target for 2020 for avoiding the tripping of the generation units during frequency events, which shows the relevance of the calculation of this parameter for stability studies.

The RoCoF measurements vary according to the chosen measurement window. The accurate choice of the measurement window is very important, given that the frequency measured at different points in the system can vary significantly under transient conditions [8]. During transient events, the generator rotor speeds at different points of the system can differ from each other due to local and interarea interactions [8]. Then, to obtain consistent system wide RoCoF measurements, the electrical transients must be removed, ensuring that only the mechanical transients are considered [8]. Larger measurement windows can remove the electrical transients from the RoCoF measurements, but they can also eliminate the mechanical transients, leading to false RoCoF values [8]. Figure 2.4 shows that higher measurement windows lead to lower RoCoF values, and that lower measurement windows lead to higher RoCoF values. The use of a large measurement window leads to neglecting mechanical transients, increasing the mechanical stress on the rotating machines [8].

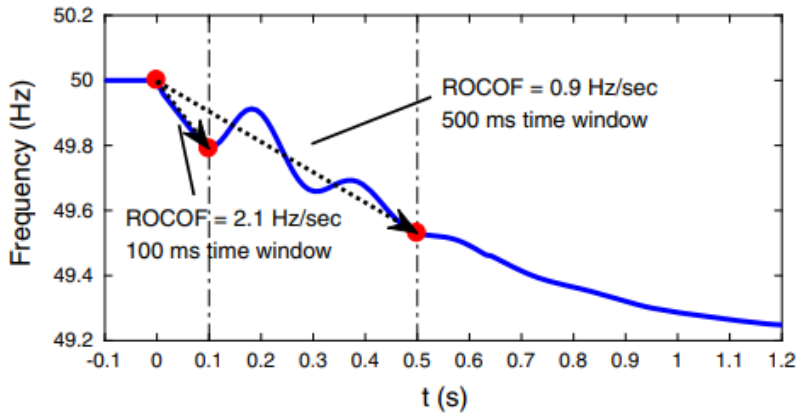

Figure 2.4 - The effect of using different measuring windows in the RoCoF calculation (source: [8]).

As previously seen in Figures 2.1 and 2.2, high RoCoF can create lower frequency nadir. This happens because, in a system with reduced inertia, a smaller number of governors participates in the frequency control because there are less synchronous machines [9]. Then, the remaining governors do not have enough time to react, which causes a low frequency nadir that can trigger the under-frequency relays, leading to under-frequency load shedding [9]. To avoid under-frequency load shedding, each country's TSO established adequate nadir ranges, RoCoF thresholds and measurement windows depending on each system's dynamics and requirements.

2.5 Review of the Requirements for Generators for the European Network

Given the impacts of RES in the power system, a set of requirements was created and harmonized between the various Transmission System Operators (TSO) to propose a solution for reducing some negative impacts of RES. This section provides an overview of the current European Network Code on Requirements for Generators (NC RfG, following the EU Commission Regulation 2016/631), which sets the requirements for the generators to be connected to the network.

The requirements for the generators are being applied to all generators, providing system security in a changing environment [14]. They also accommodate evolution in the way energy is generated, reducing costs through standardization [14]. However, these requirements are only applied provided it is technically justifiable (which is evaluated through Cost Benefit Analysis and must be approved by the National Regulatory Authority).

The RfG (Requirements for Generators) divides the Power Generating Facilities into 4 types, depending on the synchronous area, their generation capacity and voltage level. The types are listed below [14]:

- **Type A Generators:** for connections below 110 kV, and maximum capacity of 0.8 kW or more. These generators must have a stable operation over extended frequency range with limited automated response and minimum system operator control.
- **Type B Generators:** for connections below 110 kV and a capacity above threshold A/B and below B/C. These generators provide higher resilience to operational events, appropriate dynamic response, and basic system operator control.
- **Type C Generators:** for connections below 110 kV and a capacity above the threshold B/C and below C/D. They must provide a stable and a real-time dynamic response to maintain balancing services to ensure security of supply. Their requirements cover all operational network conditions and detailed specification of the functions, controls, and information exchange to handle these capabilities. They ensure real-time system response necessary to avoid, manage and respond to system events.
- **Type D Generators:** for connections at 110 kV or above and a capacity above the threshold C/D. Their requirements cover a wide area of control and range of operation [14]. They establish specific needs for high voltage networks and their operation and stability over wide areas, allowing the use of ancillary services from Europe wide generation.

The NC RfG only sets maximum thresholds for the generator types for the different synchronous areas in Europe [14]. Within the maximum thresholds, the individual capacity thresholds are decided by the national regulatory authorities through a "determination of significance" process [14]. These values are present in Table 2.1:

Table 2.1: Maximum Capacity Thresholds for type B, C and D Power Generating Modules (source: [14]).

Limit for maximum capacity threshold for each type of module			
Synchronous Area	**Type B**	**Type C**	**Type D**
Continental Europe	1 MW	50 MW	75 MW
Great Britain	1 MW	50 MW	75 MW
Nordic	1.5 MW	10 MW	30 MW
Ireland	0.1 MW	5 MW	10 MW
Baltic	0.5 MW	10 MW	15 MW

The requirements in the RfG are provided following a technology-neutral approach and they can be divided in three categories: general requirements (applied regardless of the type of connection), specific requirements for synchronously connected generators (SPGM-Synchronous Power Generation Modules) and specific requirements for non-synchronously connected generators (PPM - Power Park Modules) [14].

The Requirements for Generators are divided in the following aspects: frequency stability, robustness of power generating modules, system restoration, general system management, and voltage stability. The frequency stability covers the setting of operating frequency ranges (for types A, B, C and D), the RoCoF withstand capability (for types A, B, C, D), the constant active power output regardless of frequency changes (for types A, B, C, D), the limitation of power reduction at underfrequency (for types A, B, C, D), the automatic connection (for types A, B, C, D), the remote ON/OFF (only for types A and B), the active power reduction remote control (for type B only), the additional requirements related to frequency control and the provision of synthetic inertia (both for type B only) [14]. The robustness of the power generating modules is achieved by FRT and post-fault active power recovery (only for types B, C, and D) [14]. The system restoration defines the coordinate reconnection for types B, C, and D [14]. As for the general system management, it defines the control schemes and settings for types B, C, and D, and the electrical protection and control schemes and settings, priority ranking of protection and control, and information exchange (for types B, C, and D) [14]. It also defines the additional requirements to monitoring (for types C and D only) [14]. As for voltage stability, the reactive power capability, and the fast injection of reactive power (for types B, C, and D) are defined, as well as the additional requirements for reactive power capability and control modes (for types C and D only) [14].

The requirements of the NC RfG were set to balance European-wide system needs and local specifics [14]. So, only the requirements relevant for European-wide system stability are called "Exhaustive Requirements" [14]. All the others are called "non-Exhaustive" because other specifications and details are defined by national regulatory authorities [14].

Exhaustive Requirements define capabilities of generators by function or principle, and by specified parameters, without national level specifications [14]. Non-Exhaustive requirements only define the basic generators' capabilities, without specifying settings or parameters. These should be detailed on national level, due to specific national or regional system characteristics [14]. Non-Exhaustive requirements are therefore also called non-mandatory. For example, the NC RfG was complemented by "*Portaria nº 73/2020*", which sets the non-exhaustive requirements for generators to be connected in the Portuguese network. The NC RfG only defines a minor part of requirements, mostly concerning frequency ranges, frequency withstand capability and voltage ranges [14].

One of the most important requirements for any generator is its ability to survive frequency variations, which should be applied to all generators under NC RfG, regardless of their capacity [14]**.** According to the NC, Article 13.1 (b), "a power-generating module shall be capable of staying connected to the network and operate at rates of change of frequency up to a value specified by the relevant TSO, unless disconnection was triggered by rate-of-change-of-frequency-type loss of mains protection. The relevant system operator, in coordination with the relevant TSO, shall specify this Rate-Of-Change-Of-Frequency-type loss of mains protection." [14]

Table 2.2: Proposals for Rate-Of-Change-Of-Frequency (RoCoF) withstand capability in selected European Countries (source: [14]).

Country	**Rate of Change of Frequency (RoCoF) withstand capability**	
Continental Europe	**Requirement and measurement period**	**Applicable to**
Austria	2 Hz/s	ABCD
Belgium	2 Hz/s	
Germany	2 Hz/s; 500 ms	
Denmark	2 Hz/s; 200 ms	
France	N/A	
UK	1 Hz/s; 500 ms	
Ireland	1 Hz/s; 500 ms	
Netherlands	2 Hz/s; 500 ms	
Spain	2 Hz/s; 500 ms	
Italy	2.5 Hz/s; 100 ms	

Table 2.2 shows that most Central-European countries chose a minimum of 2 Hz/s measured over a period of 500 ms, but countries like Ireland and the UK opted for 1 Hz/s measured over 500 ms. Depending on the inertia of the power system, the typical RoCoF relays are set between 0.1 and 1 Hz/s [14]. In Ireland, there is a high integration of wind generators in the distribution network using this type of RoCoF relays [14], which explains why this country has set lower limits for RoCoF withstand capability [14] and combined this strategy with wind turbine inertia emulation at very high renewable energy integration levels. As for larger RoCoF limits, it is also known that wind turbines (such as DFIG and full converter) can handle values up to 4 Hz/s, but the assessment of impacts of high RoCoF on their control and protection schemes must be done [14].

Another set of relevant requirements is related to the ability of generators to modulate active power as a function of the grid frequency. A particular operational mode defines that generators should be capable of reducing their output power if the frequency exceeds a certain threshold ("Limited Frequency Sensitive Mode – Overfrequency (LFSM-O)") [14]. Other operational modes are the "Frequency Sensitive Modes" – FSM (stating that a generator should be able to participate in active power-frequency regulation), and the "Limited Frequency Sensitive Modes – Underfrequency (LFSM-U)" (stating that the generators should be able to increase their output power if the frequency is lower than a specified threshold). The response characteristic is defined by the relevant national TSO/authority through two parameters: frequency threshold (Hz) and P/f droop (%) [14]. This requirement will be applied to all generators, regardless of their capacity.

Table 2.3: Proposals for Limited Frequency-Sensitive mode – Overfrequency (LFSM-O) settings in selected European Countries (source: [14]).

Country	**Limited Frequency Sensitive Mode - Over Frequency**		
RfG definition	**Requirement Droop**	**Threshold**	**Delay**
Austria	5%	50.2 Hz	None
Belgium	5%	50.2 Hz	None
Germany	5%	50.2 Hz	None
Denmark	CE: 5% (SPGM/PPM); N: 4% (SPGM/PPM)	CE: 50.2 Hz; N: 50.2 Hz	None
France	5%	50.2 Hz	<2 s
UK	10%	50.4 Hz	<2 s
Ireland	4%	50.2 Hz	None
Netherlands	5%	50.2 Hz	None
Spain	5%	50.2 Hz	None
Italy	2.60%	50.2 Hz	None

From Table 2.3, it is seen that most European continental countries have opted for a 5% droop, which equals to a 40 %/Hz reduction in active power generated, to counteract the excessive frequency rise [14]. Every country except for the UK has set a frequency threshold of 50.2 Hz. This is the frequency for which the LFSM-O will be activated [14].

There are also requirements related to the reactive power capabilities for the generators, as reactive power is related to voltage stability. The generators should also inject reactive power in quasi-steady state, therefore regulating reactive power and voltage. These capabilities must be provided by all generators from type B upwards upon specification from the relevant TSO/national authorities [14]. Table 2.4 shows the proposed reactive power requirements for the individual countries for the type B PPM generator [14].

Table 2.4: Proposals for reactive power capabilities for Type B PPM in selected European Countries (source: [14]).

Country	**Reactive Power Capability for Type B PPM**	
RfG definition	**Reactive Power Range Q/Pmax**	**Voltage Range**
Austria	-0.411 to 0.411	0.875 to 1.1 pu
Belgium	0.33/0.33	0.9 to 1.1 pu
Germany	cosφ 0.9 at Pmax	0.9 to 1.1 pu
Denmark	0.33/0.33	0.9 to 1.05 pu
France	0.35/0.4	Not specified
UK	cosφ 0.9 at Pmax	0.95 to 1.05 pu
Ireland	-0.33 to 0.33	Not specified
Netherlands	-0.4 to 0.35	0.9 to 1.1 pu
Spain	-0.3 to 0.3	0.95 to 1.05 pu
Italy	-0.484 to 0.484 (LV); -0.312 to 0.312 (MV, Wind); -0,436 to 0.436 (MW, Solar)	Not specified

On Table 2.4, it is possible to observe that countries have very different reactive power and voltage requirements, which reflects the currently existing practices to include distributed generators in the local voltage management [14], showing the local nature of voltage and reactive power. For example, according to [15], “highly meshed and/or heavily loaded networks need more lagging reactive power (production)”, and “remote networks with modest power flows and low consumption need more leading reactive power (consumption) in order to keep the voltage within the permitted ranges”.

In Figure 2.5, the U-Q/Pmax and P-Q/Pmax profiles for Type D power plants in Denmark are represented. The U-Q/Pmax describes the requirements for reactive power capability at different voltage levels, and the P-Q/Pmax profile describes the requirements for reactive power capability at different active power levels below maximum capability [16]. However, as expressed in Table 2.4, some countries do not use the U-Q/Pmax profile, rather requiring the delivery of reactive power within a power factor range [16]. Reactive power capabilities below maximum active power output are considered to ensure that enough reactive power is provided at low active power levels for avoiding step changes in case of sudden wind sags (for wind generation) or clouds (for solar power plants) [16].

The steady-state reactive power requirements are defined by black lines and are set by the EU CR (European Commission Regulation) for Continental Europe, leaving each country's TSO to define its own reactive power requirements through an inner envelope [16]. The generators should then be designed to ensure that the operating point for the delivery of reactive power can be set within the specified inner envelope [16]. The inner envelope is specified by the blue lines and can assume different shapes according to the country/area to which they will be applied [16]. However, the inner envelope should always be positioned within the limits of the fixed outer envelope defined by the EU CR [16]. In other words, the blue areas in Figure 2.5 show the steady-state reactive power requirements defined by the Danish TSO, whereas the grey area represents "the area where the reactive power capability is allowed to be limited by a reduced number of operating units, due to startup and shutdown as a function of primary energy, maintenance or failure" [16].

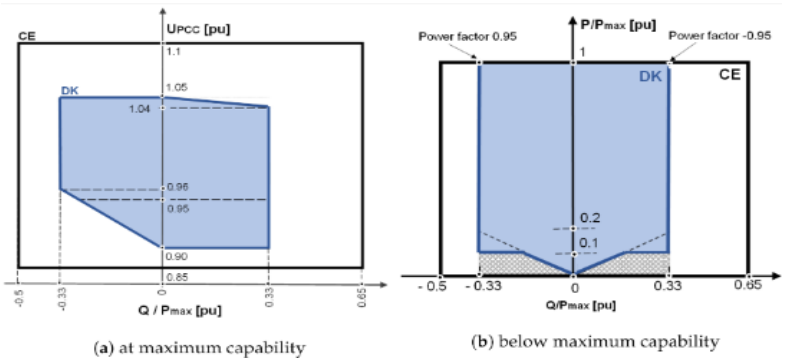

Figure 2.5 - Reactive power provision capability requirements for power generating units (source: [16]).

According to [16] and as seen in Table 2.4, large scale power generating units and electrical energy storage systems should be able to provide reactive power control using one of the following control modes: voltage, reactive power, and power factor control. Only one control mode can be activated at a time, being the choice of the control mode done in coordination between the TSO and the plant operator [16].

In voltage control, the generators should be able to control the voltage at the PoC (point of connection) by providing reactive power to the network. The reactive power of the power generating unit varies according to the PoC voltage droop to keep the voltage stable [16]. In reactive power control mode, generators and energy storage systems should control the reactive power at the PoC to the reactive power setpoint, regardless of the active power and voltage at the PoC, being the reactive power setpoint within the reactive power limits defined by the TSO [16]. The power factor control requires the generators to control the reactive power proportionally to the active power at the PoC, according to a fixed power factor set point set within the reactive power range of the generator [16]. Nevertheless, a plant should only exchange reactive power with the public electricity supply grid unless it is agreed with the TSO [16].

To ensure robustness of generators during disturbances and faults and avoid undervoltage generation tripping, all type B generators need to provide Fault Ride Through (FRT) and Fast Fault Current Injection capabilities. The Fast Fault Current Injection refers to the symmetrical and unsymmetrical current at the connection point during a voltage deviation [14] (the current is injected to rise the voltage). The generator should also provide "post-fault active power recovery" and the specifications for these currents should be provided by the relevant TSO [14].

The FRT requirement is given by the lower limit of a voltage vs. time profile of the voltage at the connection point, where a generator must be connected to the grid [14]. There are four voltage/time parameters: U_{ret} is the retained voltage during a fault, t_{clear} is the instant where the fault has been cleared, and $U_{rec1}/t_{rec1,2}$ and U_{rec2}/t_{rec3} define the lower limits during recovery of the voltage after clearance of the fault [14]. These parameters are expressed in Figure 2.6, where, as expected, the voltage is at its lowest at the time the fault appears and remains on the minimum until its clearing. For FRT, the requirements are different depending on the relevant TSO, being the major difference noted for the voltage recovery after the clearance of the fault, with the requirements varying from 1.5 to 3.0 seconds [14].

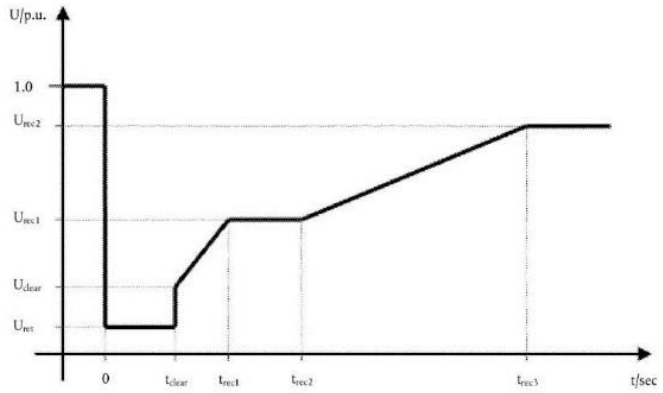

Figure 2.6: Definition of FRT (Under voltage ride through) curve in the NC RfG Figure 3 (source: [14]).

Some countries only provide a basic definition for the Fast Fault Current Injection Capability of a generator (as seen from Table 2.5, Type B PPMs is the term of comparison, as the other types and technologies differ in their specifications [14]), but the Fault Current should be injected to rise the voltage after the fault and prevent the voltage collapse. For example, according to the German Grid Code, the reactive current injection should be activated within 20 milliseconds [17]. When the voltage deviation is higher than 10%, the converter should provide 2% of reactive current per percent of voltage deviation [17]. "During voltage support, the reactive current has higher priority than that of the active current", which means that, "in case of a voltage drop below half of the nominal voltage the converter should allocate the full rated current to reactive power injection" [17]. The voltage support by reactive current injection is then shown in Figure 2.7.

Table 2.5: Proposals for Fast Fault Current Injection Capability of Type B PPMs in selected European Countries (source: [14]).

Country	Fast Fault Current Injection Capability of Type B PPMs
Austria	Yes, 2≤ k ≤6
Belgium	Yes, 0<k<6
Germany	Yes, 2≤ k ≤6
Denmark	Yes, k=2
France	Yes, 0<k<6
UK	Yes, no parameters specified
Ireland	Yes, no parameters specified
NL	Yes, 2≤ k ≤10
Spain	Yes, 2≤ k ≤6
Italy	Yes

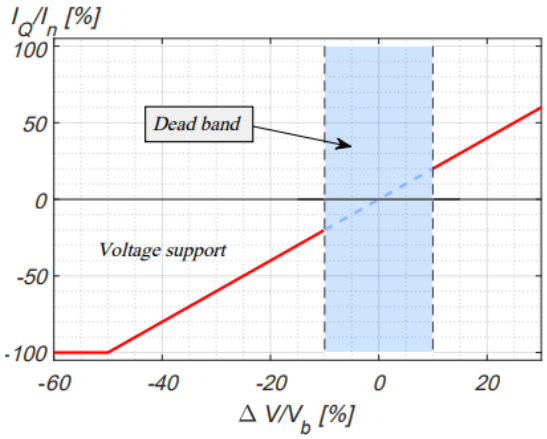

Figure 2.7: Injection of reactive current for voltage support (source: [17]).

After having reviewed the exhaustive requirements for the generators connected in the European synchronous area (as well as the UK and Ireland), the non-exhaustive requirements will be discussed in the next section. The following section will then analyse the Portuguese case, taking as a reference the document "*Portaria nº 73/2020*" [18].

2.6 Review of the Requirements for Generators in Portugal

As previously discussed, the most important aspects to define in the Requirements for Generators are their ranges of voltage and frequency, their ability of providing reactive power to the grid, their ability of surviving voltage collapse, and their sensitivity to frequency disturbances. Then, the legislation in Portugal defines the non-Exhaustive requirements for the generators. Notably, Table 2.6 defines their supported frequency ranges:

Table 2.6: Frequency ranges to be supported by the generators (source: [18]).

Frequency Ranges (Hz)	Period of Operation	Generator Types
47.5-48.5	30 minutes	ABCD
48.5-49.0	Unlimited	
49.0-51.0	Unlimited	
51.0-51.5	30 minutes	

In Portugal, the generators should support RoCoF equal or lower than 2 Hz/s measured in a moving window of 500 milliseconds, as in most European countries [18]. This requirement also includes three different operational modes: the Frequency Sensitive Mode (FSM), the Limited Frequency Sensitive Mode for Over-frequency (LFSM-O) and the Limited Frequency Sensitive Mode for Under-frequency (LFSM-U). The generators should also connect automatically to the grid between 47.5 Hz and 51.5 Hz [18]. The generators should also remain connected during three-phase symmetric and asymmetric faults and when voltage levels are low [18].

The Frequency Sensitive Modes are defined by the variation of the active power generated with frequency variations [18]. The Non-exhaustive requirements applicable in Portugal define that only generators of types C and D are required to have a full active power response for a period of at least 15 minutes.

In Table 2.7, the parameters for the active power response in this operational mode are listed. Figure 2.8 explains how this operation mode works, where P_{max} is the maximum capacity to which ΔP is related, being ΔP the change in the active power output from the power generating module [19]. The generators should provide an active power output, ΔP, up to the point ΔP_1, according to the time instants t_1 and t_2, being t_1 the initial delay, and t_2 the full activation time (Figure 2.8).

Table 2.7: Parameters used to apply the Frequency Sensitive Modes (source: [18]).

Parameters	Values	Generator Types
Range of Active Power Compared to Pmax, |ΔP1|/Pmax	5%	C, D
Insensitivity of Response to Frequency		
|Δfi|	10 mHz	
$\frac{\lvert\Delta fi\rvert}{f_n}$	0.02%	
Frequency Response Deadband	0 Hz	
Speed Droop, R (adjustable)	4%-6%	
Maximum admissible initial delay, t1, with inertia	2 s	
Maximum admissible initial delay, t1, without inertia	500 ms	
Maximum permissible for the full activation time, t2	30s	

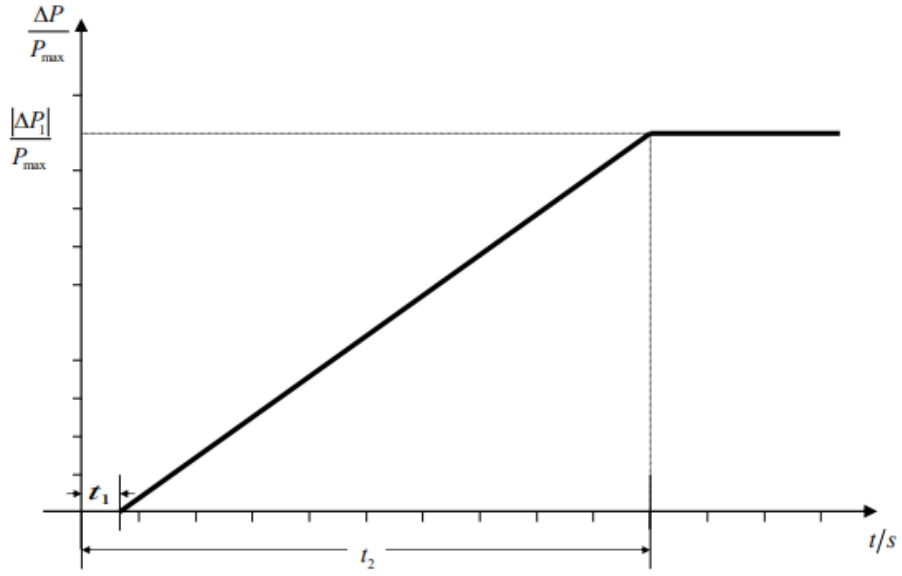

Figure 2.8 – Active power-frequency response capability (source: [19]).

Regarding the LFSM-O, it is known that it corresponds to the active power reduction when the frequency rises to unacceptable levels, using the speed droop control. According to the Non-exhaustive requirements applicable in Portugal [18], all the generators must operate after reaching the minimum frequency level: this means that types A, B, C and D should operate with frequencies higher than 50.2 Hz with a speed droop between 4% and 6 % [18]. As for the LFSM-U, the minimum of frequency should be 49.8 Hz, with a speed droop between 4% and 6%, for types C and D [18].

The Type D generators should remain connected to the network within the voltage ranges indicated in Table 2.8 [18]. In the case of Type C generators, the automatic disconnection depends on the established conditions for the connection of power units. Then, this should be defined by the relevant TSO [18].

Table 2.8: Minimum Periods of Time for which the generator must operate, with voltages deviated from 1 p.u. (source: [18]).

Voltage Levels	Voltage Range	Values	Type of Generator
110 kV-300 kV	0.85 p.u. - 0.90 p.u.	60 minutes	D
	0.90 p.u. - 1.118 p.u.	Unlimited	
	1.118 p.u. - 1.15 p.u.	20 minutes	
300 kV - 400 kV	0.85 p.u. - 0.90 p.u.	60 minutes	
	0.90 p.u. - 1.05 p.u.	Unlimited	
	1.05 p.u. - 1.10 p.u.	20 minutes	

In [17], it is also defined the admissible active power reduction according to the frequency drop. Particularly, the 3rd Point of Article 5th states that, below 49 Hz, there should be a 2%/Hz reduction of active power, when operating at a 50 Hz frequency [18] [20].

Moreover, the Requirements for Generators also include the capability of generator surviving voltage dips, as well as the additional injection of reactive current during the fault and the recovery of the active power after the fault [18] [20]. This is also called Low Voltage Ride-Through (LVRT) Capability or Fault Ride-Through in case of fault [20].

The voltage dip is defined as an abrupt reduction in the voltage between 90% and 5% of the nominal voltage, following the voltage restoration after a short period (10 milliseconds to 1 minute) [20]. In fact, the value of a voltage dip is given by the difference between the nominal voltage and the RMS voltage during the voltage dip [20].

When a short-circuit appears in the grid, it might lead to the disconnection of a generator during a voltage dip, compromising the grid's stability [20]. For example, converter-interfaced generation, especially wind generation systems, is characterized by a post-fault active power response in the moments after the clearing of the fault (Figure 2.9 -a)). Since the post-fault active power recovery phase is characterized by an active power deficit largely impacting the power-frequency dynamics after the fault clearance, such behaviour became a concern of the Grid Codes. Then, it is required that any generation module has LVRT capability: for a synchronous generator (SPGM), this is regulated by the excitation system, whereas for a PPM generator, this is achieved by the inverter, which injects reactive current during the fault, provoking a voltage rise and the recovery of active power [20].

According to the Non-exhaustive requirements applicable in Portugal [18], it is required that all generators remain connected during three-phase symmetrical and unsymmetrical faults, involving or not the ground, if the voltage in the connection points remain above the capacity profile curve [18]. The capacity profiles are defined based on the significance of the generation modules, being these requirements only applicable to all type A generators having a nominal active power higher than 15 kW [20]. Figure 2.9 represents the capacity profiles for LVRT capability of type D generators.

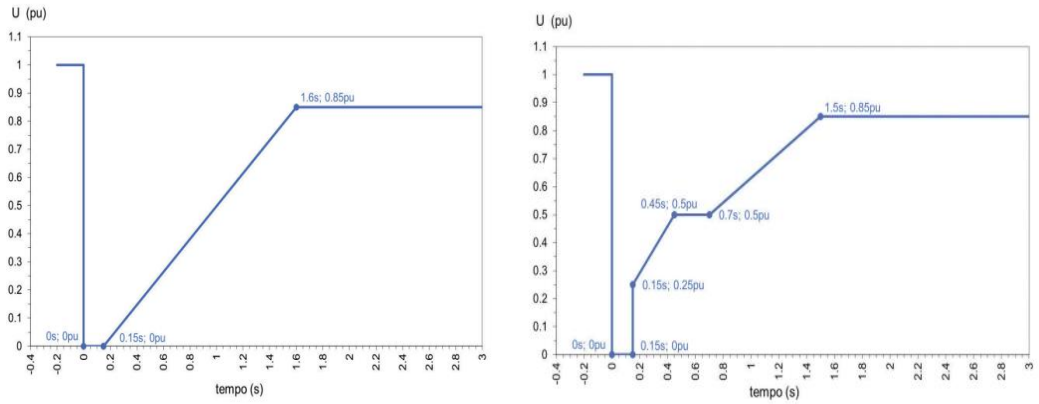

(a) **(b)**

Figure 2.9- Capacity profile for LVRT Capability for: **a)** PPM of type D (U≥110 kV) and **b)** SPGM of type D (U≥110 kV), as specified in point 9.1 of the Article 5th of [18].

According to the Non-exhaustive requirements applicable in Portugal [18], the SPGM of type B, C and D must be capable of activating the fast reactive current injection mode if a voltage in the connection point outside the permitted range is detected, or if there are abrupt voltage variations [18] [20]. The reactive current injection (Figure 2.10) must be a priority during the fault, but it is acceptable to reduce the active component, although this reduction should be as minimal as possible [18] [20].

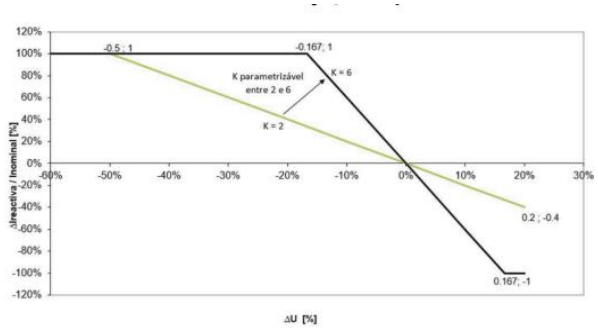

Figure 2.10 - Minimum values for the fast injection of reactive current, applied to PPM generators of types B, C, D, as specified in Point 15.5 of Article 5th of [18].

After the beginning of the fault, the response times are defined. The measurement/detection time is, at most, 20 ms (it is the maximum time for starting the injection of reactive current) [18] [20]. The response time is 30 ms, and it is the response time between the beginning of the reactive current injection until it reaches 90% of the expected current response [18] [20]. The establishment time is 60 ms, which is the time between the beginning of the reactive current injection and the time when it reaches the admissible range of the expected current response [18] [20]. If the voltage returns to values within the admissible range, or after 5s after an abrupt variation, this mode should be deactivated [18].

Another important requirement is the Fast Post-Fault Active Power Recovery. This is defined by the capacity of a generation module reaching at least 90% of its pre-fault active power, after fault elimination and beginning of voltage restoration at the connection point, having 2 seconds to reach the same active power as before the fault [18] [20]. The generator should remain connected to the system for at least 15 minutes after the fault [20].

In agreement with the non-exhaustive requirements for Portugal [18], for the SPGM and the PPM of types B, C and D, it is required that, after the fault elimination and beginning of the voltage recovery, the recovery of 95% of the active power produced before the fault is done in less than 1 second [18]. Additionally, the generators have 2 seconds to reach the same active power as before the fault [18] (as present in Point 16.2).

The reactive power requirements for Portuguese generators must also be assessed. As stated in [18] [20], within the static voltage limits, the reactive power/voltage control is done with two different operation points: at maximum capacity with varied voltage and below the maximum capacity. The U-Q Capability is specified by the relevant system operator, so that any module of types B, C and D can provide reactive power at maximum capacity [18] [20]. The SPGM as of 45 MW connected to the Very High Voltage Network should include PSS (Power System Stabilizer) [18] [20]. In Figure 2.11, the profiles for type D generation modules are present:

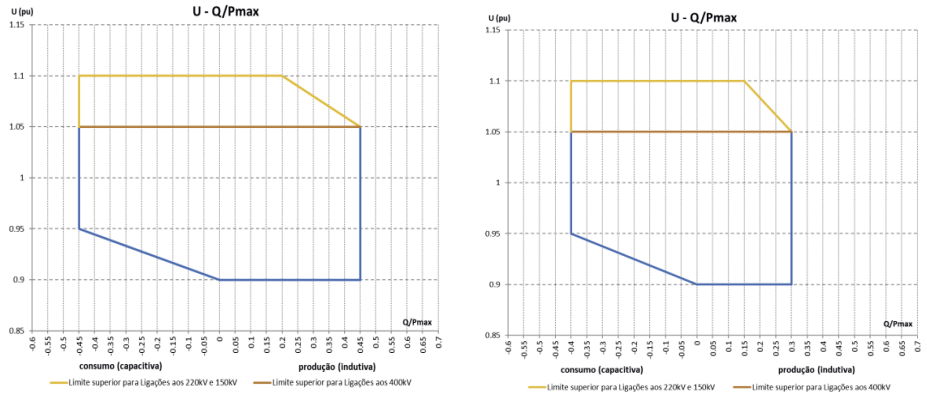

(a) **(b)**

Figure 2.11 - Capacity profile of reactive power supply, as specified in Point 12.2 of Article 5th of [18]: a) SPGM of type D (U≥ 110 kV); b) PPM of type D (U≥ 110 kV).

From Figure 2.11, it is possible to verify that synchronous generators indeed provide more reactive power than distributed generators.

The PPM of types C and D have to provide reactive power at any point of their P-Q Capability profile provided all units of the generation module are available and not in maintenance or at fault [18]. In Figure 2.12, variants 1 and 2 for the PPM of type D are represented (for U≥ 110 kV).

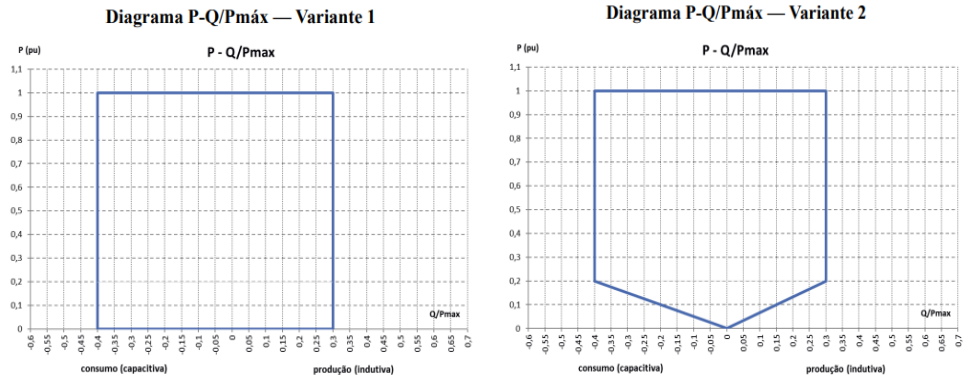

(a) **(b)**

Figure 2.12 - P-Q Capability profile for providing reactive power with the active power of type D PPM (U≥ 110 kV), as specified in Point 19.2 of Article 5th of [18]: a) Variant 1; b) Variant 2.

To conclude this section, it is important to note that one of the reasons why the Requirements for Generators are a solution for the mitigation of inertia-related problems is because they define how the generators should provide synthetic inertia. Indeed, the non-exhaustive requirements for generators applicable to Portugal [18] define that the types C and D of PPM should provide the synthetic inertia of the equivalent capacity synchronous generators [18] [20]. In fact, when considering virtual inertia, as stated in Table 2.7, the frequency sensitive mode includes a maximum time delay of 2 seconds [18] [20]. Virtual inertia increases the time to achieve the nadir, which lowers the impact of the perturbations in frequency transient stability [20]. To achieve this goal, the next sections briefly describe some strategies to implement the mentioned Grid Codes.

2.7 Strategies for Providing Virtual Inertia

Virtual inertia is the capability of emulation of the inertial response in power converter interfaces, similarly to the one obtained in conventional synchronous generators following a load-generation unbalance. As stated in [21], there are three main topologies for delivering virtual inertia. The four main models are based on the electromagnetic and electromechanical equations of synchronous generators (also called Synchronverters), on the swing equation (known as the Ise Lab's Topology), on the frequency/active power response (Virtual Synchronous Generators), and droop-based approaches [21].

The synchronverter strategy guarantees an accurate replication of synchronous generators' dynamics, and does not require frequency derivative, which is an advantage because the derivative terms usually introduce noise in the system [21]. Moreover, the PLL is only used for grid synchronization of the converter to the grid, which is advantageous because, in weak grids, the PLL usually is more prone to instabilities [21]. Even though the synchronverter can mimic the exact dynamics of a SG, the complexity introduced by the differential equations may cause numerical instability, depending on the parametrization of the damping coefficient (D) and the moment of inertia (J) [20] [21]. Furthermore, this is a voltage-source based implementation, which means that there is no protection against severe grid transients, resulting then in the need for external protection systems for safe operation [21].

In comparison to the synchronverter strategy, the Ise Lab's Topology is a simpler model [21]. Once again, the RoCoF calculation is not required and the PLL is only used for synchronization to the grid [20]. However, this model provokes power and frequency oscillations, due to incorrect tuning of the J and D parameters. This model can be applied to operate distributed generation units as grid forming modules [21].

The models based on Frequency-Power response are also named Virtual Synchronous Generators, which absorb/release kinetic energy similarly to SG, presenting the DG units as dispatchable current sources that provide dynamic frequency control [21]. The output power of the VSG converter is given by Equation 2.23:

$$P_{VSG} = K_D \Delta\omega + K_I \frac{d\Delta\omega}{dt} \tag{2.23}$$

Where $\frac{d\Delta\omega}{dt}$ corresponds to the RoCoF, K_D represents the damping constant (or Frequency Containment Reserve, in MW/rad/s) and K_I the inertia constant (or the Fast Frequency Response) [20]. The FCR helps the frequency return to a steady-state value and reduces the frequency nadir, whereas the inertia constant arrests the RoCoF by contributing to fast dynamic frequency response based on the frequency derivative [21]. This aspect is important in an island, where the initial RoCoF can be very high and cause unnecessary tripping of protection relays [21].

In this system, a PLL is adopted for measuring the change in the system frequency and RoCoF. Using the previous equation, the active power reference for the inverter is calculated, which allows the generation of current references for the current controller [21]. This topology follows a direct-quadrature (d-q) based current control approach, being the d-axis current the written according to Equation 2.24:

$$I_d^* = \frac{2}{3}\left(\frac{V_d P_{VSG} - V_q Q}{V_d^2 + V_q^2}\right) \tag{2.24}$$

Where V_d and V_q are measured according to the grid voltage [21]. The q-axis current and the reactive power are set to zero, as the active power is the only variable to be controlled [21]. The current controller then generates a PWM signal, which defines the state of the inverter's semiconductors, creating a system behaving as a current-controlled Voltage Source Inverter [21].

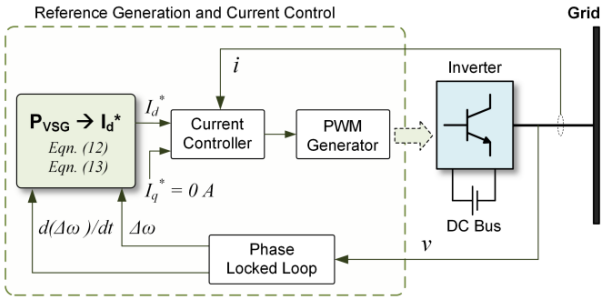

Figure 2.13 - VSG Topology (source: [21]).

The topology represented in Figure 2.13 has been used in remote microgrid applications, especially in the presence of wind systems [21]. However, its implementation is impossible in islanded modes because the virtual inertia unit must operate in a grid forming mode [21], creating a high error in the voltage phase estimation [21]. Moreover, this system creates inertia during frequency disturbances, but not when input power variations occur [21]. Other issues are related to the PLL, as their performance can degrade and compete with other PLLs, which is especially prevalent in weak grids, as they have frequency variations, harmonic distortions, and voltage sags/swells [21]. Another problem is that the computation of the frequency derivative makes this topology sensitive to noise, leading to possibly unstable operation [21].

A solution for this problem would be the use of Grid-Forming Converters with a Droop-Based control approach [20] [21] according to Equations 2.25 and 2.26:

$$f_{grid} = f^* - m_p(P_{out} - P_{in}) \tag{2.25}$$

$$v_{grid} = v^* - m_q(Q_{out} - Q_{in}) \tag{2.26}$$

Being f_{grid} the local frequency value, f^* the frequency reference value (both in Hz), m_p (Hz/MW) and m_q (kV/Mvar) the active and reactive power gain, respectively, P_{out} and P_{in} the measured and reference values for active power (both in MW), Q_{out} and Q_{in} the measured and reference values for reactive power (both in Mvar) and v_{grid} and v^* the local grid voltage and the reference voltage (respectively).

2.8 Power Electronic interfaces and associated controls

As previously discussed, converter-interfaced generation lacks the natural dynamics of a synchronous machine, meaning that the natural interactions with the grid and other grid resources depend on the control approach [22]. The converters typically have two common modes of operation: the grid-forming and the grid-following modes.

A grid-following converter requires both the amplitude and phase of the grid voltage, which are measured through the PLL at the terminal of the converter [9]. The converter follows the grid voltage phase and magnitude by injecting current at a certain phase shift so that the active component, $I_P^{\rightarrow}$, aligns with $V_g^{\rightarrow}$, and so that the reactive component, $I_Q^{\rightarrow}$, is in quadrature with the grid voltage [9]. With this control, it is possible to generate an active power reference set-point, P*, for the converter [9]. Yet, as this type of control requires the grid voltage to determine the active power, grid-following converters are uncapable of working alone, making it impossible to reach an 100% renewable energy integration [9]. If only grid-following converters were used without any synchronous machines, the voltage measurements would be more volatile, causing frequency differences between converters and producing higher power flows, leading to more changes in the output current (and in the active power generated by each converter) [9]. Then, there is a need for implementing converters capable of controlling the frequency for the proper operation of the grid-following inverters found in the grid [9]. According to [9], it would be possible to implement the inertial response in the grid-following converter controller, but "it would require the implementation of a PLL to measure changes in the frequency and then modify P*" [9]. To obtain the grid frequency, the PLL would have to measure the grid angle, but given the frequency oscillations around its nominal values, the derivative calculation would amplify the measurement noises and would require the implementation of filters, thus modifying the inertial response of the grid-following converter [9].

For these reasons, the grid-forming converter is proposed. In the grid-forming converter, the voltage magnitude and the frequency are adjusted to specified values by the converters, like a synchronous machine [22]. Grid-forming converters have full frequency and full voltage operating ranges, dynamic reactive power controls, FRT and FFCI capabilities, and act as a sink to counter harmonics and imbalances in the system's voltage [4]. All the same, the behaviour of this technology in grids with high inclusion of converter-interfaced generation is still unknown, and there are doubts about the adequacy of the current Requirements for Generators for promoting this measure.

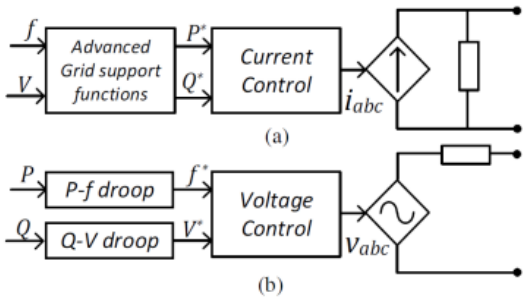

Figure 2.14: Differences between a) grid-following converter and b) grid-forming inverter (source: [9]).

Since the lines in transmission systems are predominantly inductive (i.e., the R/X ratio is low), it is possible to decouple the active and reactive power (being the active power dependent on the phase voltage, and the reactive power dependent on the voltage magnitude) [22]. Then, the previously described Droop-Control Approach can be applied, which is simple and has been widely used in microgrids [22]. Indeed, in Figure 2.14, it is shown that grid-forming inverters use active power-frequency and reactive power-voltage droop controls to set the right frequency and voltage, depending on the active and reactive power measured [9].

Other strategies allowing Grid-Forming operation are the previously described Virtual Synchronous Generator (VSG) and the Matching Control [9]. For example, the Matching Control regulates the converter's DC/AC energy exchange by matching a synchronous machine's electro-mechanical energy exchange [22]. It only requires measuring the DC voltage and does not need other inner loops, diminishing the control-induced delays typical of other strategies [22]. This strategy also imposes the DC voltage stabilization by the primary DC energy source to maintain a power balance across the converter without debilitating the DC capacitor, allowing the identification of imbalances by the evaluation of the DC side voltage measurements [22]. This control signal is widely used in back-to-back converter applications of DFIG-based wind power generators, and in nonlinear modelling of droop-controlled HVDC transmission systems [22].

Since renewable energy generation is dispersed in the power system, the new converter controllers to be developed should be decentralized, not requiring communications for fast-timescale control [23]. Then, all generation, network, and loads play a role in frequency stability [22], being the focus placed in each converter's design. There is a wide variety of control strategies applicable to CIG, according to the type of resource in use. In the case of wind turbines, the kinetic energy must be controlled, as it can be used as a fast frequency reserve, supporting the power system during faults. However, wind turbine generators may exhibit secondary frequency dips, provoked by the switching from normal operating mode and the frequency supporting mode [22]. However, these can be prevented when operating at the maximum power point (MPP) [22], which is further explained.

2.9 Wind and Solar Generation: Maximum Power Point Operation

In the previous sections, some control solutions have already been briefly mentioned. In this section, the power electronic converter design will be developed in detail, focusing on renewable energy applications and their specific control solutions.

Starting from the converter itself, it must be guaranteed that switches have a high operating voltage, as a high voltage implies lower current (hence lower losses), and a low switching time [20]. The fault current injection capability in a power electronic converter is low in comparison to synchronous generators, which creates difficulties when using conventional methods for detecting and isolating faults, as well as the worsening of voltage and angular stability [20]. To counteract the issues posed by current limitation, there are two solutions: oversizing the inverters, for at least the double of the peak demand, and the use of synchronous condensers, which rise the system's inertia and reuse the already installed synchronous generation [20].

Indeed, renewable generation, despite relying on power electronic converters, should have the same abilities as a conventional synchronous generator, notably regarding their Frequency Containment Reserves (FCR) [20]. Indeed, wind turbines (particularly the Variable Speed Wind Generators, such as DFIG – Doubly-Fed Induction Generators – and PMSG – Permanent-Magnet Synchronous Generators) and photovoltaic systems should have two operation modes: maximum power operation and below maximum power operation [20].

To operate the converter at the maximum power point, it must be noted the active power produced by a wind generator has a single well-defined maximum value [24]. The active power available in the wind is written according to Equation 2.27, where ρ is the air density (kg/m^3), the A is the area covered by the blades (m^2), and v the wind speed (m/s).

$$P_{wind} = \frac{1}{2}\rho A v^3 \tag{2.27}$$

As the wind turbine can only extract a part of the wind power, as it is limited by 59% of the capacity (Betz Limit) [24], the actual active power generated by a wind turbine should be given by Equations 2.28 and 2.29:

$$P_{generated} = \eta * C_{p,max}(\lambda, \beta = 0^\circ) * P_{wind} \tag{2.28}$$

$$\lambda = \frac{\omega_r R}{v} \tag{2.29}$$

Where η is the efficiency (the ratio between the output active power and the mechanical power of the turbine, in %), $C_{p,max}$ the maximum power coefficient of the turbine, β the pitch angle, λ the tip-speed ratio (which is the ratio between the speed at the blade's extremity, and the actual wind speed [20]), ω_r the rotor speed (rad/s), and R the rotor radius.

As such, the necessary condition for the speed to be at the maximum power point is that the derivative of the active power generated with respect to ω is null, meaning that a change in speed does not affect the output [24].

To implement this control, it is necessary to increase or decrease the speed in small increments, to evaluate the $\frac{\Delta P}{\Delta \omega}$ ratio: if positive, then an increase in speed generates higher power, whereas, if negative, the power generated decreases if the speed increases [24]. Therefore, the speed is maintained at the point when this ratio is close to zero [24]. This method does not consider the errors in the local wind speed measurement or the wind turbine design, being it the reason why this method is the most widely adopted [24]. In a wind farm, each turbine should have its own control loop, illustrated by Figure 2.15:

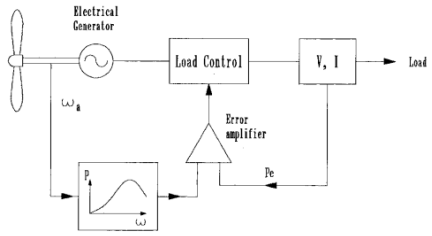

Figure 2.15 - Maximum power operation control scheme for each turbine (source: [24]).

With a higher wind speed, the maximum power limit for active power generation by the turbine is achieved, which may compromise the turbine's integrity [20]. To limit the turbine performance in strong winds, the **Pitch Angle Control** is used to put the blades in the desired position [25], reducing the C_p and adjusting the rotor speed (Figure 2.16) [20].

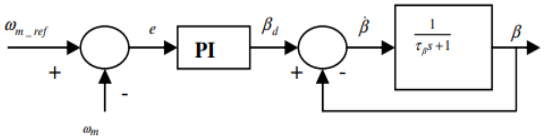

Figure 2.16 - Pitch Angle Control (source: [25]).

In photovoltaic systems, a voltage adjustment in the photovoltaic module by means of a DC/DC converter is needed for maximizing the active power generated. One of the most common control strategies for photovoltaic systems is the Perturb and Observe algorithm, which is implemented by the perturbation of the reference voltage and measuring the system's response for the determination of the next perturbation's direction [26]. The reference voltage perturbations are then induced in the direction for which the generated power increases [26].

Figure 2.17 shows a block diagram used to implement the MPPT of the PV system using a boost converter, where the reference for the voltage is the result of the MPPT algorithm itself [26]. The voltage error is controlled through a PI controller, whose output is the current in the input capacitor, i_c [26]. Since the DC/DC converter is not able to control the capacitor current directly, the inductor current, i_L, is used as a current reference to compute the current error [26]. The output of the current control loop generates the reference for the duty-cycle, which is used for controlling the semiconductors present in the DC/DC boost converter [26].

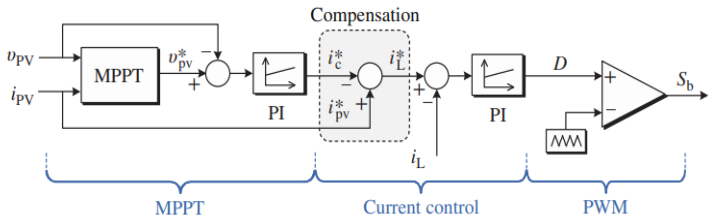

Figure 2.17 - DC/DC Converter control block diagram for photovoltaic systems (source: [26]).

As stated before, the converters can operate at the MPP and below the MPP. So far, the MPP operation was discussed. Now, the **de-loaded operation** should be addressed, as it limits the output active power, allowing the CIG to participate in the Frequency Containment Reserve [20]. This is done to provide active power/frequency control, as it is required for PPM. There are three types of constraints in this type of control: **delta power constraint** (active power reduction proportionally to the available active power), **absolute power constraint** (to protect the system from overloads, there is a limitation of the active power in the coupling point), and **ramp rate constraint** (to prevent abrupt active power variations from causing abrupt frequency variations, defining the maximum gradient of the output active power) [20].

To achieve active power/frequency control for wind turbines, [20] summarizes the **Rotor Speed Control (RSC)**, which consists of rising the rotor speed above the MPP, to have a lower output active power than the active power generated [20]. This then provides an active power additional response. This method is fast and diminishes the mechanical wear, but the Frequency Containment Reserve is limited by the rotor's speed and wind speed, being this strategy valid only for low wind speeds [20].

After having revised the fundamentals of MPP operation, the following section details the techniques for participation in frequency regulation and for virtual inertia provision.

2.10 Frequency control techniques for Wind Turbines without Energy Storage Systems

In the previous section, specific aspects regarding the design of power electronic converters to be used in wind and solar applications were discussed. However, there are other types of frequency controls suitable for wind and solar generation that can help achieve active power/frequency control [27], which are summarized in Figure 2.18.

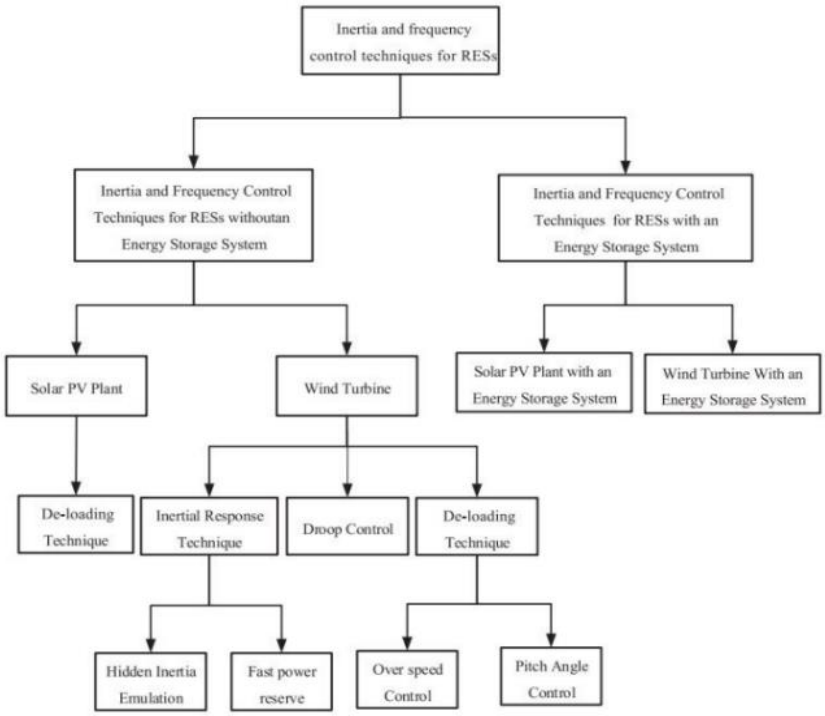

Figure 2.18 - Inertia and frequency control strategies for RES with or without energy storage systems (source: [27][28]).

In this section, the first control strategy to be covered is the de-loaded operation for both wind and solar generation. Figure 2.19 shows a combination of the de-loading controller with a proportional frequency control (droop control) using the previously described pitch control, which is a common approach:

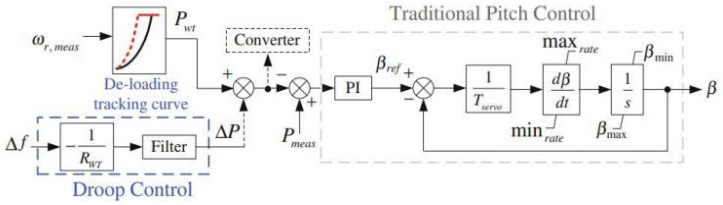

Figure 2.19 - De-load operation using pitch control (source: [27]).

For wind turbines, the de-loaded operation can be implemented through speed control and by pitch angle control. The speed control approach consists of the change in the value of the tip speed ratio, λ, by shifting the operation point towards the left or the right of the MPP [28]. When the frequency drops, the wind turbine releases active power proportionally to the frequency deviation according to Equation 2.30:

$$P_{ref} = P_{del} + (P_{max} - P_{del}) * [\frac{\omega_{rdel} - \omega_r}{\omega_{rdel} - \omega_{rmax}}] \quad (2.30)$$

Where P_{max} is the maximum power (in p.u.), P_{del} is the de-loaded power (in p.u.), ω_{rmax} is the rotor speed at the maximum power, ω_{rdel} is the rotor speed at the de-loaded power, and ω_r is the rotor speed at the reference power. The de-loading method using overspeed control is mostly used at medium wind speeds [28].

The pitch angle controller de-loads the wind turbine through the increase of the blade's angle. It is activated when the WTG arrives at the nominal speed and when the overspeed controller fails [28]. The de-loaded operation of a WTG follows this sequence: the Equation 2.30 gives the reference active power for calculating the rotor's speed, thus de-loading the generator; then, the pitch control provides a 10% active power reserve; to release the active power reserve stored in the turbine's blades, the droop control is also activated [28].

For photovoltaic energy, the de-loaded technique is achieved by increasing the PV voltage beyond the MPP voltage. Figures 2.20 and 2.21 show that this is done by increasing the value of V_{MPP} by $V_{de\text{-}load}$, allowing the PV array to function as an active power reserve [28]. This reserve will not be released until the deviation of the system's frequency, which is implemented by the addition of a control signal, $V_{dc\Delta f}$, to the DC reference voltage [28]. This strategy alone does not take in account the remaining reserve power for each PV unit, so, it considers that all PV units release the same amounts of active power needed for frequency regulation [28]. This results in some PV units with less active power reserves to reach the MPP faster, thus becoming unable to further contribute to frequency regulation, creating then a non-uniform distribution of frequency regulation [28]. So, a new control signal, $\Delta V_{reserve}$, must be added to represent the remaining reserve power. The new DC voltage reference is then given by Equation 2.31, which demonstrates that the output power of a PV unit depends on the system's frequency deviation and on its available active power reserve:

$$V_{dc,ref} = \left(V_{MPP} + V_{deload} - V_{dc\Delta f}\right) - (\Delta f * \Delta V_{reserve} * K_{P2}) \quad (2.31)$$

Where K_{P2} is a controlled variable that determines the amount of reserve power for PV plants and is limited to the range of 0.8-0.95 [28]. Therefore, this shows that PV generators can provide frequency regulation and follow load changes [28].

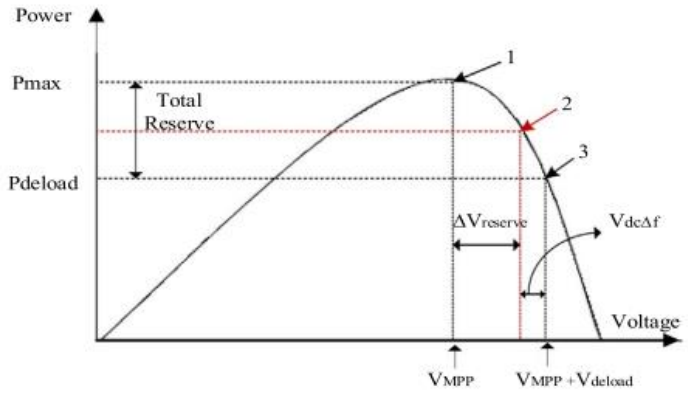

Figure 2.20 – De-loaded technique applied to Solar PV (source: [28]).

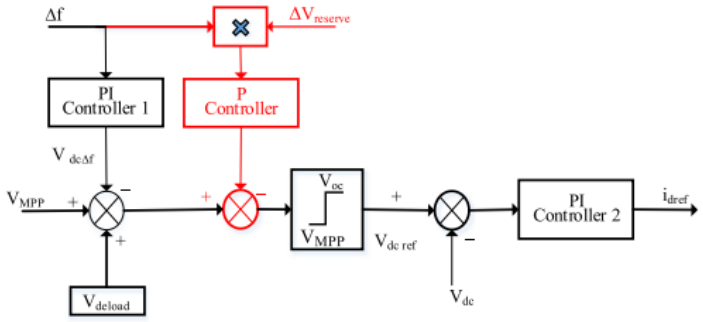

Figure 2.21 - Solar PV with the improved de-loaded technique (source: [28]).

Now, the inertial response control shall be revised. The inertial response is characterized by a generator's ability to provide automatic frequency control following a disturbance, by releasing part of the kinetic energy stored in the rotating masses [27]. Wind turbines have a reasonable amount of kinetic energy stored in their blades, gearbox, and generator, but, as they are connected to the grid through power electronic converters, they are unable to provide an inertial response on their own [27]. Then, to enable a temporary power response from WTGs (wind turbine generators), two control strategies were developed: the Hidden Inertia Emulator Controller and the Fast Power Reserve.

In the Hidden Inertia Emulator Controller, the power is withdrawn from the wind turbine's rotating parts according to Equation 2.32. This means that the active power response will be simultaneously proportional to the frequency value and to the RoCoF [27]:

$$P_{Hsyn} = 2 * H_{syn} * f_{sys} * \frac{df_{sys}}{dt} \quad (2.32)$$

Where P_{Hsyn} is the active power control signal (in p.u.GW), f_{sys} is the system frequency (in p.u. Hz), and H_{syn} is the synthetic/emulated inertia (in seconds) (Figure 2.22).

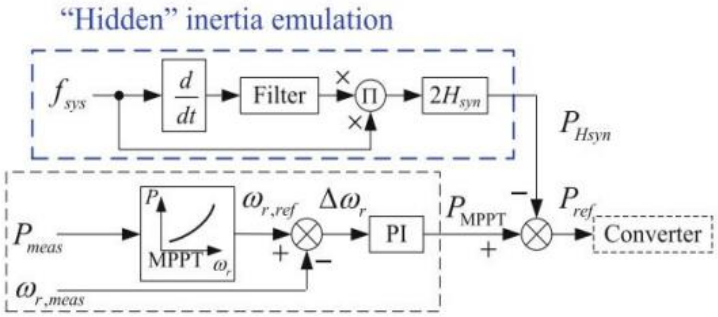

Figure 2.22 - Hidden inertia controller (source: [27]).

As for the Fast Power Reserve controller (Figure 2.23), a constant amount of power (P_{Hsyn}) is released during an amount of time t.

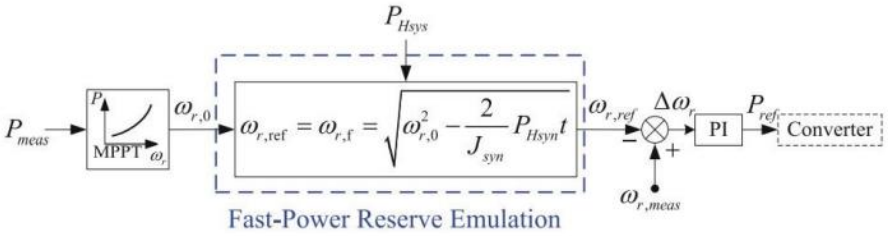

Figure 2.23 - Fast power reserve controller (source: [27]).

This controller changes the rotational speed value artificially, according to Equation 2.33, thus allowing the release of the kinetic energy stored in the wind turbine's rotor [27] [28].

$$\omega_{r,ref} = \omega_{r,f} = \sqrt{\omega_{r,0}^2 - \frac{2}{J_{syn}} * P_{Hsys} t} \tag{2.33}$$

Where $\omega_{r,0}$ is the rotor initial rotational speed, before the release of the kinetic energy (p.u.rad/s), $\omega_{r,\,ref}$ is the desired rotational speed (p.u.rad/s), and $\omega_{r,\,f}$ is the rotor rotational speed corresponding to t (in p.u.rad/s).

According to [27], when using these techniques, the wind turbine is unable to provide an unlimited active power response, given the effect that the release of the kinetic energy stored in the rotating masses has on the machine's rotational speed. The controllers stop the power response either because the frequency value is above a certain threshold, or because the machine's rotational speed has dropped below the threshold [27].

A fast power reserve controller begins its operation once the frequency deviation exceeds a certain threshold. Then, a control signal is sent to bypass the maximum power point tracking, thus enabling power shaping [28]. This control strategy provides extra power during overproduction, but, when the kinetic energy discharge is complete, the rotor speed must be set to its pre-fault value, restoring the maximum power [28]. The restoration process leads to the under-production phase, where the power is withdrawn from the grid to return the rotor speed to its desired value [28]. To prevent an instantaneous drop in the output power, the transition from overproduction to under-production should follow a sloped transition [28], as it can be seen in Figure 2.24:

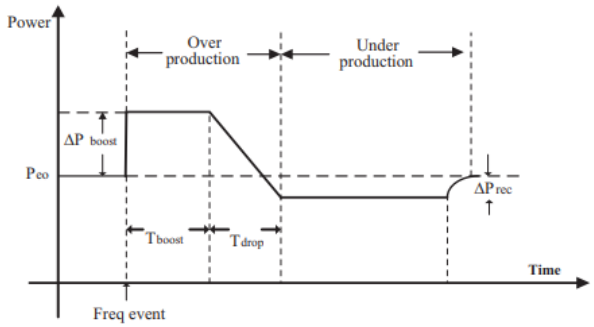

Figure 2.24 - Power characteristics for fast power reserve control [28].

The final control strategy for wind turbines to be discussed is the droop control scheme (Figure 2.25), which is used to regulate the active power output from a wind turbine according to the frequency change. The active power should then be given by Equation 2.34:

$$\Delta P = P_1 - P_0 = -\frac{f_{measured} - f_{nominal}}{R} \qquad (2.34)$$

Where R is the WTG's droop constant, $f_{measured}$ and P_1 the new frequency and wind turbine's output power, and $f_{nominal}$ and P_0 the initial frequency and active power. This linear relation shows that, when the frequency drops from its nominal value (50 Hz) to the measured value, the wind turbine increases the active power to compensate the frequency drops. According to [28], this approach improves the frequency nadir and facilitates the frequency recovery after a disturbance.

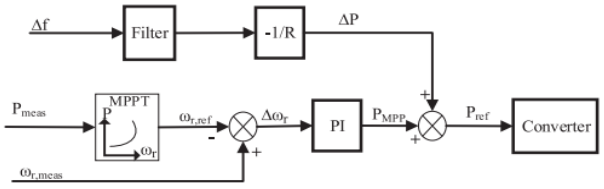

Figure 2.25- Frequency support scheme with droop speed control (source: [28]).

2.11 Frequency control techniques for Wind and Solar generators with Energy Storage Systems

In this section, the frequency support of wind and solar generators using energy storage systems (ESS) is discussed. When ESS are present in PV plants and wind farms, it is simpler to provide a frequency dependent active power response. They allow the use of various types of controllers, because all the active power reserve will be used for frequency support services. This is unlike what is observed in wind farms and PV plants, where only 5-10% of the nominal capacity is available for this function [27]. Therefore, ESS increase the reliability of frequency regulation, as they can ensure that PV plants and wind farms work with variable irradiance and wind speed, respectively.

According to [28], various techniques were tested for energy storage systems associated to wind turbines. It was firstly proposed to coordinate the behaviour of a DFIG wind turbine with an ESS, and it has been verified that this has prevented frequency oscillations and frequency drop. In this situation, the ESS provides the active power required for speed recovery, preventing the secondary frequency drop, and behaving as a backup system which provides power during faults [28]. Secondly, [28] also discussed that primary frequency control should be used in wind power plants to maintain power reserve, through the support of a flywheel storage. In steady state, a central controller distributes the power reserve between the wind turbines and the flywheel storage system. The power reserve margin is determined by the wind speed range. In [28], it is too discussed that the DFIG wind turbine can use virtual inertia techniques to provide short-term frequency regulation through supercapacitors connected to the DC link of the DFIG wind turbine inverter via a DC-DC converter. It has been shown that these techniques both improve frequency stability. Even though the inertia provision through flywheels does not require additional components, its performance depends on the fluctuations of the wind speed [28]. As for supercapacitor's virtual inertia provision, this technique does not rely on wind speed, but requires more components (which can increase its cost and complexity) [28].

For photovoltaic energy, the supercapacitors can be used to absorb the differences between the active power generated by the PV array and the active power consumed [28]. In [28], it is shown that using PV systems with Lithium-Ion batteries has also allowed active and reactive power control in the network. The frequency regulation of a PV plant supported by ESS can be done by a P-Q-based droop control, which allows the regulation of the active and reactive power when the demand exceeds the solar generation. When the demand is lower than the solar generation, the inverter control regulates the active and reactive power according to setpoints. Therefore, the controller regulates the frequency according to the output power of the PV generator and the battery state-of-charge (SoC).

2.12 Final Remarks

The increasing presence of converter-interfaced generation in the power system has been reducing the system's inertia, which is creating a power system more vulnerable to fast frequency changes and higher frequency deviations. Therefore, this chapter's aim was to provide a literature review of possible solutions for reducing the negative impacts of RES in the electric power system. Adding inertia and primary frequency control were the solutions proposed for the mitigation of these problems.

In a system with reduced inertia, the RoCoF calculation is important, because this indicator gives information about islanding and disconnection of generators. It is also very important to choose an appropriate measurement window because higher measurement windows can hide some mechanical transients and lead to false RoCoF results. It was then understood that smaller measurement windows can result in more severe RoCoF values than larger measurement windows. To achieve secure system operation, the maximum RoCoF and its measurement window must be specified by each country's TSO.

Indeed, a detailed explanation of the currently available Grid Codes of the European synchronous area was done, with a focus on the non-exhaustive requirements for Portugal, following the available legislation. Since the Requirements for Generators provide some guidelines related to the virtual inertia provision, the strategies for providing virtual inertia to the electric power system were also addressed. Regarding virtual inertia, three different strategies for its implementation were described, being them the synchronverters, the Ise's Lab Topology, and the Droop-based approach. These descriptions were followed by an overview of power electronic interfaces and controls, where the differences between grid-forming and grid-following converters were discussed. In the end, a review of specific control strategies for wind and solar generation was conducted to explain how the active power/frequency control (or the Frequency Sensitive Modes) are implemented in the power electronic converters.

The described control strategies for wind and solar generation show they should either operate at the MPP or below the MPP (which is known as de-loaded operation). As these strategies allow the adjustment of the output active power, it is possible to state that wind and solar generation systems can participate in active power/frequency control. Then, the following step for this dissertation is the study of the simulation models of these new technologies, which are applied to a test system.

Chapter 3

Modelling a system with high shares of RES

In this chapter, the dynamic modelling of a system with high levels of wind and solar PV sources is discussed. This chapter presents the test system (the IEEE 39-Bus network) and the simulation platform (PSS/E) to be used to address the power system's stability problems in face of the increase in renewable energy generation connected to the grid through a power conversion stage. Then, the models related to the synchronous generators already present in the IEEE 39-Bus network will be addressed. Moreover, the generic models of the Western Electricity Coordinating Council (WECC) for converter-based renewable energy generation are also explained, as they are suitable for transmission system stability studies.

3.1 The IEEE 39-Bus network and the use of PSS/E

To study the problem in discussion, simulation platforms capable of reproducing the dynamic power system's behaviour in various situations (such as the loss of generation or short-circuits) and models that can represent each system's components are necessary. One of the tools available at a university level is PSS/E from Siemens. It was chosen given its ability to handle power networks with a relevant dimension, even in freely available versions. Moreover, existing test networks such as the IEEE 39-Bus network [29], which has been widely used for addressing power system dynamic performance under several situations, are available in this simulation platform.

For the next phase, the IEEE 39-Bus network [29] (also known as the New England test system) is used as a test system. This test system has been widely used as a benchmark system to address power system stability problems in multi-area systems. It is characterized as a two-area power grid, hence mimicking an Iberian-Central Europe interconnection.

In [6], the interconnection between the Iberian Peninsula and Central Europe is modelled, being each control area represented by a swing equation. The relationship between [6] and this dissertation is built because, similarly to the Iberian Peninsula, this work's Control Area 1 also has high inclusion of renewable energy generation and low synchronous generation, as well as few interconnections to Control Area 2, which compromises frequency stability. This system has 39 buses and 10 synchronous generators. Notably, the bus 39 contains the generator with the largest power rating, representing an external control area. Control area 1 is then formed by the remaining 9 generators, with smaller power ratings (for better familiarization with the test system, the tables in Appendix A show the data of the synchronous generators, transformers, and lines present in this network).

.

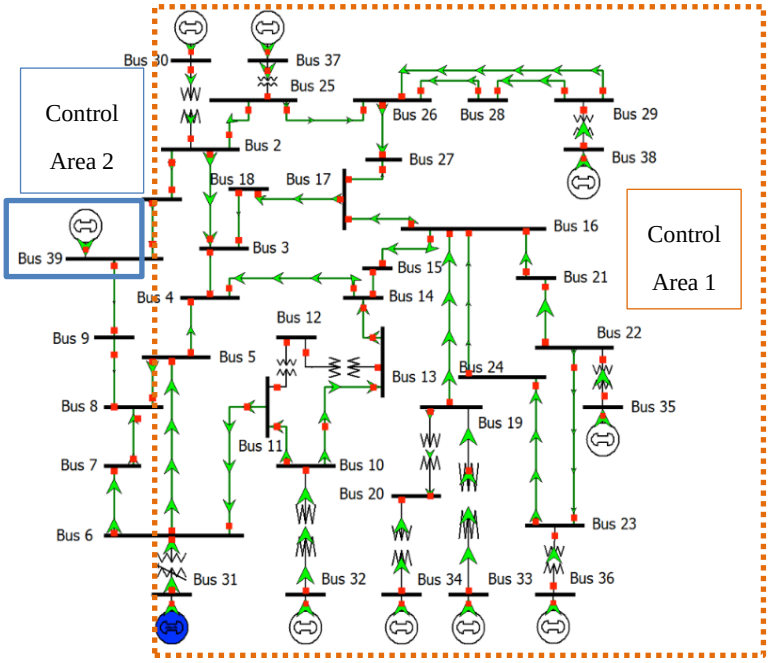

Figure 3.1: The IEEE 39-Bus network (source: [29]).

The following sections explain the dynamic models and the parametrization of conventional synchronous generation and of converter-interfaced generation. The adopted models are based on typical ones and are available on PSS/E's libraries.

3.2 Modelling Conventional Synchronous Generation

Since the IEEE 39-Bus system is originally defined as a network containing only synchronous generation and is already built on PSS/E, the dynamic models of the generators are then already defined. Within the scope of this dissertation, the conventional synchronous generation-based plant model includes the generator, the exciter, and the turbine governor.

Each generator is modelled by the GENROU model (Round Rotor Generator Model). It is important to clarify that, even though all the synchronous generators follow the GENROU dynamic model, their parameters' values are different for each generator. In Table 3.1, a description of the parameters used by the GENROU dynamic model is provided:

Table 3.1 - Parameters of the GENROU dynamic model for the synchronous machines.

Parameters	Description
T'do (<0) (sec)	Direct-axis open-circuit transient time constant
T"do (>0) (sec)	Direct-axis open-circuit sub-transient time constant
T'qo (>0) (sec)	Quadrature-axis open-circuit transient time constant
T"qo (>0) (sec)	Quadrature-axis open-circuit sub-transient time constant
H (p.u.)	Inertia constant
D (p.u.)	Speed damping
Xd (p.u.)	Direct-axis synchronous reactance
Xq (p.u.)	Quadrature-axis synchronous reactance
X'd (p.u.)	Direct-axis transient synchronous reactance
X'q (p.u.)	Quadrature-axis transient synchronous reactance
X"d=X"q (p.u.)	Direct-axis sub-transient synchronous reactance
XI (p.u.)	Leakage reactance of the stator of the generator
S (1.0)	Saturation factor for point 1.0
S (1.2)	Saturation factor for point 1.2

According to [30], the GENROU dynamic model of the synchronous machines considers two points of the typical generator open-circuit saturation curve, S (1.0) and S (1.2). The generator's open-circuit saturation curve (Figure 3.2) establishes the relationship between the field current (i.e., the DC excitation current) and the open-circuit voltage. It is verified that this curve has a linear zone, where more field current creates a higher open-circuit voltage, and a saturation zone, where the voltage reaches its limit value. The GENROU model assumes that the saturation curve is quadratic, and can be calculated using Equation 3.1, where E is the input and A and B are the points (1.0, $S_{1.0}$) and (1.2, $S_{1.2}$) on the saturation curve:

$$S = \frac{B(E-A)^2}{E} \tag{3.1}$$

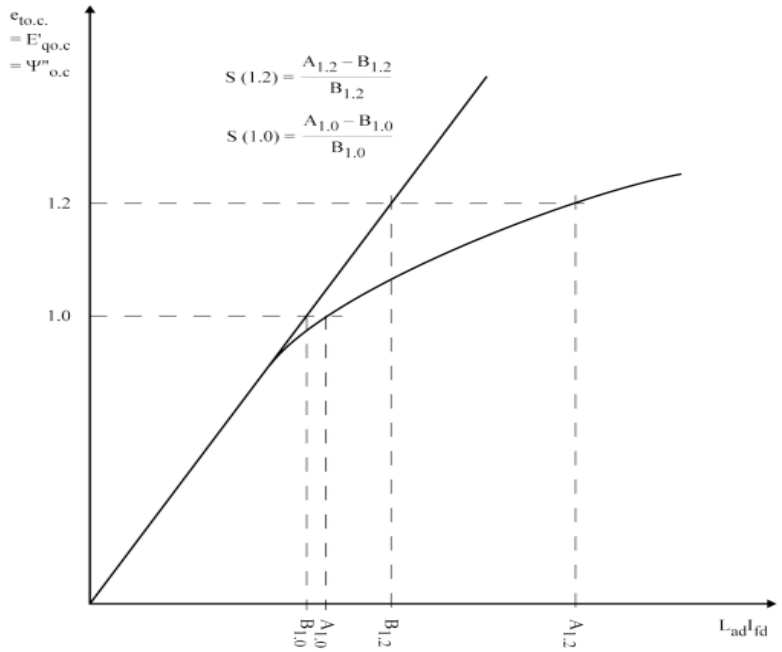

Figure 3.2: Typical saturation curve of a synchronous generator and calculation of the saturation factors (source: [30]).

In Appendix B, the parameters for each synchronous generator in the IEEE 39-Bus system are specified, as well as the parameters of the excitation system and the turbine governor. The parameters of the GENROU dynamic model (Appendix B.1) are all expressed in p.u. in the machine's base.

The exciter follows the SEXS model (Simplified Excitation System), and the turbine governor uses the TGOV1 model (the steam turbine-governor model, which is the simplest of the turbine-governors' models available in PSS/E's library). All the generators have the same parameters for the exciter and the turbine governor's model. In Figure 3.3, the block diagram of the excitation system (SEXS) is presented.

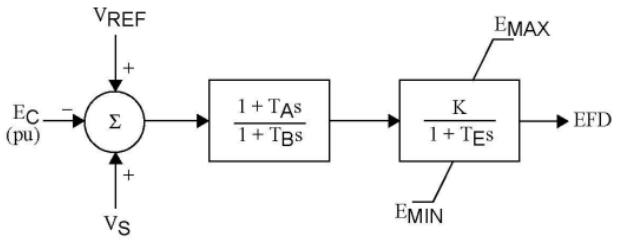

Figure 3.3 - Block diagram of the excitation system (SEXS) to be used on PSS/E (source: [31]).

The SEXS model calculates the difference between E_C, the measured voltage, and the voltage reference, V_{REF}. The voltage error signal is then processed and amplified (being T_A and T_B the time constants of the lead-lag block) for producing the voltage regulator output. The regulator is represented by the voltage regulator gain, K, and the voltage regulator time constant, T_E. The voltage regulator has operational limits, which are represented by the E_{MAX} and E_{MIN} parameters.

The turbine governor TGOV1 (which is represented on Figure 3.4) is a simple model representing the governor's action and the reheater time constant effect for a steam turbine. It has a speed-droop block, where R is known as the permanent droop. The most important parameter to control is the position of the valves, which allow the steam to flow: T_1 models the governor's time constant, T_3 models the reheater's time constant, and $\frac{T_2}{T_3}$ models the fraction of the total turbine power generated by the high-pressure section. D_t is the turbine damping factor, which is the derivative of the power produced by the turbine in relation to the turbine speed. It can be taken as zero for steam, nuclear, and gas turbines. V_{MAX} is the maximum limit of the speed governor control loop. As for V_{MIN}, it is the minimum limit of the speed governor control loop, at it should be higher than zero.

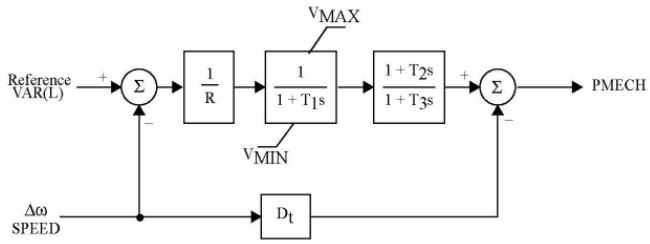

Figure 3.4 - Block diagram of the turbine governor (TGOV1) used on PSS/E (source: [31]).

3.3 General Simulation Models for Wind and Solar Generation

In [32], WECC (Western Electricity Coordinating Council) defines generic models for wind power plants, which are intended to be used for general large system planning studies and evolve based on industry experience and technology evolution. According to [32], for types 3 (DFIG) and 4 (Full Size Frequency Converter) WTGs' models were significantly improved in terms of structure and functionality. Particularly, the dynamic simulations to be performed in this work use type 4 models, as the full converter topology allows the decoupling between the network and the power electronic converter. The main models to be used for dynamic simulations can then be characterized in the following way:

- **REGC_A:** it is used to represent the generator/converter. Its inputs are the active and reactive current (I_{pcmd} and I_{qcmd}, respectively) and its outputs are the real (I_p) and reactive current (I_q) injected into the grid [33].
- **REEC_A:** it represents the electrical controls of the WTGs (i.e., the renewable energy electrical controls model a [33]), acting on the active and reactive power reference of the REPC_A module, with feedback of terminal voltage and generator power output. It then provides active and reactive current commands to the REGC_A module [32]. Its inputs are then P_{ref} (active power reference) and Q_{ref} (reactive power reference), being the outputs the real and reactive current commands (I_{pcmd} and I_{qcmd}) [33].
- **REPC_A:** it represents the plant controller (in this case, it is, according to [33], the renewable energy plant controller model a). It processes voltage and reactive power output to emulate volt/var control at the plant level, while also processing frequency and active power output to create the active power control. It provides active/reactive power commands to the REEC_A module [33]. Therefore, its inputs are V_{ref} and the measured/regulated voltage (V_{reg}) at the plant level, or Q_{ref} and measured Q_{gen} (reactive power generated) at the plant level [33]. Its output is then the reactive power command connecting Q_{ref} to the REEC_A model [33]. This model can provide "primary frequency response based on the measured total plant real power output at the point of common coupling and measured system frequency" [33].

On PSS/E, the renewable energy generators are modelled using the REGCA1 model, which stands for the Renewable Energy Generator Model. The Electrical Model is the REECA1 model, and the REPCA1 is the Auxiliary Control Model. These models define the behaviour of converter-interfaced generation connected to the grid. These models are generic, meaning that they can represent either a wind farm or a solar power plant. Unlike synchronous machines, power electronic converters decouple frequency and mechanical power, which is why the mechanical models for RES are not specified.

On PSS/E, the models have not only constant parameters (CONs), but also VAR and ICON parameters. The VAR parameters are calculated by PSS/E after a dynamic simulation is performed, based on the voltage and reactive power references provided to the program. On the other hand, the ICON parameters set which control modes of the converter should be activated. For example, in the REECA1 model, the control modes are related to the power factor control, voltage control, active and reactive power control, as required in the Grid Codes.

The REGCA1 model controls the active current so that the generator can survive voltage dips, and the reactive current to prevent over-voltages [20]. According to [20], the active current to be injected into the grid is set according to the grid voltage, V_{grid}, and by the value of the reference active current (which will be given by the electrical model, REECA1). This type of control then reduces the active current in the presence of a fault and recovers the active power to its pre-fault levels [20]. This is according to what has been described in the Grid Codes and in [20], where it is stated that the generator should have fault ride-through capabilities, as well as the capacity for recovering 95 % of its pre-fault active power in less than 1 second, having 2 additional seconds for total recovery.

To obtain the desired behaviour for the active and reactive power injected by the power electronics converters (as well as the voltage and the active and reactive current injected by them), the parametrization used for the REGCA1 model of PSS/E's library was the same as the one described in [34]. In [34], the REGCA1 model is parametrized so that the inverter complies with the requirements set by REE ("Red Eléctrica de España"). The results shown in [34] compare the active power, reactive power, and voltage results using the REGCA1 model on PSS/E and the results of a real inverter's response. It was then shown that the parametrization of the REGCA1 model was accurate, given the similarities between the two cases, which then justifies its use in this dissertation. The only differences between the parametrization used in [34] and the parametrization used in this work is the value of the converter time constant and the *Zerox* parameter: it was chosen to have a time constant equal to 0.05 seconds and a *Zerox* parameter equal to 0.6 p.u. so that the converter recovered its initial active power values more gradually.

The Electrical Model, REECA1 (the Generic Renewable Electrical Control Model), regulates the active and reactive current injected and the setting of its minimum and maximum limits. This is done by regulating the injected active and reactive powers, according to its reference values and the grid voltage [20]. As for the Auxiliary Control Model, the REPCA1 controls the reference powers for a wind park or a solar power plant. The reactive power control is done through the constant voltage control at the PCC (Point of Common Coupling), or constant reactive power in the substation's transformer [20]. On the other hand, the active power control is done according to the system's frequency, hence modelling the frequency sensitive modes defined in the grid codes [20].

3.4 Modelling Battery Energy Storage Systems

In this work, Battery Energy Storage Systems (BESS) are modelled by the REGCA1, REECCU1, and the REPCA1 models. According to [31], the REECCU1 model stands for the "Electrical Control Model for Utility Scale Battery Energy Storage". The REECCU1 model has two main control modes, being them the voltage and the power factor control. This model also controls the State-of-Charge (SoC) of the battery: if the initial battery SoC is equal to 1 p.u., it means that the battery is fully charged; if it is 0 p.u., it means that the battery is fully discharged. However, the maximum SoC may be set to 80% to represent specific manufacturing requirements [31].

3.5 Modelling Synchronous Condensers

Synchronous condensers are synchronous machines containing a voltage regulator but lacking a turbine. Therefore, any synchronous machine to be replaced by a renewable energy generator can be taken as a candidate for the operation as a synchronous condenser, provided the TGOV1 model is disabled, and the active and reactive power generated are set to 0. Hence, the synchronous condensers will solely be represented by the GENROU model for the synchronous generator and by the SEXS model for the excitation system (both parametrized as in Appendix B.2 and Appendix B.3, respectively).

3.6 Final Remarks

This chapter described the IEEE 39-bus system and has also described the models used for synchronous machines and renewable energy sources. For the renewable energy generators, generic models were used, because they are standard models representing both wind and solar generation and are publicly available. They are suitable for stability simulations of large, interconnected power systems [31], which is the case of the IEEE 39-bus system. The descriptions of these models serve as an introduction for the next chapters, which use this information to perform dynamic simulations both containing only synchronous machines and converter-based generation.

Chapter 4

Dynamics in a conventional power system

In the previous chapter, the IEEE 39-Bus system was defined, as well as the models for synchronous generation and renewable energy generation available on PSS/E. In this chapter, the first dynamic simulations will be performed in the above-described system, considering only the presence of synchronous generation. The methodology for performing these dynamic simulations is described. Notably, this chapter aims to assess the behaviour of the power system facing multiple line faults to understand the influence of the location of the disturbance in the key frequency indicators – the Nadir and the RoCoF (Rate-of-change-of-frequency).

4.1 The RoCoF calculation and the frequency of the centre of inertia

The frequency stability of this system and the severity of the encountered faults will be evaluated based on key frequency indicators, which are the nadir and the RoCoF. As defined in section 2.4, the RoCoF is the same as the frequency variation in each time frame. In Continental Europe, according to the ENTSO-E, the RoCoF should be calculated every 500 milliseconds, being this the most used measurement window [35]. However, given the fast phenomena introduced by renewable energy generation and the already described impact of the sliding window in the RoCoF measurements, it is important to also consider other sliding windows such as 250 milliseconds and 100 milliseconds. It is also important to consider the absolute values of the frequency changes in Hz/s, being the highest RoCoF experienced the one assigned to a given disturbance.

In Chapter 3 (section 3.1), when describing the test system, it was defined that the network had two control areas: the first control area consists of generators 1 to 9, and the second one consists of the generator 10, as it is the largest synchronous generator. Since the first control area has more than one synchronous generator with different characteristics, the value of the frequency of the centre of inertia should be used for this area, as it is a good approximation of the system's frequency. Indeed, the RoCoF indicator is calculated regarding the system centre of inertia, making it possible to neglect local frequency oscillations [11]. Equation 4.1 expresses how to calculate the frequency of the centre of inertia, setting an apparent power base, S_b, of 100 MVA.

$$f_{system} = \frac{\sum_{i=1}^{N} H_i \omega_i}{\sum_{i=1}^{N} H_i} f_N \tag{4.1}$$

In Equation 4.1, f_{system} is the equivalent frequency of the centre of inertia, H_i is the constant of inertia of each synchronous generator, ω_i is the rotor speed of each generator (in p.u.), and f_N is the nominal system frequency, which is 50 Hz on PSS/E. To perform this calculation, H_i, which is originally in p.u. in the machine's power base ($S_{machine}$), should be converted to the system's power base of 100 MVA. This is done by Equation 4.2, being the results present in Table 4.1:

$$H(p.u.S_b) = H(p.u.S_{machine}) * \frac{S_{machine}}{S_b} \tag{4.2}$$

Table 4.1: Conversion of the inertia constants for the machines in service in Control Area 1.

Bus Number	Machine	H (Smachine)	$S_{machine}$ (MVA)	H (system)
30	G1	4.2	1000	42
31	G2	4.329	700	30.303
32	G3	4.475	800	35.8
33	G4	3.575	800	28.6
34	G5	1.625	800	13
35	G6	4.35	800	34.8
36	G7	3.771	700	26.397
37	G8	3.471	700	24.297
38	G9	3.45	1000	34.5

With these aspects in consideration, it is possible to extract the data from PSS/E and have the first results for the power system containing only synchronous generation. To calculate the frequency deviations for each machine, it is required to extract the rotor speeds of the synchronous generators from PSS/E, which are expressed in p.u. So, to convert them to frequency, it is necessary to multiply each value by 50 Hz (the system's frequency base).

The next sections present the initial studies regarding the system dynamic performance, considering system simulations in different circumstances.

4.2 Power flow calculation

The first step to perform a dynamic simulation is to define the steady state operational conditions of the system by means of power flow studies. The results of the power flow calculation present in Table 4.2 allow the calculation of the total active power generated and consumed, as well as the losses. Therefore, the total active power generated is 6254.79 MW and the total active power consumed is 6124.5 MW. Therefore, the losses are equal to 130.29 MW.

Table 4.2: Results of the power flow calculation with the dispatch adjustments.

Bus Number	PGen (MW)	PMax (MW)	PMin (MW)	QGen (Mvar)	QMax (Mvar)	QMin (Mvar)	Voltage (p.u.)
30	319	843.9999	309	265.0	538	-184.1	1.048
31	277.8	591	216	117.0	377	-128.9	0.982
32	390	675	247	239.8	431	-147.3	0.983
33	390	675	247	106.0	431	-147.3	0.997
34	390	675	247	160.0	431	-147.0	1.012
35	390	675	247	181.8	431	-147.3	1.049
36	300	591	216	72.3	377	-128.9	1.064
37	390	591	216	165.9	377	-128.9	1.028
38	310	843.9999	309	25.3	538	-184.1	1.027
39	3098	8442	3088	709.3	5382	-1841.4	1.03

After the power flow calculation, performing a dynamic simulation on PSS/E requires, in this order, the conversion of the loads and the generators, factorizing the admittance matrix, finding a solution for switching studies, and defining the output channels. Particularly, when performing dynamic simulations, it is important to understand how loads are converted, as various types of loads are possible, such as constant impedance loads and constant power loads.

Type power loads are those in which the product between voltage and current remains constant. On the other hand, type impedance loads are those in which the voltage/current ratio remains constant. When performing dynamic simulations, it is not advised to convert the loads to constant power loads, as it provides the most pessimistic RoCoF results and may create unstable cases. Such is confirmed in [36], where the effect of load modelling on power system stability is studied using the IEEE 39-bus system as a test network. This happens because, when a fault (such as a short-circuit) is applied, to ensure that the power remains constant, the current increases, which further decreases the voltage, leading to convergence problems. In addition to creating convergence problems, loads modelled as constant power loads require a set of parameters that are not easily available. Instead, constant impedance load models are preferred for stability studies.

According to [37], type impedance loads are converted adopting the constant admittance method, which considers that the loads can be converted into equivalent impedances. Indeed, for each bus *i* containing a load, the impedance is calculated as expressed by Equation 4.3:

$$Y_{load} = -\frac{P_{load,i} - jQ_{load,i}}{V_i^2} \quad (4.3)$$

Therefore, for the dynamic simulations performed in this work, it was selected on PSS/E the option "100% constant admittance loads". Before describing the performed dynamic simulations, it is also important to understand the security criteria for a power system. According to [38], the security actions to ensure the system's security can be listed in the following way:

1. If $\Delta f < -0.5\ Hz$, the shedding of pumping units occurs.
2. If $\Delta f < -1\ Hz$, there is the load shedding with a 500-millisecond delay.
3. If $\Delta f < -1.5\ Hz$, the load shedding with a 150-millisecond delay occurs.
4. If $\Delta f < -2.5\ Hz$, the frequency tripping of generation units starts.

4.3 Scenarios for performing line faults in the IEEE 39-Bus System

The events creating more risks for the frequency stability of a power system are the loss of transmission lines, the occurrence of a short-circuit followed by the loss of a transmission line, the loss of an interconnection (leading to the loss of the injected active power in one control area occurs) and the loss of the largest generator online. This dissertation aims to provide solutions for frequency problems related to the short-circuit followed by the loss of transmission lines, which is among the most extreme events.

Aiming to find the worst locations for the faults, the same simulation scenario was defined considering faults in several lines and that they put the line out of service. All these simulations are performed with a simulation step of 1 millisecond.

For faults causing the tripping of the lines, the following case was simulated:

1. At t=5 seconds, a short-circuit occurs in the beginning of the line close to one of the connection buses.
2. The bus fault runs for 150 milliseconds.
3. At t=5.15 seconds, the line is out of service and the fault is cleared.
4. The simulation runs for 30 seconds in total.

By evaluating these faults, it is possible to understand which location creates the highest RoCoF and the lowest nadir. In the following chapter, the results presented in this scenario are compared to those of the different scenarios of renewable energy integration.

4.4 Results and observations

After performing dynamic simulations in the power system containing only synchronous machines, the obtained nadir and RoCoF results with three different measurement windows are organised on Tables 4.3 and 4.4. For the RoCoF calculation, it was necessary to calculate the frequency of the centre of inertia, which is shown in Figure 4.1 (considering that a fault has occurred in line 5-6, and that this line was set out of service).

Table 4.3: Nadir results for different line faults in a scenario containing only synchronous generation.

	Control Area 1	Control Area 2
Line	**Nadir 1**	**Nadir 2**
5-6	49.89	49.95
13-14	49.89	49.96
21-22	49.87	49.96
2-25	49.91	49.96
16-17	49.82	49.94

Table 4.4: RoCoF results for different line faults in a scenario containing only synchronous generation.

	RoCoF for Control Area 1 (Hz/s)			RoCoF for Control Area 2		
Line	**500 ms**	**250 ms**	**100 ms**	**500 ms**	**250 ms**	**100 ms**
5-6	0.309	0.815	1.363	0.24	0.438	0.678
13-4	0.366	0.821	1.432	0.24	0.3789	0.549
21-22	0.453	1.03	1.84	0.229	0.276	0.337
2-25	0.287	0.723	1.178	0.267	0.475	0.724
16-17	0.646	1.31	2.34	0.315	0.404	0.524

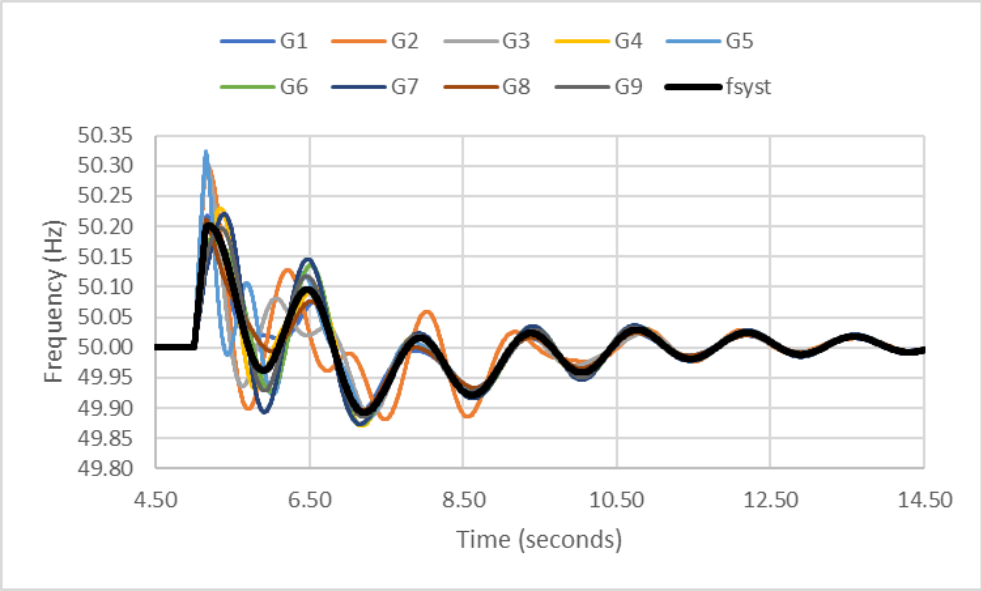

Figure 4.1- Frequency in Control Area 1 after the fault in Line 5-6.

According to Table 4.3, none of the disturbances provoked a nadir less than 49.8 Hz, which means that the activation of the Limited Frequency Sensitive Modes – Underfrequency (LFSM-U) was not required. As the nadir values are high, no action needs to be performed to ensure this power system's security. According to [38], the under-frequency load-shedding only happens when there is insufficient generation to increase the active power output, being the frequency decline determined by the frequency sensitive characteristics of the load. Since this is not the case, the power system remains secure.

Moreover, the RoCoF results in Control Area 1 remained lower than 1 Hz/s, which is another reason why this system is not at risk. The considered faults practically did not affect Control Area 2 either. Yet, the faults are more severe in Control Area 1 than in Control Area 2, which was to be expected given the high inertia in generator G10.

When a fault occurs in line 5-6 and this line is set out of service, none of the generation units lose synchronism, thus recovering its nominal frequency values. The oscillations become increasingly more damped, being the generator G2 the one experiencing the lowest frequency values after the line is set out of service. This happens because this generator is the one closest to the fault, as line 5-6 connects the rest of the network to generator G2. On the other hand, generators G1 and G3 produce more power at the time of the fault, which can be seen by the increase of their frequency values at the time of the fault. These generators are also closer to the zone where the fault occurs, thus having a more prominent role in arresting the frequency changes.

The behaviour of the frequency of the centre of inertia when the line 13-14 is set out of service is very similar to the frequency behaviour in the previous case, as both lines are in the same zone. Indeed, generator G2 is the generator directly affected by the fault, but generators G3 and G5 are the ones that are closer to this line, thus contributing more to arrest the frequency variations. Then, the generation units do not lose synchronism and its frequency returns to the nominal values. In comparison to the previous case, this fault does not lead to significantly different RoCoF and nadir results since these lines are closely located. Therefore, the loss of either line does not represent a large threat to this power system's security.

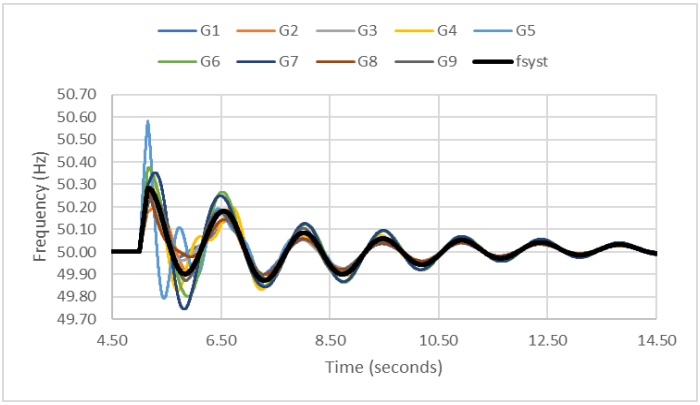

Figure 4.2: Frequency in Control Area 1 after the fault in Line 21-22.

When a fault occurs in line 21-22 and this line is lost (Figure 4.2), the more affected generators are generators G5, G6, and G7, as they are closest to the fault. However, the generators do not lose synchronism and the frequency value goes back to nominal, meaning that no external control actions needed to be performed to damp the frequency oscillations. In terms of RoCoF levels, this fault was more severe than when the lines 5-6 and 13-14 were lost. This may happen because bus 21 has active and reactive power consumptions, making it more vulnerable to perturbations. However, no RoCoF or nadir limits were violated, which means that the system returned to stability on its own.

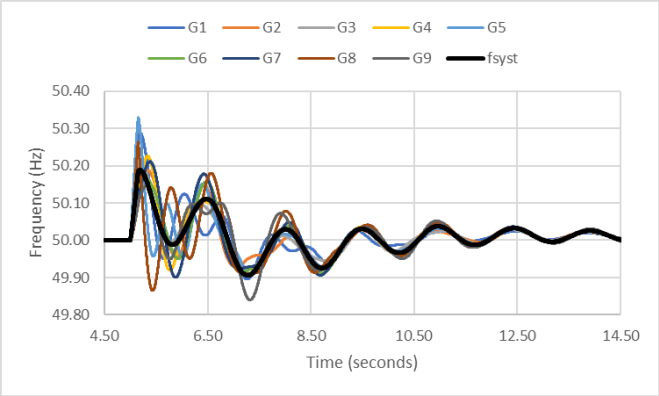

Figure 4.3: Frequency in Control Area 1 after the fault in Line 2-25.

The line 2-25 is the only line connecting bus 2 to bus 25 (Figure 4.3), which was the reason for choosing this location for the fault. In this situation, it is generator G8 the one suffering more frequency changes, because it is located at bus 37 (which is directly connected to bus 25). However, losing this line does not cause the loss of synchronism and the frequency returns to its nominal values. The RoCoF and nadir results for this perturbation show that it is not as severe as the loss of the line 21-22, therefore not violating the RoCoF limits and not needing additional control actions.

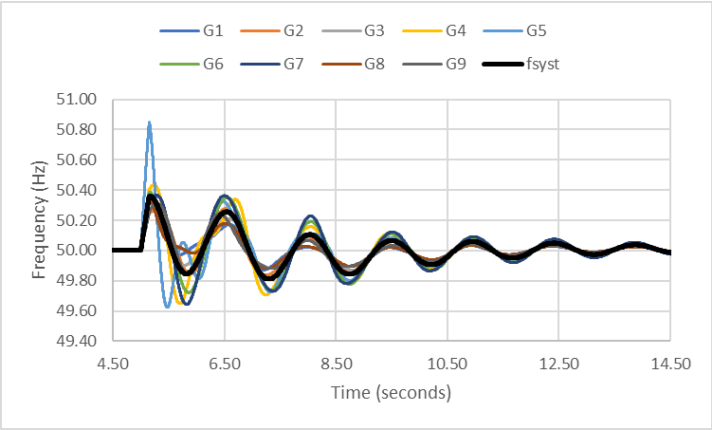

Figure 4.4: Frequency in Control Area 1 after the fault in Line 16-17.

The loss of the line 16-17 (Figure 4.4) causes higher frequency deviations in the generator G1 and G7. However, this fault did not provoke the loss of synchronism in the generation units and the system returned to its nominal values at the end of the simulation time.

4.5 Final Remarks

In this chapter, short-circuits in some lines that were cleared by setting the line out of services were tested in the IEEE 39-bus system. In all the situations, these disturbances were more severe in Control Area 1 than in Control Area 2, as the second consists of a large generator with the highest inertia. However, the low RoCoF and high nadir shown in these circumstances demonstrate that the IEEE 39-Bus network is a large and resilient power system.

The analysis presented in this chapter serves as a term of comparison for Chapter 5, where renewable energy generation will be progressively integrated in this power system. Chapter 5 will then describe the scenarios leading to the worst nadir and RoCoF results, proving the problems introduced by systems with reduced inertia.

Chapter 5

Integrating Renewable Energy Generation

After having tested some disturbances in the IEEE 39-Bus system, this chapter assumes the need of building renewable energy integration scenarios over the existing test system to characterize the resulting impacts in terms of key frequency indicators. Hence, it is assumed that the synchronous machines are progressively replaced by converter-based renewable energy generation, using the models explained in Chapter 3. The RoCoF and nadir values will be calculated for the reference disturbances previously taken in consideration in Chapter 4. The aim of this chapter is to find a scenario with low synchronous inertia in operation, which will be studied in this chapter and serve as a base case for Chapter 6, where the solutions for systems with reduced inertia will be tested.

5.1 Renewable energy integration scenarios

In this section, each synchronous machine will be replaced by a renewable energy generator with equivalent capacity until reaching a scenario with low synchronous inertia in the power system. This will be done to assess system dynamic behaviour in scenarios with reduced inertia.

Table 5.1 shows how renewable energy was progressively integrated in this power system. The 4th scenario is identical to the 3rd, except that it considers a 50% reduction in the inertia constant of each remaining synchronous generation. However, the 5th scenario was chosen to be analysed in this chapter, as it integrates more renewable energy (7 power electronic converters with a reduction of 25% of the inertia constant of the remaining synchronous machines) and leads to the most challenging situation regarding frequency stability.

Table 5.1: Renewable energy integration scenarios.

Scenario	Replaced Generators	Converters	Location (Buses)	Hsystem (s)	Additional inertia reduction
Base Case	-	-	-	233.897	-
2	G1, G3, G7, G8	C1, C2, C7, C8	30, 32, 36, 37	156.703	-
3	G1, G3, G5, G6, G7, G8	C1, C2, C5, C6, C7, C8	30, 32, 34, 35, 36, 37	108.903	-
4	G1, G3, G5, G6, G7, G8	C1, C2, C5, C6, C7, C8	30, 32, 34, 35, 36, 37	54.67	-50%
5	G1, G3, G4, G5, G6, G7, G8	C1, C2, C4, C5, C6, C7, C8	30, 32, 33, 34, 35, 36, 37	48.625	-25%

Each power electronic converter should inject the same active and reactive power as the one injected by the synchronous machine. The active and reactive power injected by the converters will then be equal to electric power required by each thermal unit, which was an assumption also made in [20].

Table 5.2: Active and reactive power injected by the converters.

Replaced generator	Converter	Bus number	Sn (MVA)	Pgen (MW)	Qgen (Mvar)
G1	C1	30	1000	319	265.024
G3	C2	32	800	390	240
G4	C4	33	800	390	106
G5	C5	34	800	390	160
G6	C6	35	800	390	181.84
G7	C7	36	700	300	72.26
G8	C8	37	700	390	165.94
G9	C9	38	1000	390	25.31

With this information, it is possible to simulate and quantify the impact resulting from the disturbances defined in section 4.4, being these aspects described in the following sections.

5.2 Power flow solution for the scenario with the lowest inertia

As seen previously, the first step for performing a dynamic simulation is to calculate the power flows. Table 5.3 presents the results of the generation dispatch for the 5th scenario (the scenario where the lowest inertia constant was achieved).

Table 5.3: Generation dispatch for scenario 5.

Generator	Bus	PGen (MW)	PMax (MW)	PMin (MW)	QGen (Mvar)	QMax (Mvar)	QMin (Mvar)
C1	30	319	843.9999	309	272.4	538	-184.1
G2	31	381.5	591	216	131.6	377	-128.9
C2	32	390	675	247	251.2	431	-147.3
C3	33	390	675	247	113.8	431	-147.3
C5	34	300	675	247	161.8	431	-147.0
C6	35	300	675	247	183.1	431	-147.3
C7	36	300	591	216	75.3	377	-128.9
C8	37	390	591	216	169.4	377	-128.9
G9	38	390	843.9999	309	27.7	538	-184.1
G10	39	3098	8442	3088	717.2	5382	-1841.4

This power flow solution will remain the same even when more equipment is integrated in Chapter 6, to ensure that the system will have the same initial conditions. This will guarantee that coherence between simulations is achieved (thus facilitating the comparison between the efficacy of different solutions).

5.3 Loss of lines with increasing renewable energy integration

In this section, the behaviour of the network after the loss of the lines presented in Chapter 4 was evaluated under a low inertia scenario. Table 5.4 and Table 5.5 show the results of the nadir and the RoCoF for sliding windows of 500, 250, and 100 milliseconds, respectively.

Table 5.4: RoCoF results for the different renewable energy integration scenarios.

		RoCoF for Control Area 1 (Hz/s)			RoCoF for Control Area 2 (Hz/s)		
Scenario	**Line**	**500 ms**	**250 ms**	**100 ms**	**500 ms**	**250 ms**	**100 ms**
Base Case	5-6	0.3088	0.815	1.363	0.24	0.438	0.678
	13-14	0.366	0.821	1.432	0.24	0.3789	0.549
	21-22	0.453	1.03	1.84	0.229	0.276	0.337
	2-25	0.287	0.723	1.178	0.267	0.475	0.724
	16-17	0.646	1.31	2.34	0.315	0.404	0.524
5	5-6	1.32	2.42	2.68	0.315	0.55	0.823
	13-14	1.36	2.23	2.52	0.294	0.492	0.714
	21-22	1.33	1.77	2.33	0.228	0.374	0.527
	2-25	1.59	1.77	2.27	0.352	0.57	0.832
	16-17	1.048	2.01	2.955	0.348	0.511	0.696

Table 5.5: Nadir results for the different renewable energy integration scenarios.

		Control Area 1	Control Area 2
Scenario	**Lines**	**Nadir 1**	**Nadir 2**
Base case	5-6	49.89	49.95
	13-14	49.89	49.96
	21-22	49.87	49.96
	2-25	49.91	49.96
	16-17	49.82	49.94
5	5-6	49.67	49.86
	13-14	49.74	49.91
	21-22	49.76	49.91
	2-25	49.73	49.88
	16-17	49.78	49.91

Table 5.4 and Table 5.5 show that, with a network containing only synchronous generation, the nadir is high and the RoCoF is generally low in every sliding window. This demonstrates that the system is secure because it has high inertia. The fault occurrence having the worst nadir and RoCoF values is line 2-25, as it is near the interconnections between the two control areas (which are weak spots in the grid due to the low number of lines connecting the two control areas). When there is only synchronous generation connected to the system, these values do not pose threats to the power system security, but, in scenario 5, the fault in line 5-6 was the one showing the largest RoCoF in all the sliding windows, as well as the lowest nadir. Therefore, the results for this fault location are taken for more detailed analysis. Such analysis is present from Figure 5.1 to Figure 5.4.

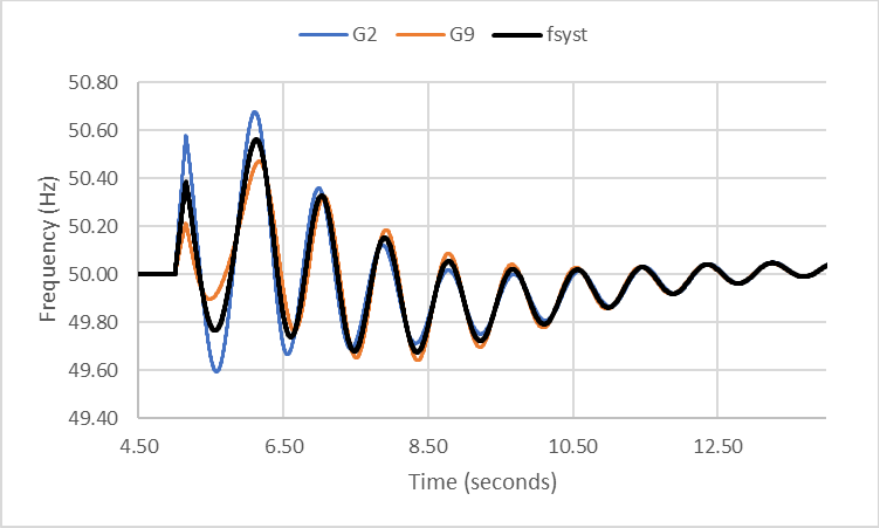

Figure 5.1: Frequency of the centre of inertia during the fault in line 5-6 in Control Area 1.

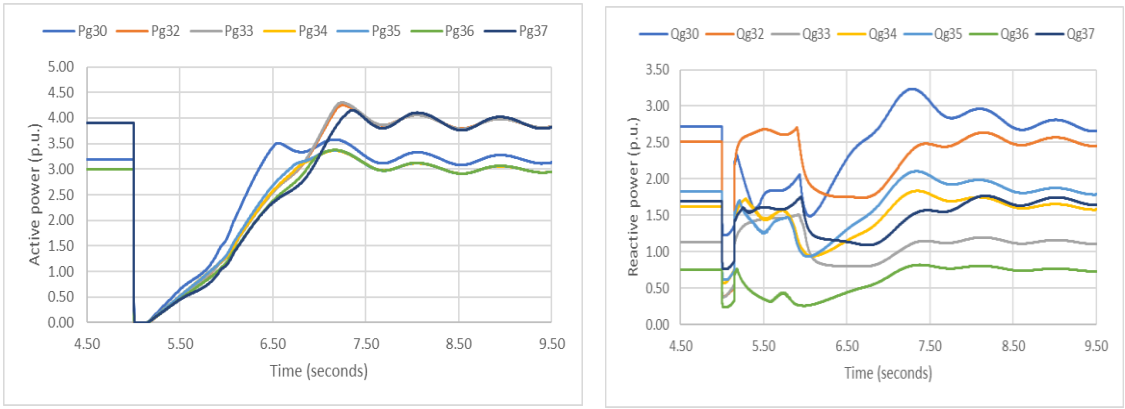

(a) **(b)**

Figure 5.2: Active (a) and reactive (b) power injected by the renewable energy sources in the power system during the fault in line 5-6.

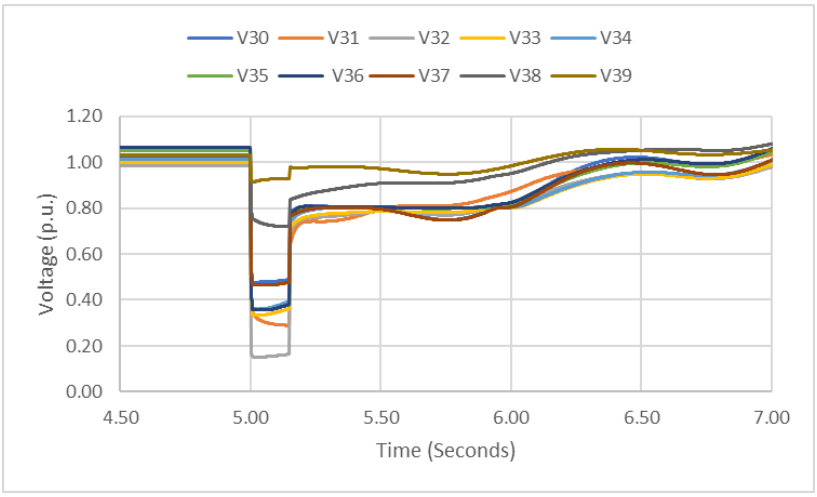

Figure 5.3: Voltage in all the generation buses of the power system during the fault in line 5-6.

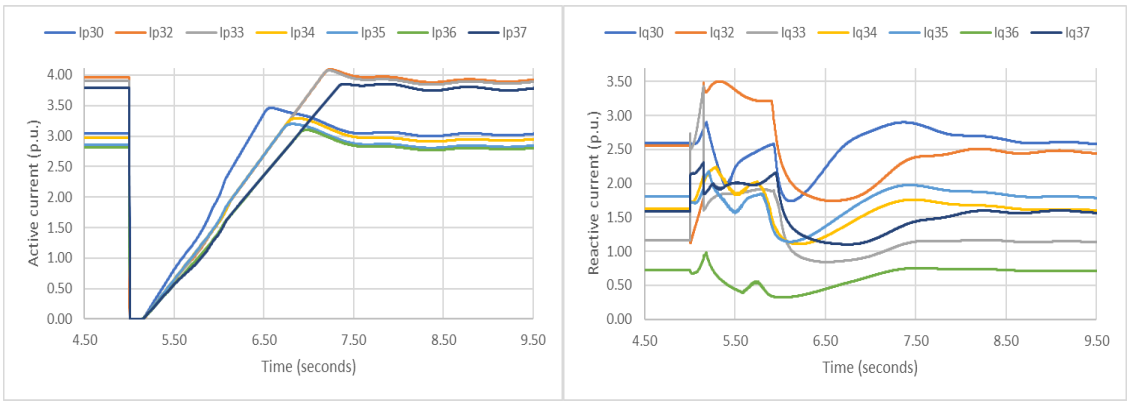

(a) **(b)**

Figure 5.4: Active (a) and reactive (b) current injected by the renewable energy sources in the power system during the fault in line 5-6.

During the short-circuit, given the current limit of the power electronic converters, the active power injected temporarily drops to zero. Then, it is given priority to the injection of reactive current (Figure 5.4 – b). When the fault is cleared and the voltage recovers, the active power starts recovering progressively, exhibiting a ramp behaviour. Such behaviour affects the balance between generation and demand after the fault. Consequently, this influences the frequency behaviour. Therefore, Figure 5.2 and Figure 5.4 show that renewable energy generation performs as expected regarding Fault Ride-Through requirements.

In scenario 5, the RoCoF has increased greatly, given the reduced synchronous inertia in the power system. Particularly, the RoCoF values in Control Area 1 were located close to the limits stated in the Grid Codes. However, the nadir was lower than in the base case, but no pump-shedding occurred, as it remained higher than 49.5 Hz. As the nadir was not close to 49.2 Hz, this shows that obtaining such low nadir requires even more severe frequency events than the loss of one transmission line. This hints that the RoCoF is an indicator more sensitive to changes in the power system than the nadir. Indeed, in [39], the impacts of reduced inertia in power systems were studied using the real data of Sardinia Island, Italy, where there is a large presence of renewable energy sources. For under-frequency events, this study found that, in a 50% reduced inertia scenario, the frequency nadir changed to 49.38 Hz, and the RoCoF to 1.07 Hz/s, being the worst frequency indicators also obtained with the lowest inertia scenario [39]. Moreover, the study presented in [6] also shows that, in the simulations performed in the Iberian system, the frequency nadir does not surpass the limit defined by European regulations, whereas the encountered RoCoF values were higher than 1 Hz/s, possibly resulting in frequency instabilities. Then, the results found in this chapter are coherent with the reality of some power systems.

5.4 Final Remarks

Since the IEEE 39-bus system is a highly robust network, several modifications were needed to create a scenario for analysing the frequency problems created by a system with reduced inertia. The progressive replacement of synchronous machines by renewable energy generation was considered until reaching scenario 5, where the inertia had an 83% reduction relatively to the base case. The observed RoCoF and nadir results for Scenario 5 were coherent with the results obtained for similar frequency events in real power systems. The key frequency indicators show a high RoCoF, exposing the need for the introduction of solutions for the mitigation of possible frequency problems. Given some countries already have set a limit of +/-1 Hz/s in the RoCoF relays, the encountered RoCoF results must be improved. In the next chapter, solutions such as fast active-power frequency reserves, synchronous condensers, and battery energy storage systems are tested.

Chapter 6

Solutions for systems with reduced inertia

The aim of this chapter is to take the 5th scenario presented in Chapter 5 as a reference case to test and compare the effectiveness of different solutions for improving the key frequency indicators. The main intent of both this chapter and this dissertation is to analyse the technological possibilities for solving frequency stability problems, while also understanding the influence of the location and sizing of the different solutions on the key frequency indicators. Therefore, the possibility of having active power-frequency regulation performed by the RES (Renewable Energy Sources), the use of BESS (battery energy storage systems) and the use of synchronous condensers (SCs) will be analysed. To better generalize the claims, the solution scenarios will be tested for some of the fault locations described in Chapter 4.

6.1 The location of the tested solutions

For each solution for improving the frequency stability of the power system, the scenarios considering the most relevant locations were built as follows:

- Active power-frequency response from the RES: this solution is placed in each generation unit, being it represented by the REPCA1 model according to Chapter 3.
- Synchronous condensers can either be installed close to the RES, close to the existing synchronous machines or close to buses with high loads.
- Battery energy storage systems: they were installed either close to the RES or close to the existing synchronous machines.

The following sections in this chapter then show the results obtained after these tests.

6.2 Active power-frequency response by the RES

The active-power frequency response represented by the REPCA1 model essentially is an implementation of the "Frequency Sensitive Modes" (FSM) presented in the Grid Codes. Tables 6.1 and 6.2 show the results of the key frequency indicators for the 5th scenario of renewable energy integration assuming the renewable energy sources participation in active power-frequency control with a speed-droop equal to 6%, as advised by the Grid Codes, and a power reserve margin of 1 %.

Table 6.1: RoCoF results for the RES incorporating active power-frequency response.

		RoCoF for Control Area 1 (Hz/s)			**RoCoF for Control Area 2 (Hz/s)**		
Scenario	**Line**	**500 ms**	**250 ms**	**100 ms**	**500 ms**	**250 ms**	**100 ms**
5	5-6	1.33	2.43	2.68	0.315	0.547	0.823
	13-14	1.36	2.236	2.52	0.293	0.492	0.715
	21-22	1.33	1.8	2.33	0.22	0.374	0.522
	2-25	1.588	1.77	2.266	0.352	0.57	0.832
	16-17	1.048	2.034	2.96	0.348	0.511	0.696

Table 6.2: Nadir results for the RES incorporating active power-frequency response.

Scenario	**Fault type**	**Nadir 1**	**Nadir 2**
5	Line 5-6	49.63	49.864
	Line 13-14	49.71	49.92
	Line 21-22	49.73	49.92
	Line 2-25	49.72	49.85
	Line 16-17	49.76	49.91

These results are not significantly different from the results obtained in the 5th renewable energy integration scenario without active-power frequency control. This can be due to the low power reserve margin (1%), because a low power reserve margin indicates that there is a low volume of power available to respond to a disturbance.

Therefore, the results evidence that the RES frequency sensitive modes alone will not improve the values of the key frequency indicators. This happens because the active power contribution of the RES during the post-fault recovery is limited. Figure 6.1 presents a comparison between the active power results of the RES present in buses 30, 32, and 35 to the loss of line 5-6 (which has the worst nadir and RoCoF) with and without FSM, proving that the inclusion of the frequency sensitive modes does not have a significant impact because they do not influence the active power recovery.

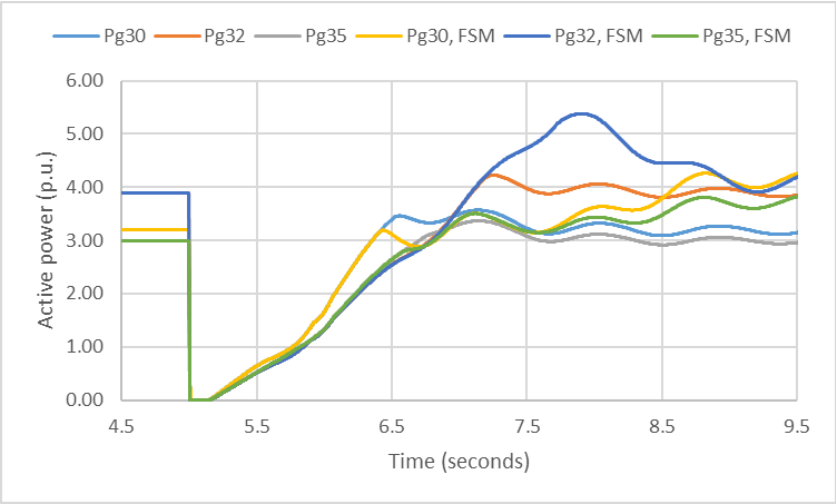

Figure 6.1: Comparison between the active power injected by the RES with and without FSM.

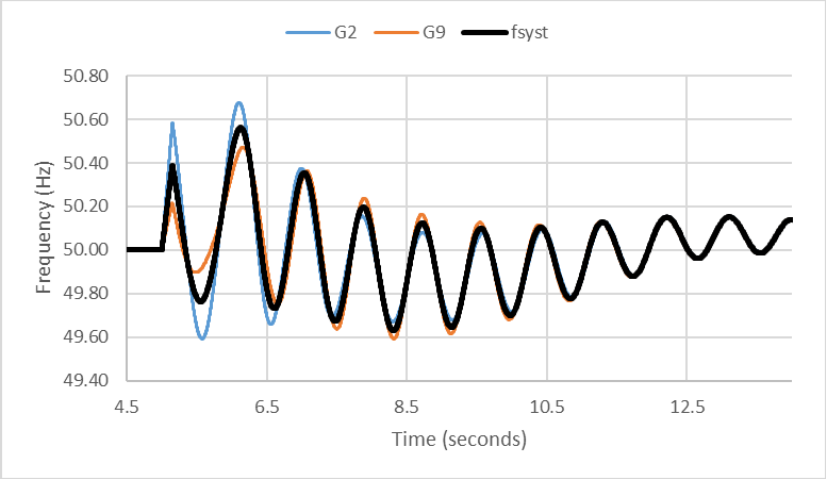

Figure 6.2: Frequency in control area 1 during the fault in line 5-6 with Frequency Sensitive Modes enabled on the RES.

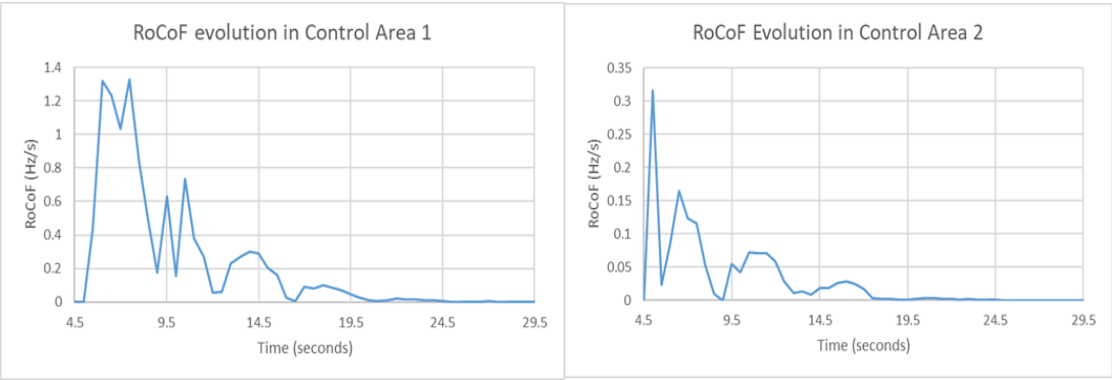

(a) **(b)**

Figure 6.3: RoCoF evolution in control area 1 (a) and in control area 2 (b) during the fault in line 5-6 with a sliding window of 500 milliseconds.

Comparing the 5th scenario of renewable energy integration presented in Chapter 5 with the same scenario but with frequency control showed that there was no significant change in the active power recovery after the fault in line 5-6. Therefore, the active power injected by the power electronic converters behaved in the same way regardless of the existence of a power plant controller performing a frequency sensitive mode response. This explains why the key frequency indicators remained practically unchanged: by looking at the RoCoF's graphical representation in both control areas, the maximum RoCoF occurs right after the fault (approximately at t=6 seconds). At t=6 seconds, it can be noted that the RES are still recovering their active power: therefore, the Frequency Sensitive Modes will be unable to respond because of the limited active power contribution and will not be enough to arrest the fast frequency changes.

6.3 Installation of synchronous condensers near the RES

The first step for the incorporation of synchronous condensers in the power system is to define their location, their apparent power (S, MVA), and their inertia constant. As mentioned in Chapter 3, the synchronous machines that have previously been replaced by RES in this power system can now serve as synchronous condensers: therefore, the inertia constants appearing in Table 6.3 are in fact the same as the ones from the decommissioned synchronous generators. To facilitate the integration of the synchronous condensers in the power system and to test their contribution in different locations, additional buses were created in the IEEE 39-bus system. For the same fault and inertia constant, synchronous condensers with different apparent powers were tested. As the inertia constant is originally in p.u.MW in the machine's base, the higher the machine's apparent power, the higher the kinetic energy stored in its rotating masses. Then, this is an important aspect to consider when aiming to arrest frequency changes. Hence, the main objective of this approach is to perform a sensitivity study with respect to synchronous condensers capacity (in terms of installed power, while keeping the inertia defined in the machine base power constant).

Table 6.3: Characteristics of the available synchronous condensers in the power system.

SC identifier	Location	Machine base power, S_m (MVA)	H (p.u.MW, S_m)	H (p.u.MW, S_b)
SC1	40	100	4.2	4.2
		300		12.6
		400		16.8
		1000		42
SC2	41	100	4.475	4.475
		300		13.425
		400		17.9
		1000		44.75
SC3	42	100	4.35	4.35
		300		13.05
		400		17.4
		1000		43.5
SC4	43	100	3.771	3.771
		300		11.313
		400		15.084
		1000		37.71
SC5	44	100	3.575	3.575
		300		10.725
		400		14.3
		1000		35.75
SC6	45	100	1.625	1.625
		300		4.875
		400		6.5
		1000		16.25
SC7	46	100	3.471	3.471
		300		10.413
		400		13.884
		1000		34.71

Having stated the characteristics of all the synchronous condensers available in the power system, it is now important to understand the role of their location with respect to the contribution for mitigating frequency changes in face of the considered disturbances. In this work, the performance of the synchronous condensers was tested considering different locations in the system. All these scenarios were tested considering a fault in line 13-14. In a second phase, aiming to understand if the main findings resulting from this assessment remained valid even if the fault location was changed, the key frequency indicators were calculated considering new fault locations taking place in lines 5-6 and 2-25, as they had the most severe frequency indicators (considering the analysis conducted in Chapter 5). This is a fundamental step to consolidate the robustness of the findings to be drawn from this analysis.

In this section, the behaviour of the synchronous condensers located near the RES was assessed using two different scenarios: either with only three synchronous condensers near buses 30, 32, and 35, or with seven synchronous condensers near all the RES (i.e., one synchronous condenser per RES). These two scenarios were considered to understand not only the influence of the synchronous condensers near the RES, but also the role of the number of SCs in arresting fast frequency changes. Table 6.4 shows the location of the SCs, as well as the value of their sub-transient reactance and the increase in the inertia constant provided by the SCs.

Table 6.4: Installing three synchronous condensers with 100 MVA, 300 MVA, 400 MVA and 1000 MVA close to the RES.

SC identifier	Location	Close to bus	S (MVA)	H(s)	Xsource (p.u.)
SC1	40	30	100	4.2	0.25
SC2	41	32		4.475	0.36
SC3	42	35		4.35	0.32
			Total (s)	+13.025	

SC identifier	Location	Close to bus	S (MVA)	H(s)	Xsource (p.u.)
SC1	40	30	300	12.6	0.25
SC2	41	32		13.425	0.36
SC3	42	35		13.05	0.32
			Total (s)	+39.075	

SC identifier	Location	Close to bus	S (MVA)	H(s)	Xsource (p.u.)
SC1	40	30	400	16.8	0.25
SC2	41	32		17.9	0.36
SC3	42	35		17.4	0.32
			Total (s)	+52.1	

SC identifier	Location	Close to bus	S (MVA)	H(s)	Xsource (p.u.)
SC1	40	30	1000	42	0.25
SC2	41	32		44.75	0.36
SC3	42	35		43.5	0.32
			Total (s)	+130.25	

Tables 6.5, 6.6, and 6.7 show the obtained nadir and RoCoF results considering a fault in line 13-14. The frequency indicators concerning faults in line 5-6 and 2-25 for the installation of synchronous condensers near the RES are in Appendix D.1.

Table 6.5: Nadir results after the loss of line 13-14 with SCs close to the RES.

Scenarios to be tested close to the RES	S (MVA)	Nadir 1	Nadir 2
Scenario 5	-	49.74	49.92
Synchronous condensers at bus 40, 41, 42	100	49.69	49.89
1 synchronous condenser per RES		49.63	49.84
Synchronous condensers at bus 40, 41, 42	300	49.7	49.89
1 synchronous condenser per RES		49.61	49.84
Synchronous condensers at bus 40, 41, 42	400	49.73	49.899
Synchronous condensers at bus 40, 41, 42	1000	49.82	49.91

The nadir results suggest that, for faults in line 13-14, 5-6, and 2-25, having 3 synchronous condensers located close to the RES did not improve the nadir significantly. However, having an extreme case where each RES had a synchronous condenser worsened the nadir. Moreover, when 7 synchronous condensers of 400 MVA were added to the power system, the system could not stabilize, which is why those results are not considered: this was concluded because the frequency oscillations continued increasing even after the time of the fault.

Table 6.6: RoCoF results after the loss of line 13-14 with SCs close to the RES.

		RoCoF for Control Area 1 (Hz/s)			RoCoF for Control Area 2 (Hz/s)			Highest RoCoF Time in Control Area 1 (s)			Highest RoCoF Time in Control Area 2 (s)		
Scenarios to be tested close to the RES	**S (MVA)**	**500 ms**	**250 ms**	**100 ms**	**500 ms**	**250 ms**	**100 ms**	**500 ms**	**250 ms**	**100 ms**	**500 ms**	**250 ms**	**100 ms**
Scenario 5	-	1.36	2.236	2.52	0.293	0.492	0.715	6	6.5	6.5	5	5.25	5.1
SCs at bus 40, 41, 42	100	1.137	1.987	2.202	0.279	0.465	0.686	6	6.5	6.4	5	5.25	5.1
1 SC per RES		1.366	2.184	2.416	0.284	0.489	0.722	6	6.5	6.5	5	5.25	5.1
SCs at buses 40, 41, 42	300	0.958	1.65	1.754	0.253	1.65	0.644	6	6.5	6.5	5	5.25	5.1
1 SC per RES		1.225	2.353	2.548	0.284	0.488	0.722	6.5	6.5	6.5	5	5.25	5.1
SCs at buses 40, 41, 42	400	0.922	1.57	1.66	0.238	0.413	0.629	6	6.5	6.5	5	5.25	5.1
SCs at buses 40, 41, 42	1000	0.587	0.796	0.976	0.178	0.365	0.576	6	6.5	6.5	5	5.25	5.1

The RoCoF results for the loss of lines 13-14, 5-6, and 2-25 with SCs close to the RES show that having 1 synchronous condenser located near each RES not only worsened the nadir, but also the RoCoF. The RoCoF has then become larger when there was 1 SC per RES, but has improved when there were only 3 SCs close to the RES. The results also show that, when the fault location corresponds to a more severe fault and when the SCs are located all close to the RES, the power system becomes unstable for lower values of the apparent power in the SCs (for example, for line 13-14, the power system did not stabilize for $S \geq 400$ MVA, whereas for lines 5-6 and 2-25, the power system did not stabilize from $S \geq 300$ MVA).

After having calculated the RoCoF for the scenarios where the synchronous condensers were located near the RES, the RoCoF percentual variations in control area 1 were determined, taking as a reference the scenario 5 achieved in Chapter 5. The RoCoF percentual variations will then serve as an indicator useful for comparing the influence of locating synchronous condensers near the RES or near the synchronous machines and buses with high loads.

Table 6.7: RoCoF percentual variations with the increasing apparent power of the synchronous condensers (line 13-14).

		RoCoF variation for Control Area 1 (%)		
Tested scenarios	**SC power rating (MVA)**	**500 ms**	**250 ms**	**100 ms**
3 SCs close to RES (close to buses 30, 32, 35)	100	-16.4	-11.14	-12.62
3 SCs close to RES (close to buses 30, 32, 35)	300	-29.56	-26.21	-30.4
3 SCs close to RES (close to buses 30, 32, 35)	400	-32.21	-29.79	-34.13
3 SCs close to RES (close to buses 30, 32, 35)	1000	-56.84	-64.4	-61.27

The results in Table 6.7 demonstrate that it is easy to improve the RoCoF regardless of the location of the synchronous condensers, because the RoCoF is more sensitive to the increase in the inertia constant, as it is inversely proportional to it. Even though the RoCoF improved, it is still possible to improve the nadir, which is why the same approach will be tested, but with the SCs near the synchronous machines (SMs) instead.

For a more detailed exploration of these findings, the following figures show the dynamic behaviour of the frequency (Figure 6.4), the active and reactive power contributions of the synchronous condensers (Figure 6.5), the voltage (Figure 6.6), and the active power injected by the synchronous machine in bus 38 (Figure 6.7), as these are the most relevant variables to be analysed in this circumstance.

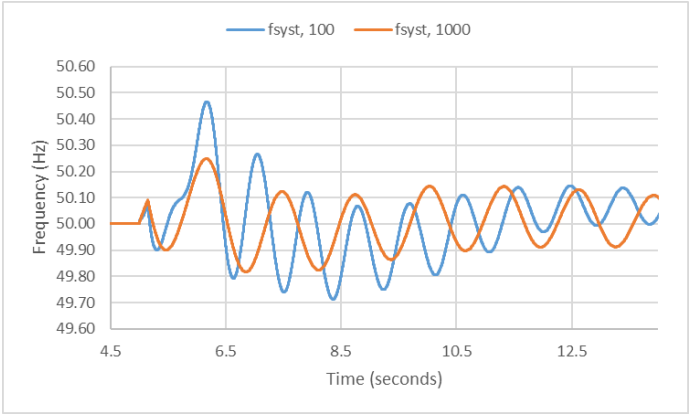

Figure 6.4: Frequency of the centre of inertia in Control Area 1 during the fault in line 13-14 when 3 synchronous condensers with 100 MVA and 1000 MVA are close to the RES.

Figure 6.4 compares the frequency of the centre of inertia with three SCs having 100 MVA and 1000 MVA, respectively. In the first frequency oscillation, the highest frequency achieved is approximately 50.4 Hz for SCs with 100 MVA, and 50.23 Hz for SCs with 1000 MVA. This means that having synchronous condensers with higher apparent power ratings helps containing frequency deviations. Moreover, the frequency signal is slightly delayed when considering SCs with 1000 MVA, which means that the largest frequency oscillations appear later than when considering SCs with 100 MVA.

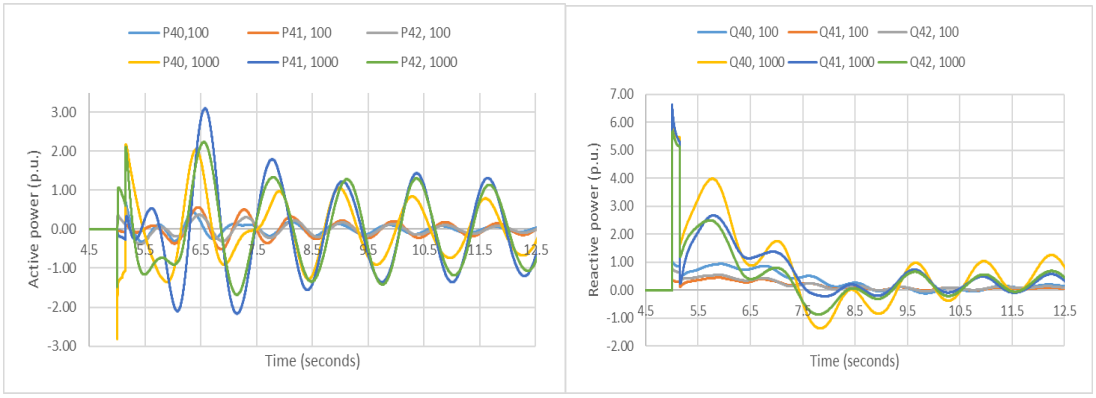

(a) **(b)**

Figure 6.5: Active (a) and reactive (b) power injected during the fault by the 3 synchronous condensers with different apparent powers close to the RES.

By observing Figure 6.5, it is possible to conclude that the higher the apparent power of the synchronous condensers, the higher the active and reactive power injected by the SCs (thus, the higher the voltage in the generation buses and the lower frequency deviations).

Figure 6.6 shows with more detail the sensitivity of the voltage in buses 34 and 38 to the changes in the SCs' apparent power. Buses 34 and 38 were chosen because bus 34 does not have a synchronous condenser installed and because bus 38 is a bus containing a synchronous machine. Then, this figure makes it possible to evaluate the voltage sensitivity to the SC's apparent power in buses that are not directly impacted by synchronous condensers.

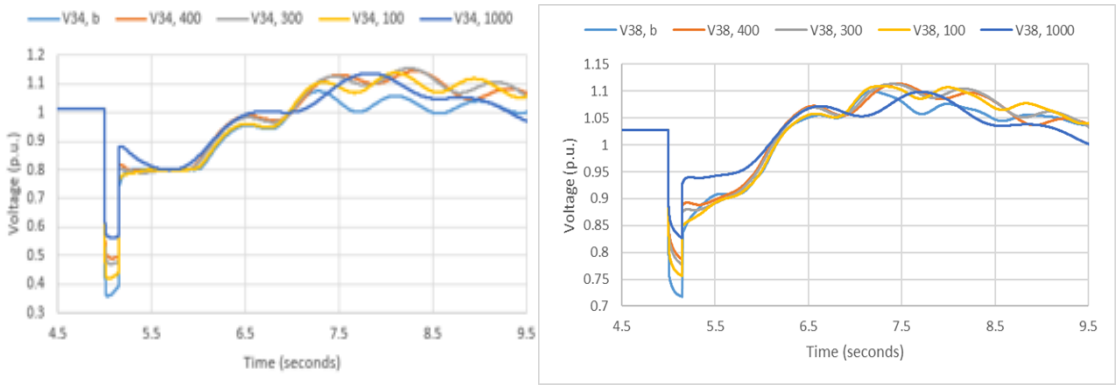

Figure 6.6: Voltage sensitivity to the SCs' apparent power (after a fault in line 13-14 with 3 SCs near the RES).

Figure 6.6 shows that, when 3 synchronous condensers were installed near the RES, buses 34 (containing RES) and 38 (containing a synchronous machine) both had higher voltages, regardless of their type of generation (renewable or synchronous generation). Both buses also showed that SCs with higher apparent powers lead to higher voltages in each bus.

After the analysis of the voltage sensitivity to the changes in the SCs' apparent power, the influence of the apparent power of the SCs in the frequency deviations of the synchronous machines (and in its generated active power) was also tested and is shown in Figure 6.7:

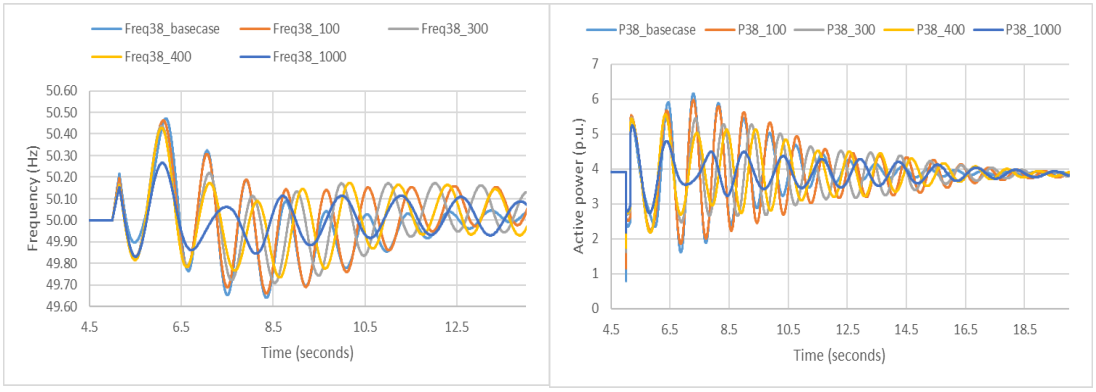

(a) **(b)**

Figure 6.7: Frequency deviations (a) and power deviations (b) of the synchronous machine in bus 38 after a fault in line 13-14 with 3 synchronous condensers with different apparent powers near the RES.

The results shown in this section prove that it is easy to improve the RoCoF regardless of the location of the synchronous condensers, because the RoCoF is more sensitive to the increase in the inertia constant, as it is inversely proportional to it. Even though the RoCoF improved after installing three synchronous condensers near the RES, it is still possible to improve the nadir, which is why the same approach will be tested, but with the SCs near the synchronous machines (SMs).

6.4 Installation of synchronous condensers near the synchronous machines

In this section, the same analysis will be conducted, but considering that 3 synchronous condensers will be installed near the 3 existing synchronous machines. This section will conduct a sensitivity analysis of the voltage to the increase in the SCs' apparent power, which will be compared to the one made for the scenario with 3 SCs near the RES. The key frequency indicators of this scenario (Table 6.10) are presented and analysed in the next section, along with the results of other simulations near the SMs. The scenario to be discussed in this section is built in Table 6.8:

Table 6.8: Installing 3 SCs near the existing synchronous machines with 100 MVA, 300 MVA, 400 MVA, and 1000 MVA.

SC identifier	Location	Close to bus	S (MVA)	H(s)	Xsource (p.u.)
SC1	40	31	100	4.2	0.35
SC2	41	38		4.475	0.45
SC3	42	39		4.35	1.0
			Total (s)	+13.025	

SC identifier	Location	Close to bus	S (MVA)	H(s)	Xsource (p.u.)
SC1	40	31	300	12.6	0.35
SC2	41	38		13.425	0.45
SC3	42	39		13.05	1.0
			Total (s)	+39.075	

SC identifier	Location	Close to bus	S (MVA)	H(s)	Xsource (p.u.)
SC1	40	31	400	16.8	0.35
SC2	41	38		17.9	0.45
SC3	42	39		17.4	1.0
			Total (s)	+52.1	

SC identifier	Location	Close to bus	S (MVA)	H(s)	Xsource (p.u.)
SC1	40	31	1000	42	0.35
SC2	41	38		44.75	0.45
SC3	42	39		43.5	1.0
			Total (s)	+130.25	

According to Table 6.10, the best nadir and RoCoF results were obtained when SCs with 1000 MVA were located close to the synchronous machines. Then, a comparison between these results and those obtained in the previous section should be made.

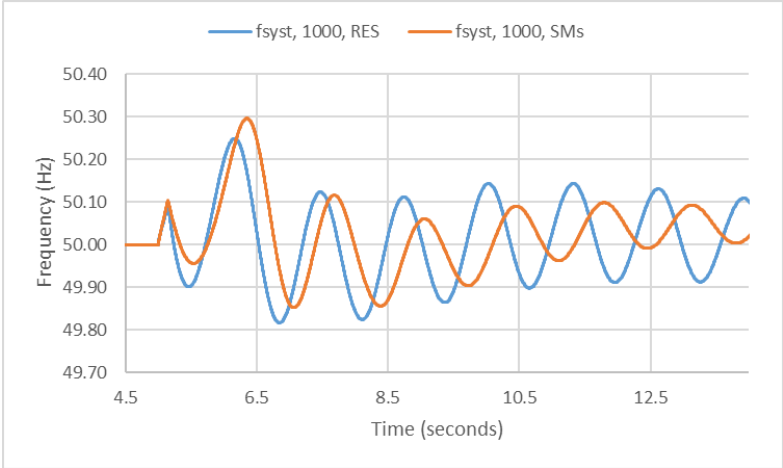

Figure 6.8: Comparison between the frequency in Control Area 1 during the fault in line 13-14 when 3 synchronous condensers with 1000 MVA are close to the SMs and close to the RES.

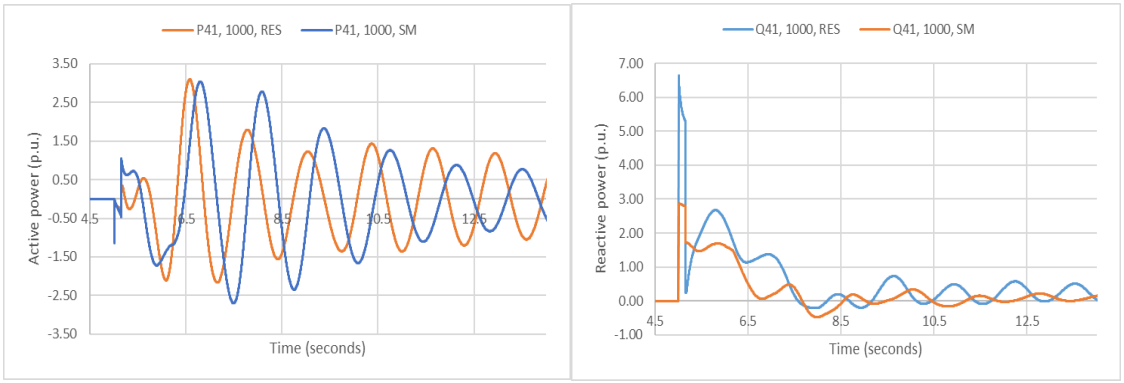

(a) **(b)**

Figure 6.9: Comparison between the active (a) and reactive (b) power injected with 3 1000 MVA-SCs close to the RES and close to the synchronous machines.

Figure 6.8 shows that, when the synchronous condensers are located near the synchronous machines, the first frequency oscillation is slightly delayed. Figure 6.9 shows that, when the synchronous condenser in bus 41 is installed near the synchronous machines, the synchronous condenser injects more active power than when located near the RES.

To better investigate the voltage sensitivity of the remaining generation buses to the increase of the apparent power of the SCs, bus 36 can be chosen as a term of comparison between the case with synchronous condensers near RES and near SMs because it does not have a synchronous condenser next to it in neither of the scenarios. It is therefore useful to assess the impact of the location of synchronous condensers in buses that are not directly affected by them.

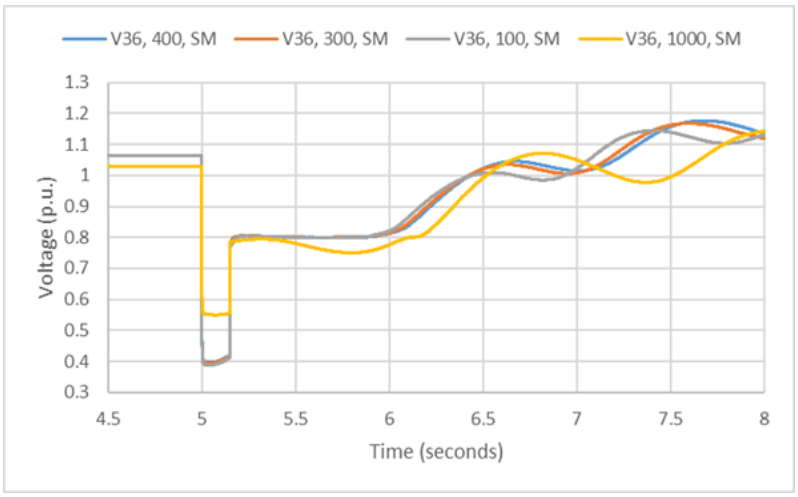

Figure 6.10: Voltage sensitivity to the SCs' apparent power (after a fault in line 13-14 with 3 SCs near the synchronous machines).

When the synchronous condensers are located near the buses with synchronous machines, the voltage in the buses containing only renewable energy generation tends to remain practically the same regardless of the value of the SC's apparent power.

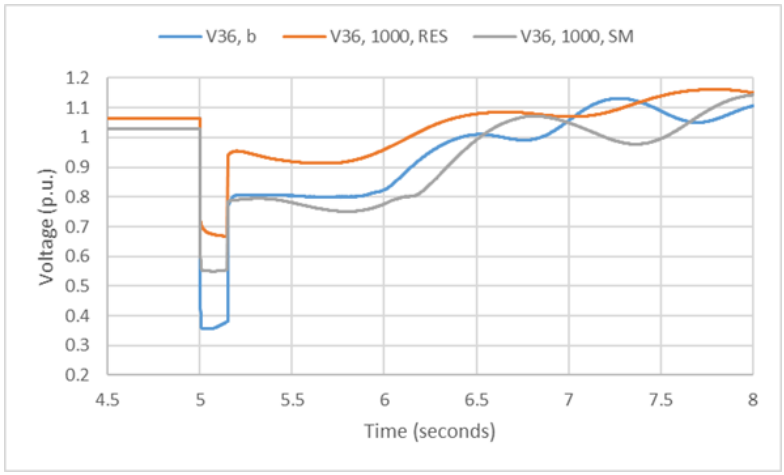

Figure 6.11: Comparison between the voltages in Bus 36: base case, 3 SCs of 1000 MVA near RES, and 3 SCs of 1000 MVA near the SMs (for the loss of line 13-14).

Figure 6.11 compares the voltage in bus 36 when synchronous condensers are installed near the RES and near the synchronous machines. In a bus not directly connected to the SCs and for the same apparent power, the voltage tends to be higher when the synchronous condensers are located near the RES than when they are located near the synchronous machines. However, when examining the voltages in buses 31 and 38, the opposite is observed, as they are directly connected to the SCs.

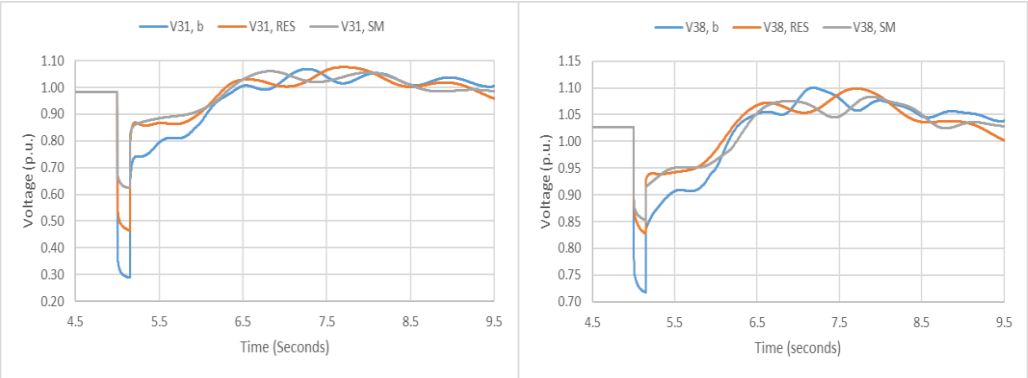

(a) **(b)**

Figure 6.12: Comparison between the voltages in Bus 31 (a) and in Bus 38 (b): base case, 3 SCs of 1000 MVA near RES, and 3 SCs of 1000 MVA near the SMs (for the loss of line 13-14).

Figure 6.12 demonstrates that, when synchronous condensers are installed near the synchronous machines, the voltage in the bus 31 and 38 is higher than when the synchronous condensers are located near the RES. The fact that the voltage is higher when the synchronous condensers are located near the synchronous machines is one of the factors improving the frequency indicators. This can be explained by the Equal Area Criterion, which states that the voltage increase is one of the factors improving transient stability, because the energy transferred during an event becomes higher, making the system more able to cope with the energy losses caused by an event. Synchronous condensers installed near the synchronous machines mean higher reactive power provision, higher voltage, and higher inertia, which augments the system's ability to balance the energy exchanged during a fault, thus maintaining frequency stability. Therefore, the higher the voltage near the synchronous machines, the better the frequency indicators will be, demonstrating that the system's stability improves.

In a scenario where only 3 SCs are located near the synchronous machines, the voltage improved locally. In contrast, installing 3 synchronous condensers near the RES showed that the voltage in the remaining generation buses without synchronous condensers was more sensitive to apparent power variations. Hence, installing 3 synchronous condensers near the RES showed a more global voltage improvement, but installing synchronous condensers near the synchronous machines only showed a high voltage increase near buses 31 and 38. Even though both locations led to significant improvements regarding the frequency indicators (especially in terms of RoCoF), the results suggest that increasing the voltage near the synchronous machines is more effective for improving frequency stability.

6.5 Installation of synchronous condensers near the synchronous machines and near buses with high loads

To conclude the analysis of the installation of synchronous condensers in the power system, this section explores the influence of having 3 synchronous condensers located close to the synchronous machines and 2 extra synchronous condensers located near buses 16 and 8 (having high loads). To assess the influence of the number of SCs near the synchronous machines, it also analyses and compares the key frequency indicators for this scenario and for the scenarios with 3 SCs and 2 SCs near the synchronous machines.

To test the influence of having 3 SCs located near the synchronous machines, and 2 SCs near the buses with high consumptions, the following scenarios were built in Table 6.9:

Table 6.9: Installing 3 SCs near the existing synchronous machines and 2 SCs near buses 16 and 8 with 100 MVA, 300 MVA, 400 MVA, and 1000 MVA.

SC identifier	Location	Close to bus	S (MVA)	H(s)	Xsource (p.u.)
SC1	40	31	100	4.2	0.35
SC2	41	38		4.475	0.45
SC3	42	39		4.35	1
SC4	43	16		3.771	0.3
SC5	44	8		3.575	0.28
			Total (s)	+20.371	

SC identifier	Location	Close to bus	S (MVA)	H(s)	Xsource (p.u.)
SC1	40	31	300	12.6	0.35
SC2	41	38		13.425	0.45
SC3	42	39		13.05	1
SC4	43	16		11.313	0.3
SC5	44	8		10.725	0.28
			Total (s)	+61.113	

SC identifier	Location	Close to bus	S (MVA)	H(s)	Xsource (p.u.)
SC1	40	31	400	16.8	0.35
SC2	41	38		17.9	0.45
SC3	42	39		17.4	1
SC4	43	16		15.084	0.3
SC5	44	8		14.3	0.28
			Total (s)	+81.484	

SC identifier	Location	Close to bus	S (MVA)	H(s)	Xsource (p.u.)
SC1	40	31	1000	42	0.35
SC2	41	38		44.75	0.45
SC3	42	39		43.5	1
SC4	43	16		37.71	0.3
SC5	44	8		35.75	0.28
			Total (s)	+203.71	

Then, the key frequency indicators for this scenario were calculated, along with those related to the previous section. Tables 6.10, 6.11 and 6.12 show the nadir results for the base case, the case with 3 SCs and 2 SCs near the synchronous machines, as well as the case of 3 SCs near SMs and 2 SCs near the buses with high loads.

Table 6.10: Nadir results after the loss of line 13-14 with SCs close to the SMs and to loads.

Tested scenarios	**S (MVA)**	**Nadir 1**	**Nadir 2**
Scenario 5	-	49.74	49.92
Synchronous condensers at bus 40, 41, 42	100	49.78	49.92
Synchronous condenser only near bus 31 and 38		49.77	49.92
3 Synchronous condensers near SM + 1 SC at bus 16 + 1 SC at bus 8		49.74	49.9
Synchronous condensers at bus 40, 41, 42	300	49.82	49.92
Synchronous condenser only near bus 31 and 38		49.79	49.92
3 Synchronous condensers near SM + 1 SC at bus 16 + 1 SC at bus 8		49.71	49.89
Synchronous condensers at bus 40, 41, 42	400	49.82	49.93
Synchronous condenser only near bus 31 and 38		49.79	49.93
3 Synchronous condensers near SM + 1 SC at bus 16 + 1 SC at bus 8		49.69	49.88
Synchronous condensers at bus 40, 41, 42	1000	49.85	49.96
Synchronous condenser only near bus 31 and 38		49.78	49.95

By comparing the results from the scenario with 3 SCs to the ones from the scenario with 2 SCs, it is observed that having more synchronous condensers installed near the synchronous machines tends to improve the nadir. Moreover, increasing the SCs' apparent power did not greatly affect the nadir when only 2 SCs were installed close to buses 31 and 38. It can, too, be observed that the nadir increases more when the apparent power increases from 100 MVA to 300 MVA, and that it tends to remain the same when the apparent power is increased above 300 MVA. In other words, even if the apparent power is the highest (e.g., 1000 MVA), the nadir practically remains the same (which remains true even if different fault locations are considered – Appendix D). Thus, this suggests that, in certain locations, the influence of the apparent power of the synchronous condensers is limited to a certain value, meaning that indefinitely increasing the SCs' apparent power does not guarantee the improvement of the nadir.

Table 6.11: RoCoF results after the loss of line 13-14 with SCs close to the SMs and to loads.

		RoCoF for Control Area 1 (Hz/s)			RoCoF for Control Area 2 (Hz/s)			Max. RoCoF Time in Control Area 1 (s)			Max. RoCoF Time in Control Area 2 (s)		
Tested scenarios	**S (MVA)**	**500 ms**	**250 ms**	**100 ms**	**500 ms**	**250 ms**	**100 ms**	**500 ms**	**250 ms**	**100 ms**	**500 ms**	**250 ms**	**100 ms**
Scenario 5	-	1.36	2.236	2.52	0.293	0.492	0.715	6	6.5	6.5	5	5.25	5.1
SCs at bus 40, 41, 42	100	1.065	1.84	1.955	0.279	0.477	0.706	6	6.5	6.5	5	5.25	5.1
SCs only near bus 31 and 38		1.147	1.975	2.102	0.2	0.48	0.711	6	6.5	6.5	5	5.25	5.1
3 SCs near SM + 1 SC at bus 16 + 1 SC at bus 8		0.999	1.777	1.929	0.263	0.453	0.673	6	6.5	6.5	5	5.25	5.1
SCs at bus 40, 41, 42	300	0.828	1.26	1.638	0.257	0.452	0.679	6	6.5	6.5	5	5.25	5.1
SCs only near buses 31 and 38		0.876	1.444	1.827	0.266	0.481	0.687	6	6.5	6.5	5	5.25	5.1
3 SCs near SM + 1 SC at bus 16 + 1 SC at bus 8		0.713	1.465	1.712	0.218	0.39	0.592	8	6.75	6.6	5	5.25	5.1
SCs at bus 40, 41, 42	400	0.739	1.196	1.574	0.248	0.441	0.667	6	6.5	6.5	5	5.25	5.1
SCs near bus 31 and 38		0.786	1.326	1.702	0.259	0.455	0.686	6	6.75	6.5	5	5.25	5.1
3 SCs near SM + 1 SC at bus 16 + 1 SC at bus 8		1.059	1.525	1.635	0.2	0.363	0.558	7	6.75	6.7	5	5.25	5.1
SCs at bus 40, 41, 42	1000	0.777	0.879	0.951	0.209	0.3944	0.61	7	6.75	6.8	5	5.25	5.1
SCs only near bus 31 and 38		1.082	1.21	1.336	0.233	0.425	0.647	7	6.75	6.7	5	5.25	5.1

Table 6.12: RoCoF percentual variations with the increasing apparent power of the synchronous condensers (line 13-14) when located close to the SMs and loads.

		RoCoF variation for Control Area 1 (%)		
Tested scenarios	**SC power rating (MVA)**	**500 ms**	**250 ms**	**100 ms**
3 SCs near synchronous machines	100	-21.69	-17.71	-22.42
3 SCs near synchronous machines	300	-39.12	-43.65	-35
3 SCs near synchronous machines	400	-45.66	-46.51	-37.54
3 SCs near synchronous machines	1000	-42.87	-60.69	-62.26
2 SCs near bus 31 and 38	100	-15.66	-11.67	-16.59
2 SCs near bus 31 and 38	300	-35.59	-35.42	-27.5
2 SCs near bus 31 and 38	400	-42.21	-40.7	-32.46
2 SCs near bus 31 and 38	1000	-20.44	-45.89	-46.98
3 SCs near buses 31, 38, and 39 + 1 SC near bus 16 + 1 SC near bus 8	100	-26.54	-20.53	-23.45
3 SCs near buses 31, 38, and 39 + 1 SC near bus 16 + 1 SC near bus 8	300	-47.57	-34.48	-32.06
3 SCs near buses 31, 38, and 39 + 1 SC near bus 16 + 1 SC near bus 8	400	-22.13	-31.8	-54.13

When three synchronous condensers were located near the RES, the RoCoF was significantly lower, but the nadir did not suffer many changes for small increments in the SCs' apparent power. When the SCs were located near the RES, only a large increment in the apparent power improved the nadir significantly (for example, for a fault in line 13-14, going from 100 MVA to 300 MVA caused the nadir to rise from 49.78 Hz to 49.82 Hz).

However, the RoCoF percentual variations considering an increasing apparent power in the SCs show that, when the 3 SCs were located near the synchronous machines, there was a more significant RoCoF percentual reduction than when the 3 SCs were located near the renewables. When the SCs were located near the synchronous machines, the nadir significantly improved even for small increments in the synchronous condensers' apparent power.

By comparing the case of 3 SCs with the case of 2 SCs near the synchronous machines, it was noticed that the RoCoF improved more when more synchronous condensers were installed near the synchronous machines, which was to be expected.

It was also perceived that, when the synchronous condensers were installed close to the synchronous machines and to the loads, the higher their apparent power, the later the largest RoCoF appeared in the power system. For example, during a fault in line 2-25, the highest RoCoF appeared later for $S \geq 300$ MVA.

Installing two extra synchronous condensers close to the loads did not always improve the nadir and provoked instabilities for higher apparent power values. These instabilities typically happened for S= 1000 MVA, depending on the severity of the fault: for lines 13-14 and 5-6, the instabilities appeared when S=1000 MVA, whereas for line 2-25, the instabilities start when $S \geq$ 400 MVA. Adding two extra SCs close to the loads improved the RoCoF when the SCs had an apparent power of 100 MVA. However, the RoCoF results tended to worsen with the increase of the apparent power in the SCs close to the loads.

6.6 Installation of BESS near the RES

To compare the influence of installing BESS with installing synchronous condensers near the RES, 3 BESS were initially installed near buses 30, 32, and 35. To conduct a similar sensitivity analysis to the one done for the synchronous condensers, BESS with 100 MVA, 300 MVA, 400 MVA, and 1000 MVA were tested. In this scenario, the apparent powers of the BESS are high because the IEEE 39-Bus network is a large power system. The nadir and RoCoF results for the above-described scenario and different fault locations can be found in Tables 6.13, 6.14, and 6.15:

Table 6.13: Nadir results after the installation of 3 BESS near the RES (loss of line 5-6).

Scenario no.	Scenarios	S, BESS (MVA)	Nadir 1	Nadir 2
Base case	Scenario 5	-	49.67	49.86
1	3 BESS near RES (near buses 30, 32, and 35)	100	49.65	49.86
2	3 BESS near RES (near buses 30, 32, and 35)	300	49.69	49.86
3	3 BESS near RES (near buses 30, 32, and 35)	400	49.71	49.86
4	3 BESS near RES (near buses 30, 32, and 35)	1000	49.74	49.85

Table 6.14: RoCoF results after the installation of 3 BESS near the RES (loss of line 5-6).

		RoCoF for Control Area 1 (Hz/s)			RoCoF for Control Area 2 (Hz/s)			Max. RoCoF Time in Control Area 1 (s)			Max. RoCoF Time in Control Area 2 (s)		
Scenario no.	**S, BESS (MVA)**	**500 ms**	**250 ms**	**100 ms**	**500 ms**	**250 ms**	**100 ms**	**500 ms**	**250 ms**	**100 ms**	**500 ms**	**250 ms**	**100 ms**
Base case	-	1.32	2.42	2.68	0.315	0.55	0.823	6	6.5	6.5	5	5.25	5.1
1	100	1.32	2.41	2.66	0.315	0.55	0.83	6	6.5	6.4	5	5.25	5.1
2	300	1.32	2.39	2.63	0.315	0.55	0.83	6	6.5	6.4	5	5.25	5.1
3	400	1.301	2.37	2.58	0.314	0.544	0.828	6	6.5	6.4	5	5.25	5.1
4	1000	1.22	2.029	2.553	0.315	0.542	0.823	6	6.5	6.4	5	5.25	5.1

Table 6.15: RoCoF percentual variations with the increasing apparent power of the BESS (line 5-6) when located close to 3 RES.

		RoCoF variation for Control Area 1 (%)		
Tested scenarios	**SC power rating (MVA)**	**500 ms**	**250 ms**	**100 ms**
3 BESS near RES (near buses 30, 32, and 35)	100	0	-0.41	-0.75
3 BESS near RES (near buses 30, 32, and 35)	300	0	-1.24	-1.87
3 BESS near RES (near buses 30, 32, and 35)	400	-1.44	-2.07	-3.73
3 BESS near RES (near buses 30, 32, and 35)	1000	-7.58	-16.16	-4.74

By comparing the frequency indicators for the scenarios where 3 BESS are connected near buses 30, 32, and 35 and where 3 synchronous condensers are connected near these buses, it was observed that synchronous condensers reduced more the RoCoF than the BESS. This happens because synchronous condensers inject more active power than BESS, as explained by Figure 6.13:

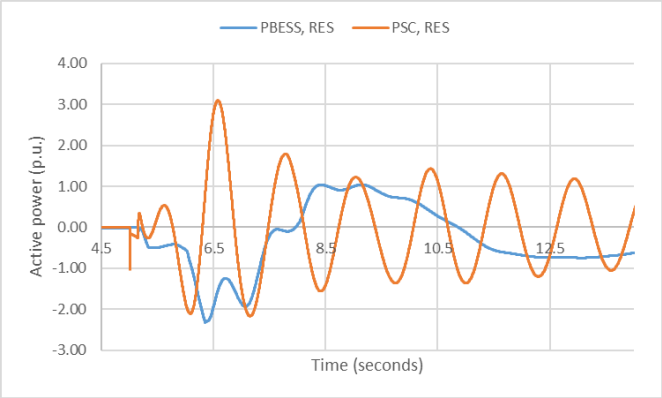

Figure 6.13: Comparison between the active power produced by the SC and BESS in bus 41 during the fault in line 13-14.

Moreover, the installation of 3 BESS near the RES did not significantly alter the nadir, even for a large apparent power in the BESS. For an apparent power of 1000 MVA, the RoCoF improved more than for S=100 MVA, 300 MVA or 400 MVA. However, even for a large apparent power, the RoCoF still remained higher than 1 Hz/s, therefore still not showing grid code compliance. The observation of the frequency indicators hints that, unlike what was observed with synchronous condensers, a higher apparent power in the BESS does not directly influence the equivalent inertia constant of the power system, hence the minimal RoCoF reduction. However, to better understand the influence of the apparent power in the BESS, Figure 6.14 shows the active and reactive power injected by BESS with different apparent powers:

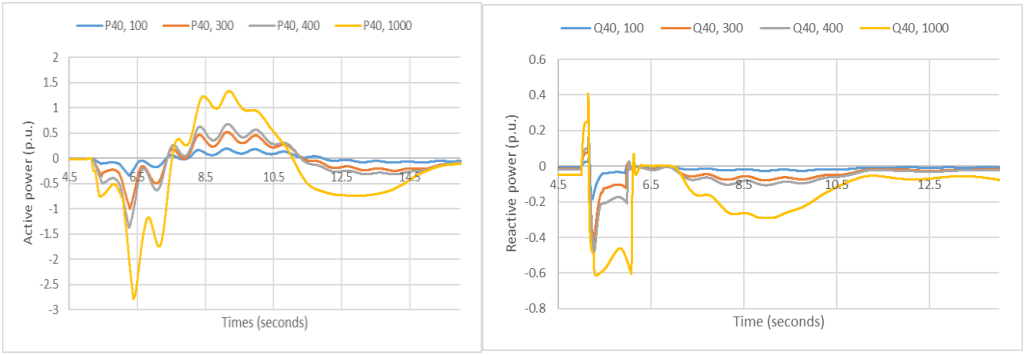

(a) **(b)**

Figure 6.14: Active (a) and reactive (b) power injected and absorbed by the BESS in bus 40 during the fault in line 5-6.

Before the fault, the batteries are not injecting any active or reactive power; during the fault, they absorb active and reactive power to reduce the system active power demand and to stabilize the voltage and frequency. Figure 6.14 also shows that the higher the apparent power of the BESS, the higher the injected active and reactive power, which already has been observed when the inclusion of synchronous condensers was analysed.

Figure 6.15 tests the influence of the BESS apparent power in bus 40 (with BESS) and in bus 36 (without BESS). It demonstrates that, for a fault in line 5-6, the voltage remains almost unchanged even if the apparent power of the BESS is varied.

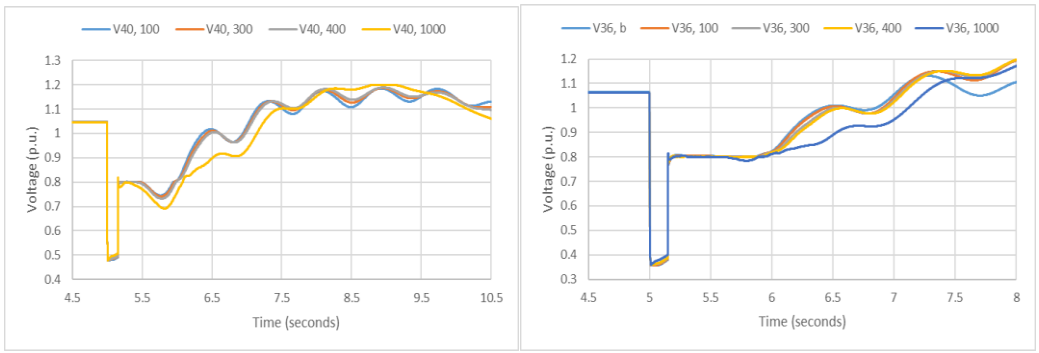

(a) **(b)**

Figure 6.15: The influence of the BESS' apparent power in the voltage at bus 40 (a) and at bus 36 (b).

To understand the influence of the number of BESS near the RES in the nadir and the RoCoF, a second scenario containing one BESS (of 100 MVA, 300 MVA, 400 MVA, and 1000 MVA) near each renewable energy generator was tested, being the frequency indicators displayed in Tables 6.16, 6.17, and 6.18.

Table 6.16: Nadir results after the installation of 7 BESS near each RES (loss of line 5-6).

Scenario no.	S, BESS (MVA)	Nadir 1	Nadir 2
Scenario 5	-	49.67	49.86
1	100	49.67	49.86
2	300	49.75	49.85
3	400	49.75	49.84

Table 6.17: RoCoF results after the installation of 7 BESS near each RES (loss of line 5-6).

		RoCoF for Control Area 1 (Hz/s)			RoCoF for Control Area 2 (Hz/s)			Max. RoCoF Time in Control Area 1 (s)			Max. RoCoF Time in Control Area 2 (s)		
Scenario no.	**S, BESS (MVA)**	**500 ms**	**250 ms**	**100 ms**	**500 ms**	**250 ms**	**100 ms**	**500 ms**	**250 ms**	**100 ms**	**500 ms**	**250 ms**	**100 ms**
Scenario 5	-	1.32	2.42	2.68	0.315	0.55	0.823	6	6.5	6.5	5	5.25	5.1
1	100	1.301	2.379	2.598	0.315	0.546	0.829	6	6.5	6.4	5	5.25	5.1
2	300	1.237	2.095	2.558	0.315	0.543	0.826	6	6.5	6.4	5	5.25	5.1
3	400	1.203	1.902	2.543	0.314	0.541	0.824	6	6.5	5.1	5	5.25	5.1

Table 6.18: RoCoF percentual variations with the increasing apparent power of the BESS (line 5-6) when located close to 7 RES.

		RoCoF variation for Control Area 1 (%)		
Scenario no.	**SC power rating (MVA)**	**500 ms**	**250 ms**	**100 ms**
1	100	-1.44	-1.69	-3.06
2	300	-6.29	-13.43	-4.55
3	400	-8.86	-21.4	-5.11

According to Table 6.18, the RoCoF still remains higher than 1 Hz/s for faults in line 5-6 and 13-14 when installing 7 BESS near the RES. Therefore, it can then be concluded that the RoCoF reduction is not achieved by installing more BESS with large apparent powers, as the RoCoF reduction is significantly lower than when synchronous condensers are preferred. Even if installing synchronous condensers close to the RES does not lead to as significant RoCoF reductions (the highest RoCoF reductions are achieved by installing the SCs close to the synchronous machines), these reductions are still larger than when BESS are installed near the RES.

The installation of 7 BESS (1 per RES) lead to instabilities in the power system when considering that each battery had an apparent power of 1000 MVA. Moreover, when the fault was applied to line 2-25, it was observed that the power system could not stabilize regardless of the apparent power rating of the battery. This happened because the line 2-25 corresponds to a very severe fault, and the high number of batteries with high apparent powers leads to an excessive absorption of reactive power, causing voltage instabilities leading to undamped voltage

and frequency oscillations. Comparatively to installing synchronous condensers near the RES, BESS with the same apparent power as the synchronous condensers lead to slightly higher nadir and less stabilization problems (especially when one BESS was installed near each RES). For example, considering a fault in line 5-6, when one synchronous condenser was installed near each RES, the instabilities were observed for $S \geq 300$ MVA. On the other hand, for the same fault but considering instead one BESS per RES, the instabilities were only observed when installing 1000 MVA in each battery.

Therefore, installing BESS near the RES can pose less stabilization problems than installing synchronous condensers near the RES and can slightly improve the nadir. However, the nadir improvements are not significant even for large increments of the apparent powers in the BESS. Unlike what was observed for synchronous condensers (more synchronous condensers lead to higher RoCoF reductions if they were located to the synchronous machines), the number and size of BESS does not greatly influence the RoCoF reductions.

To complement the analysis related to the influence of BESS in the key frequency indicators, the next section will assess the combination of having synchronous condensers near the synchronous machines and BESS near the RES.

6.7 Combining synchronous condensers with BESS near the RES

This section studies the influence of combining synchronous condensers with 1000 MVA with BESS of different apparent powers (100 MVA, 300 MVA, 400 MVA, and 1000 MVA). The synchronous condensers with 1000 MVA were installed close to the synchronous machines, since this combination of location and apparent power provided the best key frequency indicators. Moreover, only three BESS were kept in the power system given that the number of BESS did not greatly influence the results. The frequency indicators were calculated once again for lines 13-14 and 5-6. The results can be found in Tables 6.19, 6.20, and 6.21:

Table 6.19: Nadir results after the installation of 3 synchronous condensers with 1000 MVA and 3 BESS near the RES (loss of line 5-6).

Scenario no.	Scenarios	S, BESS (MVA)	Nadir 1	Nadir 2
Base case	Scenario 5	-	49.67	49.86
1	3 SCs near the synchronous machines + 3 BESS near the RES (30, 32, 35)	100	49.8	49.92
2	3 SCs near the synchronous machines + 3 BESS near the RES (30, 32, 35)	300	49.81	49.9
3	3 SCs near the synchronous machines + 3 BESS near the RES (30, 32, 35)	400	49.83	49.9
4	3 SCs near the synchronous machines + 3 BESS near the RES (30, 32, 35)	1000	49.87	49.89

Table 6.20: RoCoF results after the installation of 3 synchronous condensers with 1000 MVA and 3 BESS near the RES (loss of line 5-6).

		RoCoF for Control Area 1 (Hz/s)			RoCoF for Control Area 2 (Hz/s)			Max. RoCoF Time in Control Area 1 (s)			Max. RoCoF Time in Control Area 2 (s)		
Scenario no.	**S, BESS (MVA)**	**500 ms**	**250 ms**	**100 ms**	**500 ms**	**250 ms**	**100 ms**	**500 ms**	**250 ms**	**100 ms**	**500 ms**	**250 ms**	**100 ms**
Base case	-	1.32	2.42	2.68	0.315	0.55	0.823	6	6.5	6.5	5	5.25	5.1
1	100	0.847	0.919	1.032	0.231	0.468	0.753	7	6.75	6.7	5	5.25	5.1
2	300	0.799	0.8	0.964	0.231	0.468	0.752	7	7	6.7	5	5.25	5.1
3	400	0.725	0.792	0.863	0.231	0.468	0.751	7	6.75	6.7	5	5.25	5.1
4	1000	0.6	0.725	0.765	0.246	0.473	0.747	7	6.75	6.8	5	5.25	5.1

Table 6.21: RoCoF percentual variations with the increasing apparent power of the BESS (line 5-6) for the above-described scenario.

		RoCoF variation for Control Area 1 (%)		
Tested scenarios	**SC power rating (MVA)**	**500 ms**	**250 ms**	**100 ms**
1	100	-35.83	-62.02	-61.49
2	300	-39.47	-66.94	-64.03
3	400	-45.08	-67.27	-67.8
4	1000	-54.55	-70.04	-71.46

Combining synchronous condensers with BESS significantly reduced the RoCoF and improved the nadir even for lower apparent power values in the BESS. It was shown that having a combination of synchronous condensers with BESS led to higher nadir than when only 3 synchronous condensers with the same characteristics were installed. It was also shown that the highest RoCoF happened later in these circumstances: for example, in a sliding window of 500 milliseconds, the highest RoCoF appears at 7 seconds, which corresponds to a time when the RES have already recovered their initial active power, being now able to participate in active power/frequency control. This has, then, caused the power system to become less vulnerable to frequency changes.

This section showed that installing synchronous condensers near the synchronous machines and BESS near the RES improved the RoCoF and nadir, being them almost equal to the indicators obtained with only synchronous generation. The following section assesses the installation of BESS near the synchronous machines, comparing this scenario with the indicators obtained after the installation of synchronous condensers near the synchronous machines.

6.8 Installing BESS near the synchronous machines

When BESS were installed near the RES (without synchronous condensers near the synchronous machines), it was seen that the number and apparent power of the BESS did not greatly influence the nadir and the RoCoF. Then, it is important to evaluate if the same happens when the batteries are installed near the synchronous machines. In this section, the sensitivity of the key frequency indicators to the number and apparent power of the BESS installed near the synchronous machines will be assessed. In the end, a comparison between this scenario with having synchronous condensers near the synchronous machines will be established. Tables 6.22, 6.23 and 6.24 show the nadir and RoCoF results obtained for faults in line 5-6.

Table 6.22: Nadir results after the installation of 3 BESS near the synchronous machines (loss of line 5-6).

Scenario no.	Scenarios for the integration of BESS	S, BESS (MVA)	Nadir 1	Nadir 2
Base Case	7 renewables -25% inertia in the synchronous generators	-	49.67	49.86
1	3 BESS near the synchronous machines	100	49.7	49.86
2	3 BESS near the synchronous machines	300	49.76	49.87
3	3 BESS near the synchronous machines	400	49.76	49.88
4	3 BESS near the synchronous machines	1000	49.76	49.89

Table 6.23: RoCoF results after the installation of 3 BESS near the synchronous machines (loss of line 5-6).

		RoCoF for Control Area 1 (Hz/s)			RoCoF for Control Area 2 (Hz/s)			Max. RoCoF Time in Control Area 1 (s)			Max. RoCoF Time in Control Area 2 (s)		
Scenario no.	**S, BESS (MVA)**	**500 ms**	**250 ms**	**100 ms**	**500 ms**	**250 ms**	**100 ms**	**500 ms**	**250 ms**	**100 ms**	**500 ms**	**250 ms**	**100 ms**
Base Case	-	1.32	2.42	2.68	0.315	0.55	0.823	6	6.5	6.5	5	5.25	5.1
1	100	1.28	2.23	2.6	0.311	0.546	0.831	6	6.5	5.1	5	5.25	5.1
2	300	1.199	1.833	2.597	0.301	0.541	0.831	6	6.5	5.1	5	5.25	5.1
3	400	1.163	1.66	2.595	0.298	0.539	0.831	6	6	5.1	5	5.25	5.1
4	1000	1	1.709	2.58	0.273	0.528	0.831	6	5.5	5.1	5	5.25	5.1

Table 6.24: RoCoF percentual variations with the increasing apparent power of the BESS (line 5-6) for the above-described scenario.

Tested scenarios	SC power rating (MVA)	RoCoF variation for Control Area 1 (%)		
		500 ms	250 ms	100 ms
3 BESS near the synchronous machines	100	-3.03	-7.85	-2.99
3 BESS near the synchronous machines	300	-9.17	-24.26	-3.1
3 BESS near the synchronous machines	400	-11.89	-31.4	-3.17
3 BESS near the synchronous machines	1000	-24.24	-29.38	-3.73

The results show that installing BESS near the synchronous machines without any other equipment (such as synchronous condensers) does not lead to RoCoF lower than 1 Hz/s in a sliding window of 500 milliseconds, regardless of the BESS' apparent power. However, it was seen that installing 3 BESS near the RES had lower RoCoF percentual reductions than installing 3 BESS near the synchronous machines. Even though the 3 BESS near the synchronous machines led to lower RoCoF than the 3 BESS near the RES, installing synchronous condensers near the synchronous machines still produced higher RoCoF reductions.

The nadir did not increase greatly even if the apparent power in the BESS was increased. When 3 BESS were installed near the synchronous machines, the nadir was slightly lower than the one obtained when synchronous condensers were installed near the synchronous machines. This once again suggests that BESS may be almost as effective as synchronous condensers at increasing the nadir, but not as effective at arresting frequency changes.

The fact that the installation of BESS alone near the synchronous machines was not enough to fight the rapid frequency changes can be explained by Figure 6.16, where it is established a comparison between the active and reactive power injected by a 1000 MVA BESS and a 1000 MVA synchronous condenser when either is located near the synchronous generator in bus 38.

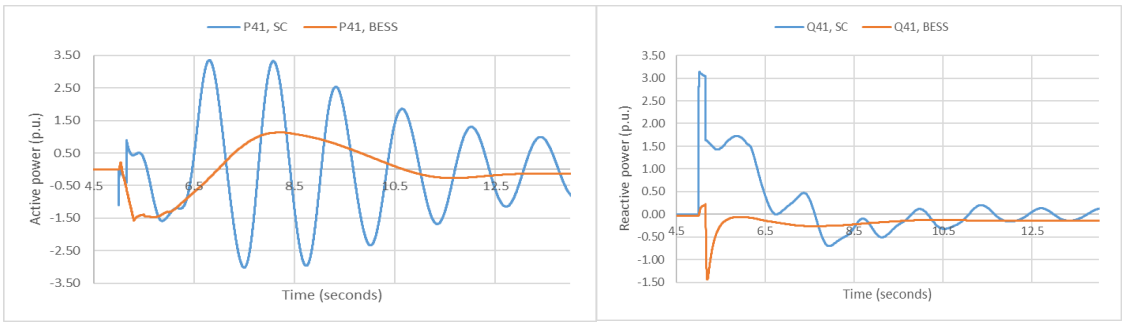

(a) **(b)**

Figure 6.16 – Comparison between the active and reactive power injected during a fault in line 5-6 by one 1000 MVA BESS and a 1000 MVA synchronous condenser.

Figure 6.16 shows that, for the same location and the same apparent power, the BESS responds instantaneously, but injects less active and reactive power than the synchronous condenser. Since the active and reactive power contributions of the BESS are limited, they are not capable of arresting the frequency changes, hence explaining the high RoCoF and low nadir values that are still found even for large BESS located near the synchronous machines. The fact that, for the same location, the synchronous condenser injects more active and reactive power also explains the larger reductions in the RoCoF when these strategies are employed.

When the BESS are located near the synchronous machines, the frequency is more sensitive to the variation of the BESS' apparent power. This is the opposite of what happens when the BESS are located near the RES, where changes in apparent power practically did not influence the frequency or the voltage in the selected buses. Such behaviour has been observed when synchronous condensers with different apparent powers were located near the synchronous machines, as the frequency also reacted more to changes in the apparent power. Regardless of the location of the BESS, the voltage in the generation buses remained unaltered by the changes in the apparent power. So far, the best combination achieved regarding the RoCoF reduction was still the installation of 3 BESS near the RES combined with the installation of the 3 synchronous condensers near the synchronous machines.

6.9 Combining synchronous condensers with BESS near the loads

Similarly to the analysis conducted for synchronous condensers, the combination of synchronous condensers near the synchronous machines and BESS near buses 16 and 8 was tested. The results for the loss of line 5-6 (being the results for the loss of line 13-14 present in Appendix D) are presented in Tables 6.25, 6.26, and 6.27.

Table 6.25: Nadir results after the installation of 3 synchronous condensers near the synchronous machines and 3 BESS near the loads (loss of line 5-6).

Scenario no.	Scenarios for the integration of BESS	S, BESS (MVA)	Nadir 1	Nadir 2
Base Case	7 renewables -25% inertia in the synchronous generators	-	49.67	49.86
1	3 Synchronous condensers near SM + 1 BESS at bus 16 + 1 BESS at bus 8	100	49.81	49.93
2	3 Synchronous condensers near SM + 1 BESS at bus 16 + 1 BESS at bus 8	300	49.83	49.94
3	3 Synchronous condensers near SM + 1 BESS at bus 16 + 1 BESS at bus 8	400	49.83	49.94
4	3 Synchronous condensers near SM + 1 BESS at bus 16 + 1 BESS at bus 8	1000	49.87	49.96

Table 6.26: RoCoF results after the installation of synchronous condensers near the synchronous machines and 3 BESS near the loads (loss of line 5-6).

		RoCoF for Control Area 1 (Hz/s)			RoCoF for Control Area 2 (Hz/s)			Max. RoCoF Time in Control Area 1 (s)			Max. RoCoF Time in Control Area 2 (s)		
Scenario no.	**S, BESS (MVA)**	**500 ms**	**250 ms**	**100 ms**	**500 ms**	**250 ms**	**100 ms**	**500 ms**	**250 ms**	**100 ms**	**500 ms**	**250 ms**	**100 ms**
Base Case	-	1.32	2.42	2.68	0.315	0.55	0.823	6	6.5	6.5	5	5.25	5.1
1	100	0.846	0.972	1.046	0.23	0.467	0.754	7	6.75	6.7	5	5.25	5.1
2	300	0.835	0.969	1.041	0.229	0.466	0.753	7	6.75	6.8	5	5.25	5.1
3	400	0.829	0.966	1.038	0.229	0.465	0.753	7	6.75	6.8	5	5.25	5.1
4	1000	0.788	0.933	1.009	0.226	0.462	0.751	7	6.75	6.7	5	5.25	5.1

Table 6.27: RoCoF percentual variations with the increasing apparent power of the BESS (line 5-6) for the above-described scenario.

		RoCoF variation for Control Area 1 (%)		
Tested scenarios	**SC power rating (MVA)**	**500 ms**	**250 ms**	**100 ms**
3 Synchronous condensers near SM + 1 BESS at bus 16 + 1 BESS at bus 8	100	-35.91	-59.83	-60.97
3 Synchronous condensers near SM + 1 BESS at bus 16 + 1 BESS at bus 8	300	-36.74	-59.96	-61.16
3 Synchronous condensers near SM + 1 BESS at bus 16 + 1 BESS at bus 8	400	-37.2	-60.08	-61.27
3 Synchronous condensers near SM + 1 BESS at bus 16 + 1 BESS at bus 8	1000	-40.3	-61.45	-62.35

When three synchronous condensers were placed near the synchronous machines and two extra synchronous condensers were installed near the buses with high loads, the system did not stabilize for apparent powers of 400 MVA and 1000 MVA. When BESS were placed near the loads instead of synchronous condensers, the system stabilized at the end of each dynamic simulation, even for large apparent powers in the BESS. Besides, the RoCoF reduction was not as high as when the BESS were installed near the loads together with three synchronous condensers of 1000 MVA near the synchronous machines. Unlike when synchronous condensers were installed near the loads, BESS have caused an increase in the nadir. When synchronous condensers were placed near the loads, the nadir decreased even more than when no control action was taken to counteract the ill-effects of operating a system with reduced inertia. Therefore, it is possible to conclude that BESS can mitigate stabilization issues if installed near the loads combined with synchronous condensers.

6.10 Combining synchronous condensers with BESS near the SMs

This section aims to study the influence of adding the same three synchronous condensers with the same inertia as in the previous scenarios and three BESS, both near the synchronous machines. The results will then be compared to the situation where the three synchronous condensers are located near the synchronous machines and the three BESS are located near the RES. The tested fault locations will still be lines 13-14 (present in Appendix D) and 5-6 (Tables 6.28, 6.29, and 6.30).

Table 6.28: Nadir results after the installation of 3 BESS and 3 synchronous condensers near the synchronous machines (loss of line 5-6).

Scenario no.	Scenarios for the integration of BESS	S, BESS (MVA)	Nadir 1	Nadir 2
Base Case	7 renewables -25% inertia in the synchronous generators	-	49.67	49.86
1	3 SCs+ 3 BESS near the synchronous machines	100	49.83	49.92
2	3 SCs+ 3 BESS near the synchronous machines	300	49.87	49.91
3	3 SCs+ 3 BESS near the synchronous machines	400	49.88	49.91
4	3 SCs+ 3 BESS near the synchronous machines	1000	49.9	49.89

Table 6.29: RoCoF results after the installation of 3 BESS and 3 synchronous condensers near the synchronous machines (loss of line 5-6).

		RoCoF for Control Area 1 (Hz/s)			RoCoF for Control Area 2 (Hz/s)			Max. RoCoF Time in Control Area 1 (s)			Max. RoCoF Time in Control Area 2 (s)		
Scenario no.	S, BESS (MVA)	500 ms	250 ms	100 ms	500 ms	250 ms	100 ms	500 ms	250 ms	100 ms	500 ms	250 ms	100 ms
Base Case	-	1.32	2.42	2.68	0.315	0.55	0.823	6	6.5	6.5	5	5.25	5.1
1	100	0.77	0.88	0.943	0.227	0.466	0.754	7	6.75	6.8	5	5.25	5.1
2	300	0.626	0.714	0.765	0.22	0.463	0.754	7	6.75	6.8	5	5.25	5.1
3	400	0.568	0.647	0.727	0.217	0.461	0.754	7	6.75	5.1	5	5.25	5.1
4	1000	0.347	0.364	0.735	0.229	0.47	0.754	7	7	5.1	5	5.25	5.1

Table 6.30: RoCoF percentual variations with the increasing apparent power of the BESS (line 5-6) for the above-described scenario.

		RoCoF variation for Control Area 1 (%)		
Tested scenarios	SC power rating (MVA)	500 ms	250 ms	100 ms
3 SCs+3 BESS near the synchronous machines	100	-41.67	-63.64	-64.81
3 SCs+3 BESS near the synchronous machines	300	-52.58	-70.5	-71.46
3 SCs+3 BESS near the synchronous machines	400	-56.97	-73.26	-72.87
3 SCs+3 BESS near the synchronous machines	1000	-73.71	-84.96	-72.57

Installing three synchronous condensers and three BESS near the synchronous machines led to the largest reduction of the RoCoF and the largest increase in the nadir for both fault locations. This RoCoF reduction was even larger than when three synchronous condensers were installed near the synchronous machines and the three BESS were installed near the RES. With three synchronous condensers and three BESS both installed near the synchronous machines, the frequency in Control Area 1 became more damped for larger apparent power values in the BESS. Moreover, the combination of BESS with synchronous condensers near the synchronous machines led to RoCoF and nadir values very similar to those obtained when the network contained only synchronous generation.

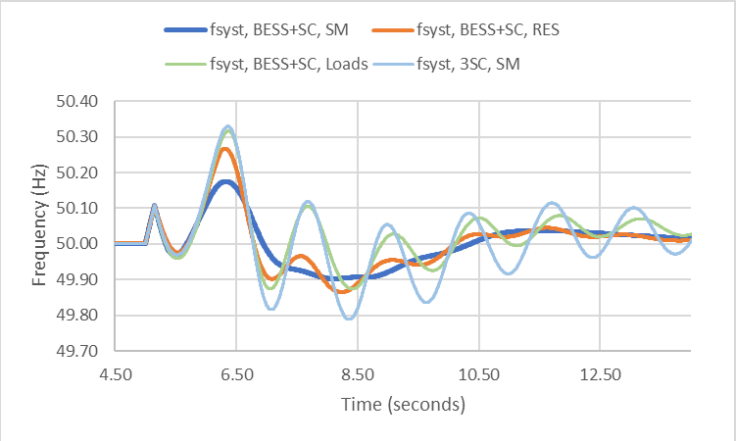

Figure 6.17: Comparison between the frequency of the centre of inertia when 3 1000 MVA synchronous condensers near the SMs and BESS in various locations.

To conclude, Figure 6.17 compares the frequency of the centre of inertia when the three 1000 MVA synchronous condensers are located near the synchronous machines and the BESS are located near the RES, near the loads or near the synchronous machines. When both SCs and BESS are located near the synchronous machines, there is better synchronism in the machines of this power system. Indeed, there are more improvements regarding frequency stability when both BESS and SCs are installed near the synchronous machines because they are installed close to each other: therefore, their inertia contribution becomes higher, improving the RoCoF and the nadir. Moreover, given that both synchronous condensers, BESS and synchronous machines respond fast to the frequency changes, and both provide active and reactive power, they respond faster when located in the same area.

Therefore, the combination of both control strategies shows that it is possible to operate a system with reduced inertia and have frequency indicators as acceptable as the ones obtained for a system containing only synchronous generation. Such is coherent to the findings in [40], where it is stated that the combined inertial response of a synchronous condenser and a BESS make it possible to emulate the response of a synchronous generator to a frequency event.

6.11 Final Remarks

First, this chapter included the Frequency Sensitive Modes in each converter, concluding that they were not enough to mitigate the RoCoF results given their limited active power contribution. Hence, other control strategies were tested.

When installing synchronous condensers, the first scenarios to be compared were the installation of 3 SCs near RES and the installation of 3 SCs near the synchronous machines. Since the synchronous condensers used for both scenarios had the same characteristics, the increase in the power system's inertia constant was the same, being the only difference the location of the synchronous condensers. This led to different nadir and RoCoF results, which proves that it is not enough to simply provide the power system with more inertia: the location of the devices is also an important factor to consider.

By analysing and comparing the nadir results for 3 SCs near the RES and 3 SCs near the SMs, it was concluded that there must be a compromise between wanting a higher nadir (which is achieved by placing the synchronous condensers near the synchronous machines) or better voltage improvement in all the generation buses (which is achieved by placing the synchronous condensers near the renewables). Installing synchronous condensers near the synchronous machines led to local voltage improvement (mostly near the synchronous machines), and to lower RoCoF. However, when installing synchronous condensers near the synchronous machines, the voltage in the remaining generation buses with RES did not vary significantly with the SC's apparent power. On the other hand, installing synchronous condensers near RES led to global voltage improvement, but to lower nadir improvement.

Regarding BESS, it was seen that the number or the apparent power of the batteries did not greatly influence the nadir and RoCoF when installed close to the renewable energy sources. The apparent power of the BESS did not greatly influence the voltage in the generation buses either, despite the different BESS locations. Regardless of their location, BESS alone do not lead to significant RoCoF improvements. Moreover, when located near the RES or near the loads, BESS alone can create less stabilization issues than synchronous condensers.

Unlike BESS, synchronous condensers alone are a promising solution because they can improve both the RoCoF and the nadir when installed near the synchronous machines. Synchronous condensers alone can provide RoCoF lower than 1 Hz/s provided they have large apparent powers. However, the best results were achieved with a combination of synchronous condensers and BESS located near the synchronous machines.

Chapter 7

Contributions of this Dissertation

7.1 Main outcomes of this work

This work relies on the dynamic/transient behaviour of a transmission grid with reduced inertia, taking as a reference the IEEE 39-Bus system, which contained only synchronous generation in the reference case. This work has created a reduced inertia scenario by installing 83% of renewable energy generation, and by reducing in 25% the inertia constant in the remaining synchronous machines. By analysing the frequency indicators (RoCoF – Rate of Change of Frequency – and nadir, the minimum frequency value) in these circumstances, it was shown that indeed a system with reduced inertia is prone to high RoCoF and lower nadir.

If no strategies to improve the frequency indicators during faults are employed, the high RoCoF and low nadir can trigger the protections of the synchronous machines and distributed generation, which can lead to under-frequency load shedding and further aggravate the existing problem. To arrest the frequency changes, three solutions were tested and compared in this dissertation: the inclusion of active power-frequency control in the RES, the inclusion of synchronous condensers and the inclusion of BESS (Battery Energy Storage Systems). Given the importance of the accurate sizing of these solutions, a sensitivity analysis was carried to understand the influence of the location and the apparent power of the BESS/synchronous condensers in the frequency indicators.

The active power-frequency control (i.e., the inclusion of Frequency Sensitive Modes, represented by the Power Plant Controller of the renewables) alone was not enough to mitigate the frequency problems, as it did not strongly influence the results obtained because of its limited active power provision.

The inclusion of synchronous condensers has revealed to be a promising solution because they provide high active and reactive power, hence improving the RoCoF and nadir. However, their effectiveness is very dependent on their location, and their apparent power/inertia time constant are also important aspects to consider. In this study, the synchronous condensers' apparent power was progressively increased, and the value of the inertia constant was maintained. Instead, testing the effects of progressively increasing the inertia constant for the same apparent power values would have also been relevant. If synchronous condensers are to be operated alone, they are more efficient when located near the synchronous machines and with high apparent powers, as more inertia is provided to the power system and because the voltage in near the synchronous machines is higher, which ensures that more energy is produced to counteract the effects of the fault.

Finally, battery energy storage systems were also tested. Battery energy storage systems, when operating alone and regardless of their location, are unable to reduce the RoCoF to acceptable levels. Regardless of their location, they can slightly improve the nadir, even if the improvements do not significantly vary with the BESS' apparent power.

The most promising results were achieved when both BESS and synchronous condensers were installed. For testing this hypothesis, the three synchronous condensers had 1000 MVA and were placed near the three remaining synchronous machines, being the BESS either placed near the RES or near the synchronous machines. In both situations, the frequency indicators improved, but the highest RoCoF reductions were accomplished by having both BESS and synchronous condensers near the synchronous machines. This happens because synchronous condensers, BESS and synchronous machines respond fast to the frequency changes, and both provide active and reactive power. Therefore, these advantages are enhanced when these devices located in the same area. It was also seen that, when three synchronous condensers with 1000 MVA are installed near the synchronous machines, installing additional BESS near the loads can be more effective than installing additional synchronous condensers in this exact location. Therefore, although BESS alone do not solve the frequency problems of transmission systems with reduced inertia, they can enhance the action of synchronous condensers.

7.2 Future work

In this work, it has been demonstrated that synchronous condensers alone or in combination with BESS are a solution with potential to improve the RoCoF and nadir after the loss of transmission lines, which are challenging events regarding frequency stability. For a fixed scenario of renewable energy integration, the location of the synchronous condensers and BESS played an important role, being the improvement more significant when they were located near the synchronous machines than when they were located near the RES. Even though this statement remained valid for different fault locations within the same scenario of renewable energy integration, it is not yet understood if it still applies to different renewable energy integration scenarios. Therefore, it is important to conduct a sensitivity analysis of the key frequency indicators to the location and apparent power of the synchronous condensers where both the fault locations and the renewable energy integration scenario is varied.

Another method for improving the key frequency indicators to be tested in future works should be the integration of the grid forming converters in weak grids. There are not yet PSS/E models of grid forming converters, which was the reason why this work only admitted that all the considered converters worked in a grid-following mode. Then, future works should focus on creating the dynamic models of grid forming converters to perform the same sensitivity analysis in systems with reduced inertia.

Appendix A

Modelling the IEEE 39-bus network

This appendix presents the main data of the IEEE 39-bus system, therefore showing the data of synchronous generators, transformers, and lines composing this system.

A.1 Characteristics of the synchronous machines in the IEEE 39-bus system

Generator	Bus	Un (kV)	Sn (MVA)	Pmax (MW)	Pmin (MW)	Qmax (MW)	Qmin (MW)
G1	30	22	1000	843.9999	309	538	-184.136
G2	31	22	700	591	216	377	-128.8952
G3	32	22	800	675	247	431	-147.3088
G4	33	22	800	675	247	431	-147.3088
G5	34	22	800	675	247	431	-147
G6	35	22	800	675	247	431	-147.3088
G7	36	22	700	591	216	377	-128.8952
G8	37	22	700	591	216	377	-128.8952
G9	38	22	1000	843.9999	309	538	-184.136
G10	39	22	10000	8442	3088	5382	-1841.36

A.2 The parameters of the transformers of the IEEE 39-bus system

Transformer	From bus	V1 (p.u.)	To bus	V2 (p.u.)	Sb_{system} (MVA)
T1	2	345	30	22	100
T2	6	345	31	22	
T3	10	345	32	22	
T4	11	345	12	138	
T5	12	138	13	345	
T6	19	345	20	230	
T7	19	345	33	22	
T8	20	230	34	22	
T9	22	345	35	22	
T10	23	345	36	22	
T11	25	345	37	22	
T12	29	345	38	22	

A.3 The parameters of the lines of the IEEE 39-bus system

From bus	To bus	R (p.u.)	X (p.u.)	Charging B (p.u.)
1	2	0.0035	0.0411	0.6987
1	39	0.001	0.025	0.75
2	3	0.0013	0.0151	0.2572
2	25	0.007	0.0086	0.146
3	4	0.0013	0.0213	0.2214
3	18	0.0011	0.0133	0.2138
4	5	0.0008	0.0128	0.1342
4	14	0.0008	0.0129	0.1382
5	6	0.0002	0.0026	0.0434
5	8	0.0008	0.0112	0.1476
6	7	0.0006	0.0092	0.113
6	11	0.0007	0.0082	0.1389
7	8	0.0004	0.0046	0.078
8	9	0.0023	0.0363	0.3804
9	39	0.001	0.025	1.2
10	11	0.0004	0.0043	0.0729
10	13	0.0004	0.0043	0.0729
13	14	0.0009	0.0101	0.1723
14	15	0.0018	0.0217	0.366
15	16	0.0009	0.0094	0.171
16	17	0.0007	0.0089	0.1342
16	19	0.0016	0.0195	0.304
16	21	0.0008	0.0135	0.2548
16	24	0.0003	0.0059	0.068
17	18	0.0007	0.0082	0.1319
17	27	0.0013	0.0173	0.3216
21	22	0.0008	0.014	0.2565
22	23	0.0006	0.0096	0.1846
23	24	0.0022	0.035	0.361
25	26	0.0032	0.0323	0.513
26	27	0.0014	0.0147	0.2396
26	28	0.0043	0.0474	0.7802
26	29	0.0057	0.0625	1.029
28	29	0.0014	0.0151	0.249

A.4 The loads in the IEEE 39-bus system

Bus Number	Voltage (kV)	Pload (MW)	Qload (Mvar)
1	345	0	0
2	345	0	0
3	345	322	2.4
4	345	500	184
5	345	0	0
6	345	0	0
7	345	233.8	84
8	345	522	176
9	345	0	0
10	345	0	0
11	345	0	0
12	138	7.5	88
13	345	0	0
14	345	0	0
15	345	320	153
16	345	329.4	32.3
17	345	0	0
18	345	158	30
19	345	0	0
20	230	628	103
21	345	274	115
22	345	0	0
23	345	274.5	84.6
24	345	308.6	-92.2
25	345	224	47.2
26	345	139	17
27	345	281	75.5
28	345	206	27.6
29	345	283.5	26.9
31	22	9.2	4.6
39	22	1104	250

Appendix B

Dynamic models of conventional synchronous machines

B.1 GENROU parameters for each synchronous machine

Parameters	Bus 30	Bus 31	Bus 32	Bus 33	Bus 34	Bus 35	Bus 36	Bus 37	Bus 38	Bus 39
T'do (<0) (sec)	10.2	6.56	5.7	5.69	5.4	7.3	5.66	6.7	4.79	7
T"do (>0) (sec)	0.05	0.05	0.05	0.05	0.05	0.05	0.05	0.05	0.05	0.05
T'qo (>0) (sec)	0.2	1.5	1.5	1.5	0.44	0.4	1.5	0.41	1.96	0.7
T"qo (>0) (sec)	0.035	0.035	0.035	0.035	0.035	0.035	0.035	0.035	0.035	0.035
H, Inertia (p.u.)	4.2	4.329	4.475	3.575	1.625	4.35	3.771	3.471	3.45	5
D, Speed damping (p.u.)	1.5	1.5	1.5	1.5	1.5	1.5	1.5	1.5	1.5	1.5
Xd (p.u.)	1	2.065	1.996	2.096	5.36	2.032	2.065	2.03	2.106	2
Xq (p.u.)	0.69	1.974	1.896	2.064	4.96	1.928	2.044	1.96	2.05	1.9
X'd (p.u.)	0.31	0.4879	0.4248	0.3488	1.056	0.4	0.343	0.399	0.57	0.6
X'q (p.u.)	0.5	1.19	0.7008	1.328	1.328	0.6512	1.302	0.6377	0.587	0.8
X"d=X"q (p.u.)	0.25	0.35	0.36	0.28	0.712	0.32	0.308	0.315	0.45	1.0
XI (p.u.)	0.125	0.245	0.2432	0.236	0.432	0.1792	0.2254	0.196	0.298	0.3
S (1.0)	0.03	0.03	0.03	0.03	0.03	0.03	0.03	0.03	0.03	0.03
S (1.2)	0.4	0.4	0.4	0.4	0.4	0.4	0.4	0.4	0.4	0.4

B.2 Excitation System (SEXS) of each synchronous machine

Parameters	Values
TA/TB	0.1
TB (>0)	15
K	55
TE	0.35
Emin	0
Emax	5.55

B.3 Turbine Governor (TGOV1) of each synchronous machine

Parameters	Generators in Control Area 1	Generator G10 (Control Area 2)
R	0.06	0.09
T1 (>0) (sec)	0.4	0.4
V MAX	0.86	0.86
V MIN	0.3	0
T2 (sec)	2	2
T3 (>0) (sec)	6	6
Dt	0	0

Appendix C

Dynamic model parameters of RES and Battery Energy Storage Systems

C.1 "CONs" and "ICON" parameters of the REGCA1 model

CONs	Value	Description
ICON M	1	Lvplsw (Low Voltage Power Logic) switch (0: LVPL not present, 1: LVPL present)
J	0.05	Tg, Converter time constant (s)
J+1	0.25	Rrpwr, Low Voltage Power Logic (LVPL) ramp rate limit (pu/s)
J+2	0.85	Brkpt, LVPL characteristic voltage 2 (p.u.)
J+3	0.6	Zerox, LVPL characteristic voltage 1 (p.u.)
J+4	0.3	Lvpl1, LVPL gain (p.u.)
J+5	1.2	Volim, Voltage limit (p.u.) for high voltage reactive current management
J+6	0.85	Lvpnt1, High voltage point for low voltage active current management (p.u.)
J+7	0	Lvpnt0, Low voltage point for low voltage active current management (p.u.)
J+8	-1.7	Iolim, Current limit (p.u.) for high voltage reactive current management (specified as a negative value)
J+9	0.005	Tfltr, Voltage filter time constant for low voltage active current management (s)
J+10	0	Khv, Overvoltage compensation gain used in the high voltage reactive current management
J+11	999	Iqrmax, Upper limit on rate of change for reactive current (p.u.)
J+12	-999	Iqrmin, Lower limit on rate of change for reactive current (p.u.)
J+13	1	Accel, acceleration factor (0 < Accel <= 1)

C.2 STATE variables of the REGCA1 model

STATEs	Description
K	Converter lag for Ipcmd
K+1	Converter lag for Iqcmd
K+2	Voltage filter for low voltage active current management

C.3 VARs of the REGCA1 model

VARs	Description
L	Previous terminal voltage
L+1	Previous terminal voltage angle
L+2	Reactive current overvoltage correction
L+3	Initial machine reactive power from power flow

C.4 Block diagram of the REGCA1 model [31]

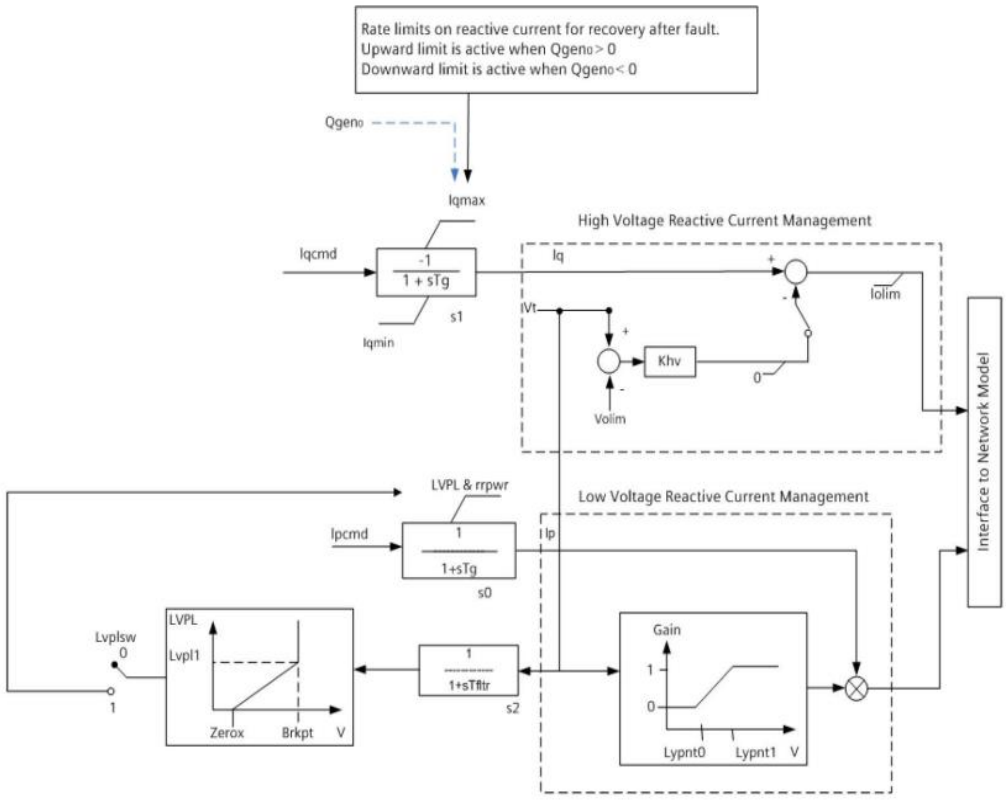

C.5 ICONs of the REECA1 model to be activated during the dynamic simulations

ICONs	Value	Description
M	0	Bus number for voltage control
M+1	1	PFFLAG: 1 if power factor control; 0 if Q control (which can be controlled by an external signal)
M+2	0	VFLAG: 1 if Q control; 0 if voltage control
M+3	0	QFLAG: 1 if voltage or Q control; 0 if constant pf or Q control
M+4	0	PFLAG: 1 if active current command has speed dependency; 0 for no dependency
M+5	1	PQFLAG, P/Q priority flag for current limit: 0 for Q priority; 1 for P priority

C.6 Block diagram of the REECA1 model [31]

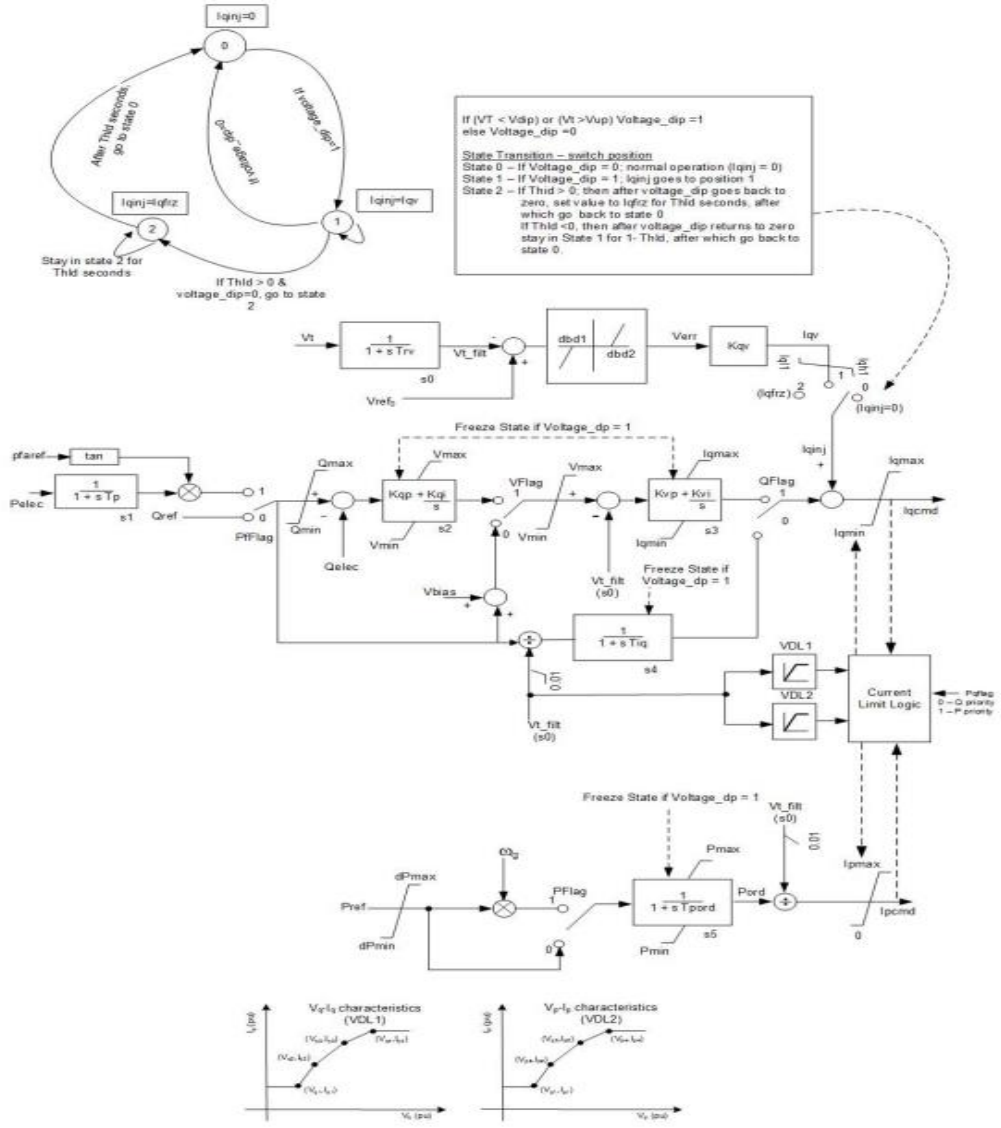

C.7 CONs of the REECA1 model

CONs	Value	Description
J	0.8	Vdip (pu), low voltage threshold to activate reactive current injection logic
J+1	1.2	Vup (pu), Voltage above which reactive current injection logic is activated
J+2	0.5	Trv (s), Voltage filter time constant
J+3	-0.02	dbd1 (pu), Voltage error dead band lower threshold (≤0)
J+4	0.02	dbd2 (pu), Voltage error dead band upper threshold (≥0)
J+5	0.5	Kqv (pu), Reactive current injection gain during over and undervoltage conditions
J+6	999	Iqh1 (pu), Upper limit on reactive current injection Iqinj
J+7	-999	Iql1 (pu), Lower limit on reactive current injection Iqinj
J+8	1	Vref0 (pu), User defined reference (if 0, model initializes it to initial terminal voltage)
J+9	0	Iqfrz (pu), Value at which Iqinj is held for Thld seconds following a voltage dip if Thld > 0
J+10	0	Thld (s), Time for which Iqinj is held at Iqfrz after voltage dip returns to zero (see Note 1)
J+11	0	Thld2 (s) (≥0), Time for which the active current limit (IPMAX) is held at the faulted value after voltage dip returns to zero
J+12	0.02	Tp (s), Filter time constant for electrical power
J+13	999	QMax (pu), limit for reactive power regulator
J+14	-999	QMin (pu) limit for reactive power regulator
J+15	999	VMAX (pu), Max. limit for voltage control
J+16	-999	VMIN (pu), Min. limit for voltage control
J+17	0.5	Kqp (pu), Reactive power regulator proportional gain
J+18	0.5	Kqi (pu), Reactive power regulator integral gain
J+19	0	Kvp (pu), Voltage regulator proportional gain
J+20	0.5	Kvi (pu), Voltage regulator integral gain
J+21	0	Vbias (pu), User-defined bias (normally 0)
J+22	0.5	Tiq (s), Time constant on delay s4
J+23	999	dPmax (pu/s) (>0) Power reference max. ramp rate
J+24	-999	dPmin (pu/s) (<0) Power reference min. ramp rate
J+25	999	PMAX (pu), Max. power limit
J+26	0	PMIN (pu), Min. power limit
J+27	999	Imax (pu), Maximum limit on total converter current
J+28	0.5	Tpord (s), Power filter time constant
J+29	0.2	Vq1 (pu), Reactive Power V-I pair, voltage
J+30	1.1	Iq1 (pu), Reactive Power V-I pair, current
J+31	0.4	Vq2 (pu) (Vq2>Vq1), Reactive Power V-I pair, voltage
J+32	1.1	Iq2 (pu) (Iq2>Iq1), Reactive Power V-I pair, current
J+33	0.6	Vq3 (pu) (Vq3>Vq2), Reactive Power V-I pair, voltage
J+34	1.1	Iq3 (pu) (Iq3>Iq2), Reactive Power V-I pair, current
J+35	0.8	Vq4 (pu) (Vq4>Vq3), Reactive Power V-I pair, voltage
J+36	1.1	Iq4 (pu) (Iq4>Iq3), Reactive Power V-I pair, current
J+37	0.2	Vp1 (pu), Real Power V-I pair, voltage
J+38	1.1	Ip1 (pu), Real Power V-I pair, current
J+39	0.3	Vp2 (pu) (Vp2>Vp1), Real Power V-I pair, voltage
J+40	1.1	Ip2 (pu) (Ip2>Ip1), Real Power V-I pair, current
J+41	0.4	Vp3 (pu) (Vp3>Vp2), Real Power V-I pair, voltage
J+42	1.1	Ip3 (pu) (Ip3>Ip2), Real Power V-I pair, current
J+43	0.85	Vp4 (pu) (Vp4>Vp3), Real Power V-I pair, voltage
J+44	1.1	Ip4 (pu) (Ip4>Ip3), Real Power V-I pair, current

C.8 STATEs of the REECA1 model

STATEs	Description
K	Voltage Measurement filter
K+1	Real power filter
K+2	PI controller for reactive power
K+3	PI controller for voltage error
K+4	First Order lag for reactive current
K+5	First order lag for Pord

C.9 VARs of the REECA1 model

VAR	Description
L	Bus reference voltage (Vref0)
L+1	Storage of current state for state transition (possible values: 0, 1 or 2)
L+2	Power factor reference angle (P_{faref}), radians
L+3	user defined bias as calculated by the model
L+4	Timer for Thld counter
L+5	Previous value of power reference
L+6	Stored Ipmax value
L+7	Timer for Thld2 counter
L+8	Storage for voltage_dip (used only when Thld2 > 0)

C.10 ICONs of the REPCA1 model

ICONs	Value	Description
M	0	Bus number for voltage control
M+1	0	Monitored branch FROM bus number for line drop compensation (if 0 generator power will be used)
M+2	0	Monitored branch TO bus number for line drop compensation (if 0 generator power will be used)
M+3	0	Branch circuit id for line drop compensation (enter in single quotes) (if 0 generator power will be used)
M+4	0	VC Flag (droop flag): 0 - with droop if power factor control; 1 - with line drop compensation
M+5	0	RefFlag (flag for V or Q control): 0 - Q control; 1 - voltage control
M+6	1	Fflag (flag to disable frequency control): 1 - enable control; 0 - disable

C.11 CONs of the REPCA1 model

CONs	Value	Description
J	0.001	Tfltr, Voltage or reactive power measurement filter time constant (s)
J+1	0.000	Kp, Reactive power PI control proportional gain (pu)
J+2	0.000	Ki, Reactive power PI control integral gain (pu)
J+3	0.000	Tft, Lead time constant (s)
J+4	0.005	Tfv, Lag time constant (s)
J+5	0.800	Vfrz, Voltage below which State s2 is frozen (pu)
J+6	0.000	Rc, Line drop compensation resistance (pu)
J+7	0.000	Xc, Line drop compensation reactance (pu)
J+8	0.000	Kc, Reactive current compensation gain (pu)
J+9	999.000	emax, upper limit on deadband output (pu)
J+10	-999.000	emin, lower limit on deadband output (pu)
J+11	-0.005	dbd1, lower threshold for reactive power control deadband (<=0)
J+12	0.005	dbd2, upper threshold for reactive power control deadband (>=0)
J+13	0.010	Qmax, Upper limit on output of V/Q control (pu)
J+14	-0.010	Qmin, Lower limit on output of V/Q control (pu)
J+15	2.000	Kpg, Proportional gain for power control (pu)
J+16	1.000	Kig, Integral gain for power control (pu)
J+17	0.500	Tp, Real power measurement filter time constant (s)
J+18	-0.001	fdbd1, Deadband for frequency control, lower threshold (specified as per unit frequency deviation) (<=0)
J+19	0.001	fdbd2, Deadband for frequency control, upper threshold (specified as per unit frequency deviation) (>=0)
J+20	999.000	femax, frequency error upper limit (pu)
J+21	-999.000	femin, frequency error lower limit (pu)
J+22	1.000	Pmax, upper limit on power reference (pu)
J+23	0.000	Pmin, lower limit on power reference (pu)
J+24	0.500	Tg, Power Controller lag time constant (s)
J+25	100.000	Ddn, reciprocal of droop for over-frequency conditions (pu)
J+26	100.000	Dup, reciprocal of droop for under-frequency conditions (pu)

C.12 STATEs of the REPCA1 model

STATEs	Description
K	Voltage Measurement filter
K+1	Reactive power control filter
K+2	PI controller for reactive power
K+3	Lead-lag in reactive power path
K+4	Real power filter
K+5	PI controller for real power
K+6	Power controller first order lag

C.13 VARs of the REPCA1 model

VARs	Description
L	Reference for voltage control (Vref)
L+1	Reactive power reference (Qref)
L+2	Frequency reference (Freq_ref)
L+3	Active Power reference (Plant_pref)
L+4	Line flow P (MW)
L+5	Line flow Q (Mvar)
L+6	Line flow (MVA)
L+7	Q/V deadband output
L+8	Frequency deadband output

C.14 Block diagram of the REPCA1 model [31]

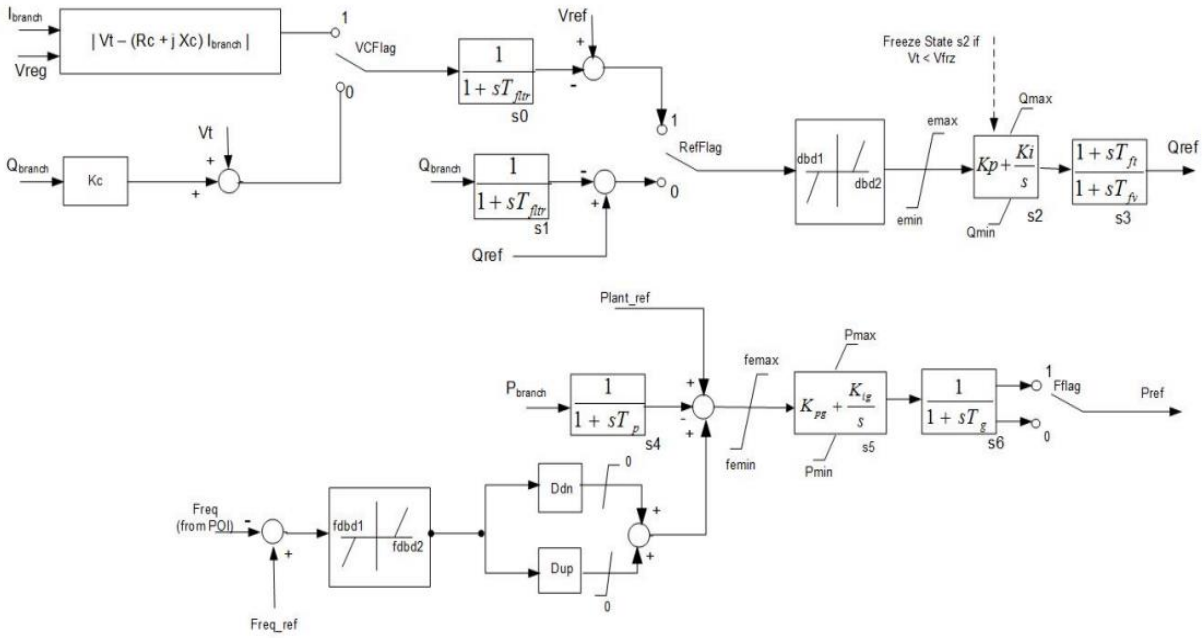

C.15 Parameters of the REGCA1 model representing BESS

CONs	Value	Description
ICONM	0	LVPL switch, 0: LVPL not present, 1: LVPL present
J	0.01	Tg, Converter time constant, second
J+1	0.6667	Rrpwr, LVPL ramp rate limit (pu/s)
J+2	0.9	Brkpt, LVPL voltage 2 (pu)
J+3	0.4	Zerox, LVPL voltage 1 (pu)
J+4	1.22	Lvpl1, LVPL gail (pu)
J+5	1.2	Volim, Voltage limit for High Voltage Reactive Current Management, pu
J+6	0.85	Lvpnt1, High Voltage point for Low Voltage Active Current Management, pu
J+7	0.5	Lvpnt0, Low Voltage point for Low Voltage Active Current Management, pu
J+8	-3	Iolim, Current limit for HVRCM, pu (< 0)
J+9	0.02	Tfltr, Voltage filter time constant for LVRCM (s)
J+10	0	Khv, Overvoltage compensation gain used in HVRCM (>=0 and < 1)
J+11	999	Iqrmax, Upper limit on Rate of change for reactive curent (pu/s)
J+12	-999	Iqrmin, Lower limit on Rate of change for reactive curent (pu/s)
J+13	0	Accel, Acc. factor for smoothing out voltage & angle calculations (>0 and <=1)

C.16 Block diagram of the REECCU1 model for BESS [31]

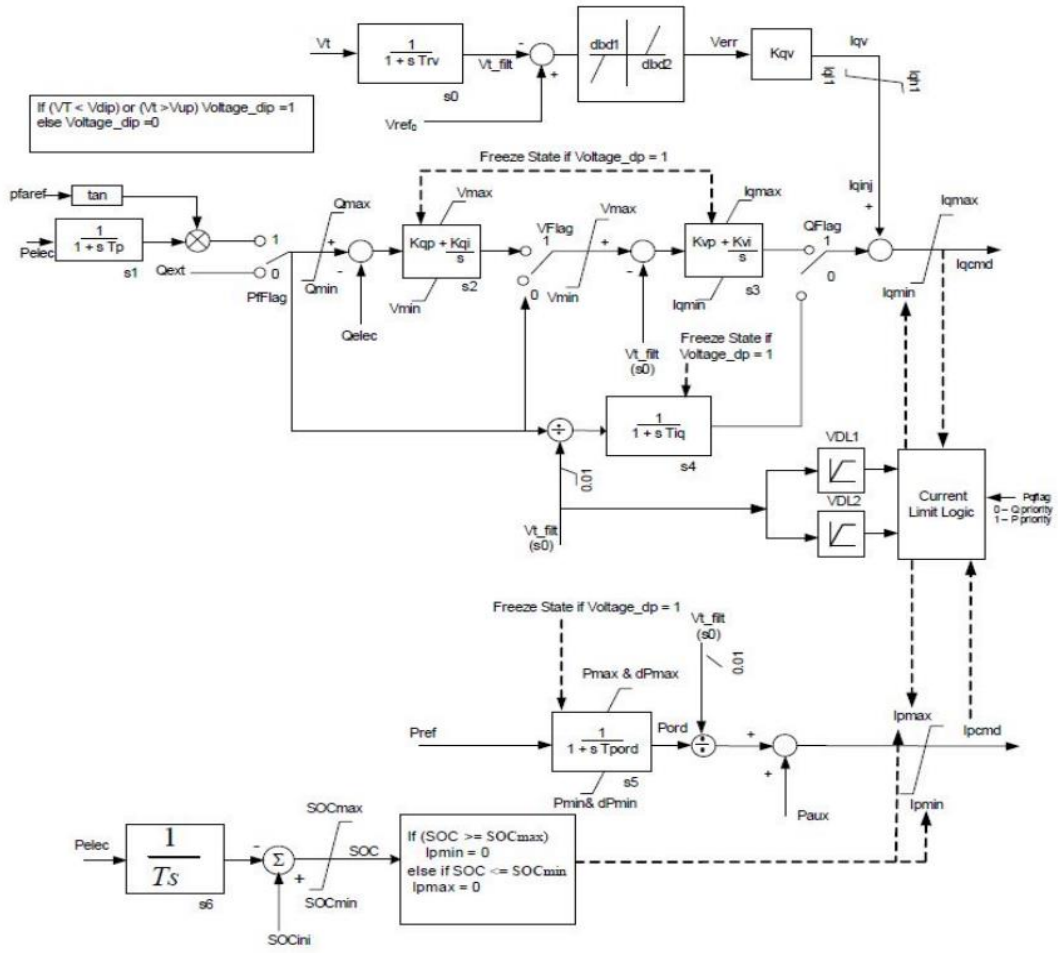

C.17 CONs of the RECCU1 model

CONs	Value	Description
J	0.8	Vdip (pu), low voltage threshold for reactive current injection
J+1	1.2	Vup (pu), high voltage threshold for reactive current injection
J+2	0.02	Trv (s), Voltage filter time constant
J+3	0	dbd1 (pu), Voltage error dead band lower threshold (<=0)
J+4	0	dbd2 (pu), Voltage error dead band upper threshold (>=0)
J+5	0.1	Kqv (pu), Reactive current injection gain
J+6	1.1	Iqhl (pu), Upper limit on reactive current injection Iqinj
J+7	-1.1	Iqll (pu), Lower limit on reactive current injection Iqinj
J+8	1	Vref0 (pu), User defined reference (if 0, initialized by model)
J+9	0.01	Tp (s), Filter time constant for electrical power
J+10	0.4	QMax (pu), limit for reactive power regulator
J+11	-0.4	QMin (pu) limit for reactive power regulator
J+12	1.1	VMAX (pu), Max. limit for voltage control
J+13	0.9	VMIN (pu), Min. limit for voltage control
J+14	0	Kqp (pu), Reactive power regulator proportional gain
J+15	1	Kqi (pu), Reactive power regulator integral gain
J+16	0	Kvp (pu), Voltage regulator proportional gain
J+17	1	Kvi (pu), Voltage regulator integral gain
J+18	0.01	Tiq (s), Time constant on delay s4
J+19	99	dPmax (pu/s) (>0) Power reference max. ramprate
J+20	-99	dPmin (pu/s) (<0) Power reference min. ramprate
J+21	1	PMAX (pu), Max. power limit
J+22	-1	PMIN (pu), Min. power limit
J+23	1.1	Imax (pu), Maximum allowable total converter current limit
J+24	0.01	Tpord (s), Power filter time constant
J+25	0	Vq1 (pu), Reactive Power V-I pair, voltage
J+26	1	Iq1 (pu), Reactive Power V-I pair, current
J+27	0.2	Vq2 (pu) (Vq2>Vq1), Reactive Power V-I pair, voltage
J+28	1	Iq2 (pu) (Iq2>=Iq1), Reactive Power V-I pair, current
J+29	0.5	Vq3 (pu) (Vq3>Vq2), Reactive Power V-I pair, voltage
J+30	1	Iq3 (pu) (Iq3>=Iq2), Reactive Power V-I pair, current
J+31	0.9	Vq4 (pu) (Vq4>Vq3), Reactive Power V-I pair, voltage
J+32	1	Iq4 (pu) (Iq4>=Iq3), Reactive Power V-I pair, current
J+33	0	Vp1 (pu), Real Power V-I pair, voltage
J+34	1.1	Ip1 (pu), Real Power V-I pair, current
J+35	0.2	Vp2 (pu) (Vp2>Vp1), Real Power V-I pair, voltage
J+36	1.1	Ip2 (pu) (Ip2>=Ip1), Real Power V-I pair, current
J+37	0.5	Vp3 (pu) (Vp3>Vp2), Real Power V-I pair, voltage
J+38	1.1	Ip3 (pu) (Ip3>=Ip2), Real Power V-I pair, current
J+39	0.9	Vp4 (pu) (Vp4>Vp3), Real Power V-I pair, voltage
J+40	1.1	Ip4 (pu) (Ip4>=Ip3), Real Power V-I pair, current
J+41	99999	T (s), Battery discharge time (>0)
J+42	20	SOCini (pu), Initial state of charge
J+43	40	SOCmax (pu), Maximum allowable state of charge
J+44	0	SOCmin (pu), Minimum allowable state of charge

C.18 ICONs of the RECCU1 model

ICONs	Value	Description
M	40	Input this as 0. For remote bus control use the plant controller model
M+1	0	PFFLAG (Power factor flag): 1 - power factor control; 0: Q control
M+2	1	VFLAG: 1 if Q control; 0 voltage control
M+3	0	QFLAG: 1 if voltage/Q control; 0 if pf/Q control
M+5	0	PQFLAG: 1 for P priority, 0 for Q priority

C.19 STATEs of the RECCU1 model

STATEs	Description
K	Voltage measurement filter
K+1	Real power filter
K+2	PI controller for reactive power
K+3	PI controller for voltage error
K+4	First order lag for reactive current
K+5	First order lag for Pord
K+6	Energy output from battery

C.20 STATEs of the RECCU1 model

STATEs	Description
K	Voltage measurement filter
K+1	Real power filter
K+2	PI controller for reactive power
K+3	PI controller for voltage error
K+4	First order lag for reactive current
K+5	First order lag for Pord
K+6	Energy output from battery

C.21 VARs of the RECCU1 model

VARs	Description
L	Bus reference voltage (Vref0)
L+1	Power factor reference angle (pfaref), radians
L+2	Real current command (Ipcmd)
L+3	Reactive current command (Iqcmd)
L+4	Battery residual energy
L+5	Auxiliary input signal, Paux

C.22 ICONs of the RECCU1 model

ICONs	Value	Description
M	42	Remote bus number or 0 for local voltage control
M+1	0	Monitored branch FROM bus
M+2	0	Monitored branch TO bus
M+3	'0'	Monitored branch ID (enter within single quotes)
M+4	1	VCFlag, droop flag (0: with droop,1: line drop compensation)
M+5	0	RefFlag, flag for V or Q control (0: Q control, 1: V control)
M+6	1	Fflag, 0: disable frequency control, 1: enable

C.23 ICONs of the REPCA1 model for BESS

ICONs	Value	Description
M	42	Remote bus number or 0 for local voltage control
M+1	0	Monitored branch FROM bus
M+2	0	Monitored branch TO bus
M+3	'0'	Monitored branch ID (enter within single quotes)
M+4	1	VCFlag, droop flag (0: with droop,1: line drop compensation)
M+5	0	RefFlag, flag for V or Q control (0: Q control, 1: V control)
M+6	1	Fflag, 0: disable frequency control, 1: enable

C.24 CONs of the REPCA1 model for BESS

CONs	Value	Description
J	0	Tfltr, Voltage or reactive power measurement filter time constant (s)
J+1	18	Kp, Reactive power PI control proportional gain (pu)
J+2	5	Ki, Reactive power PI control integral gain (pu)
J+3	0	Tft, Lead time constant (s)
J+4	0.15	Tfv, Lag time constant (s)
J+5	0	Vfrz, Voltage below which State s2 is frozen (pu)
J+6	0	Rc, Line drop compensation resistance (pu)
J+7	0	Xc, Line drop compensation reactance (pu)
J+8	0	Kc, Reactive current compensation gain (pu)
J+9	99	emax, upper limit on deadband output (pu)
J+10	-99	emin, lower limit on deadband output (pu)
J+11	0	dbd1, lower threshold for reactive power control deadband (<=0)
J+12	1	dbd2, upper threshold for reactive power control deadband (>=0)
J+13	0.4	Qmax, Upper limit on output of V/Q control (pu)
J+14	-0.4	Qmin, Lower limit on output of V/Q control (pu)
J+15	1	Kpg, Proportional gain for power control (pu)
J+16	0.5	Kig, Integral gain for power control (pu)
J+17	0.05	Tp, Real power measurement filter time constant (s)
J+18	0	fdbd1, Deadband for frequency control, lower threshold (<=0)
J+19	0	fdbd2, Deadband for frequency control, upper threshold (>=0)
J+20	999	femax, frequency error upper limit (pu)
J+21	-999	femin, frequency error lower limit (pu)
J+22	1	Pmax, upper limit on power reference (pu)
J+23	-1	Pmin, lower limit on power reference (pu)
J+24	0	Tg, Power Controller lag time constant (s)
J+25	100	Ddn, droop for over-frequency conditions (pu)
J+26	100	Dup, droop for under-frequency conditions (pu)

Appendix D

Ensuring robustness of the proposed solutions for reduced inertia systems

To ensure robustness of the proposed solutions in Chapter 6, where the detailed results for line 13-14 are analysed, this appendix reunites the results obtained for lines 5-6 and 2-25 for each performed scenario. These results validated the conclusions discussed in Chapter 6 and Chapter 7, proving that these statements remained true for different fault locations.

D.1 Installation of synchronous condensers close to RES

D.1.1 Nadir results for Line 5-6

Scenarios to be tested close to the RES	S (MVA)	Nadir 1	Nadir 2
7 renewables -25% inertia in the Synchronous Generators	-	49.67	49.86
Synchronous condensers at bus 40, 41, 42	100	49.61	49.82
1 synchronous condenser per RES		49.61	49.82
Synchronous condensers at bus 40, 41, 42	300	49.6	49.82
Synchronous condensers at bus 40, 41, 42	400	49.6	49.92

D.1.2 RoCoF results for Line 5-6

		RoCoF for Control Area 1 (Hz/s)			RoCoF for Control Area 2 (Hz/s)			Highest RoCoF Time in Control Area 1 (s)			Highest RoCoF Time in Control Area 2 (s)		
Scenarios to be tested close to the RES	**S (MVA)**	**500 ms**	**250 ms**	**100 ms**	**500 ms**	**250 ms**	**100 ms**	**500 ms**	**250 ms**	**100 ms**	**500 ms**	**250 ms**	**100 ms**
7 RES -25 % in SMs	-	1.32	2.42	2.68	0.315	0.55	0.823	6	6.5	6.5	5	5.25	5.1
SCs at bus 40, 41, 42	100	1.538	2.206	2.587	0.314	0.573	0.879	6	6.5	6.5	5	5.25	5.1
1 SC per RES		1.3989	2.335	2.585	0.304	0.553	0.853	6.5	6.5	6.5	5	5.25	5.1
SCs at buses 40, 41, 42	300	1.206	2.118	2.286	0.29	0.541	0.844	6	6.5	6.5	5	5.25	5.1
SCs at buses 40, 41, 42	400	1.094	1.818	2.29	0.28	0.527	0.829	6	6.5	6.5	5	5.25	5.1

D.1.3 RoCoF reduction percentage for Line 5-6

		RoCoF variation for Control Area 1 (%)		
Tested scenarios	**SC power rating (MVA)**	**500 ms**	**250 ms**	**100 ms**
3 SCs close to RES (close to buses 30, 32, 35)	100	16.52	-8.84	-3.47
3 SCs close to RES (close to buses 30, 32, 35)	300	-8.64	-12.48	-14.7
3 SCs close to RES (close to buses 30, 32, 35)	400	-17.12	-24.88	-14.55

D.1.4 Nadir results for line 2-25

Scenarios to be tested close to the RES	**S (MVA)**	**Nadir 1**	**Nadir 2**
7 renewables -25% inertia in the Synchronous Generators	-	49.73	49.88
Synchronous condensers at bus 40, 41, 42	100	49.57	49.797
1 synchronous condenser per RES		49.51	49.78
Synchronous condensers at bus 40, 41, 42	300	49.51	49.795
Synchronous condensers at bus 40, 41, 42	400	49.488	49.783

D.1.5 RoCoF results for line 2-25

		RoCoF for Control Area 1 (Hz/s)			RoCoF for Control Area 2 (Hz/s)			Highest RoCoF Time in Control Area 1 (s)			Highest RoCoF Time in Control Area 2 (s)		
Scenarios to be tested close to the RES	**S (MVA)**	**500 ms**	**250 ms**	**100 ms**	**500 ms**	**250 ms**	**100 ms**	**500 ms**	**250 ms**	**100 ms**	**500 ms**	**250 ms**	**100 ms**
7 renewables -25% inertia in the Synchronous Generators	-	1.59	1.77	2.27	0.352	0.57	0.832	6	6.5	6.5	5	5.25	5.1
Synchronous condensers at bus 40, 41, 42	100	1.518	2.507	2.748	0.368	0.602	0.877	6	6.5	6.5	5	5.25	5.1
1 synchronous condenser per RES		1.3	2.267	2.668	0.377	0.59	0.862	6	6.5	6.5	5	5.25	5.1
Synchronous condensers at bus 40, 41, 42	300	1.163	1.846	2.585	0.343	0.569	0.848	6	6.5	6.5	5	5.25	5.1
Synchronous condensers at bus 40, 41, 42	400	1.341	2.394	2.639	0.332	0.556	0.836	8	6.75	6.6	5	5.25	5.1

D.1.6 RoCoF reduction percentage for line 2-25

		RoCoF variation for Control Area 1 (%)		
Tested scenarios	**SC power rating (MVA)**	**500 ms**	**250 ms**	**100 ms**
3 SCs close to RES (close to buses 30, 32, 35)	100	-4.53	41.64	21.06
3 SCs close to RES (close to buses 30, 32, 35)	300	-26.86	4.29	13.88
3 SCs close to RES (close to buses 30, 32, 35)	400	-15.66	35.25	16.26

D.2 Installation of synchronous condensers close to the synchronous machines and to buses with high loads

D.2.1 Nadir results for Line 5-6

Scenarios to be tested close to the synchronous machines	**S (MVA)**	**Nadir 1**	**Nadir 2**
Scenario 5	-	49.67	49.86
Synchronous condensers at bus 40, 41, 42	100	49.72	49.87
Synchronous condenser only near bus 31 and 38		49.72	49.84
3 Synchronous condensers near SM + 1 SC at bus 16 + 1 SC at bus 8		49.67	49.86
Synchronous condensers at bus 40, 41, 42	300	49.77	49.88
Synchronous condenser only near bus 31 and 38		49.74	49.88
3 Synchronous condensers near SM + 1 SC at bus 16 + 1 SC at bus 8		49.68	49.86
Synchronous condensers at bus 40, 41, 42	400	49.78	49.9
Synchronous condenser only near bus 31 and 38		49.74	49.89
3 Synchronous condensers near SM + 1 SC at bus 16 + 1 SC at bus 8		49.66	49.85
Synchronous condensers at bus 40, 41, 42	1000	49.8	49.93
Synchronous condenser only near bus 31 and 38		49.73	49.92

D.2.2 RoCoF results for Line 5-6

		RoCoF for Control Area 1 (Hz/s)			RoCoF for Control Area 2 (Hz/s)			Max. RoCoF Time in Control Area 1 (s)			Max. RoCoF Time in Control Area 2 (s)		
Scs. Close to the SMs	**SC (MVA)**	**500 ms**	**250 ms**	**100 ms**	**500 ms**	**250 ms**	**100 ms**	**500 ms**	**250 ms**	**100 ms**	**500 ms**	**250 ms**	**100 ms**
Scenario 5	-	1.32	2.42	2.68	0.315	0.55	0.823	6	6.5	6.5	5	5.25	5.1
Synchronous condensers at bus 40, 41, 42	100	1.049	1.944	2.06	0.3	0.536	0.823	6	6.5	6.5	5	5.25	5.1
Synchronous condenser only near bus 31 and 38		1.37	1.734	2.299	0.361	0.569	0.828	6	6	5.3	5	5.25	5.1
3 Synchronous condensers near SM + 1 SC at bus 16 + 1 SC at bus 8		0.729	1.823	1.936	0.287	0.519	0.8	6.5	6.5	6.5	5	5.25	5.1
Synchronous condensers at bus 40, 41, 42	300	0.732	1.298	1.648	0.277	0.516	0.8044	6	6.5	6.6	5	5.25	5.1
Synchronous condenser only near buses 31 and 38		0.872	1.523	1.944	0.287	0.528	0.821	6	6.5	6.6	5	5.25	5.1
3 Synchronous condensers near SM + 1 SC at bus 16 + 1 SC at bus 8		0.764	1.634	1.895	0.246	0.471	0.743	9.5	6.75	6.6	5	5.25	5.1
Synchronous condensers at bus 40, 41, 42	400	0.639	1.163	1.492	0.268	0.508	0.796	6	6.5	6.5	5	5.25	5.1
Synchronous condenser only near bus 31 and 38		0.789	1.421	1.825	0.28	0.524	0.819	6	6.75	6.5	5	5.25	5.1
3 Synchronous condensers near SM + 1 SC at bus 16 + 1 SC at bus 8		1.177	1.732	1.871	0.23	0.45	0.718	7	6.75	6.8	5	5.25	5.1
Synchronous condensers at bus 40, 41, 42	1000	0.849	0.969	1.045	0.23	0.468	0.754	7	6.75	6.8	5	5.25	5.1
Synchronous condenser only near bus 31 and 38		1.181	1.324	1.462	0.259	0.504	0.81	7	6.75	6.8	5	5.25	5.1

D.2.3 RoCoF reduction percentage for Line 5-6

		RoCoF variation for Control Area 1 (%)		
Tested scenarios	**SC power rating (MVA)**	**500 ms**	**250 ms**	**100 ms**
3 SCs near synchronous machines	100	-20.53	-19.67	-23.13
3 SCs near synchronous machines	300	-44.55	-46.36	-38.51
3 SCs near synchronous machines	400	-51.59	-51.94	-44.33
3 SCs near synchronous machines	1000	-35.68	-59.96	-61.01
2 SCs near bus 31 and 38	100	3.79	-28.35	-14.22
2 SCs near bus 31 and 38	300	-33.94	-37.07	-27.46
2 SCs near bus 31 and 38	400	-40.23	-41.28	-31.9
2 SCs near bus 31 and 38	1000	-10.53	-45.29	-45.45
3 Scs near the SMs + 1 SC near bus 16 + 1 SC near bus 8	100	-44.77	-32.75	-27.76
3 Scs near the SMs + 1 SC near bus 16 + 1 SC near bus 8	300	-42.12	-32.48	-29.29
3 Scs near the SMs + 1 SC near bus 16 + 1 SC near bus 8	400	-10.83	-28.43	-30.19

D.2.4 Nadir results for Line 2-25

Scenarios to be tested close to the synchronous machines	S (MVA)	Nadir 1	Nadir 2
Scenario 5	-	49.73	49.88
Synchronous condensers at bus 40, 41, 42	100	49.79	49.86
Synchronous condenser only near bus 31 and 38		49.76	49.85
3 SCs near SM + 1 SC at bus 16 + 1 SC at bus 8		49.77	49.82
SCs at bus 40, 41, 42	300	49.82	49.86
SCs only near bus 31 and 38		49.79	49.86
3 SCs near SM + 1 SC at bus 16 + 1 SC at bus 8		49.57	49.78
SCs at bus 40, 41, 42	400	49.81	49.86
SCs only near bus 31 and 38		49.79	49.86
SCs at bus 40, 41, 42	1000	49.8	49.9
SCs only near bus 31 and 38		49.75	49.88

D.2.5 RoCoF results for Line 2-25

		RoCoF for Control Area 1 (Hz/s)			RoCoF for Control Area 2 (Hz/s)			Max. RoCoF Time in Control Area 1 (s)			Max. RoCoF Time in Control Area 2 (s)		
Scenarios to be tested close to the synchronous machines	**S (MVA)**	**500 ms**	**250 ms**	**100 ms**	**500 ms**	**250 ms**	**100 ms**	**500 ms**	**250 ms**	**100 ms**	**500 ms**	**250 ms**	**100 ms**
Scenario 5	-	1.59	1.77	2.27	0.352	0.57	0.832	6	6.5	6.5	5	5.25	5.1
SCs at bus 40, 41, 42	100	1.307	1.491	1.801	0.34	0.556	0.825	6	6	5.3	5	5.25	5.1
SCs near bus 31 and 38		1.394	1.596	1.955	0.344	0.56	0.831	6	6	5.3	5	5.25	5.1
3 SCs near SMs + 1 SC at bus 16 + 1 SC at bus 8		1.222	1.397	1.617	0.325	0.532	0.797	6	6	5.3	5	5.25	5.1
SCs at bus 40, 41, 42	300	0.988	1.182	1.296	0.319	0.531	0.798	6	6	5.3	5	5.25	5.1
SCs near buses 31 and 38		1.138	1.374	1.557	0.331	0.543	0.814	6	6	5.3	5	5.25	5.1
3 SCs near SM + 1 SC at bus 16 + 1 SC at bus 8		1.332	1.374	2	0.336	0.472	0.728	7	6.25	6.8	8	5.25	5.1
SCs at bus 40, 41, 42	400	0.884	1.077	1.143	0.31	0.52	0.786	6	6	5.3	5	5.25	5.1
SCs near bus 31 and 38		1.037	1.24	1.466	0.325	0.536	0.808	6	6	5.3	5	5.25	5.1
SCs at bus 40, 41, 42	1000	0.696	0.805	0.865	0.268	0.47	0.729	6.5	6.25	8.9	5	5.25	5.1
SCs near bus 31 and 38		0.92	1.075	1.19	0.317	0.51	0.78	6.5	6.25	9	7	5.25	5.1

D.2.6 RoCoF reduction percentage for Line 2-25

		RoCoF variation for Control Area 1 (%)		
Tested scenarios	**SC power rating (MVA)**	**500 ms**	**250 ms**	**100 ms**
3 SCs near synchronous machines	100	-17.8	-15.76	-20.66
3 SCs near synchronous machines	300	-37.86	-33.22	-42.91
3 SCs near synchronous machines	400	-44.4	-39.15	-49.65
3 SCs near synchronous machines	1000	-56.23	-54.52	-61.89
2 SCs near bus 31 and 38	100	-12.33	-9.83	-13.88
2 SCs near bus 31 and 38	300	-28.43	-22.37	-31.41
2 SCs near bus 31 and 38	400	-34.78	-29.94	-35.42
2 SCs near bus 31 and 38	1000	-42.14	-39.27	-47.58
3 Scs near buses 31, 38, and 39 + 1 SC near bus 16 + 1 SC near bus 8	100	-23.14	-21.07	-28.77
3 Scs near buses 31, 38, and 39 + 1 SC near bus 16 + 1 SC near bus 8	300	-16.23	-22.37	-11.89

D.3 Installation of BESS close to the RES

D.3.1 Nadir results for Line 13-14

Scenario no.	**Scenarios**	**S, BESS (MVA)**	**Nadir 1**	**Nadir 2**
Base case	Scenario 5	-	49.74	49.92
1	3 BESS near RES (near buses 30, 32, and 35)	100	49.72	49.91
2	3 BESS near RES (near buses 30, 32, and 35)	300	49.75	49.89
3	3 BESS near RES (near buses 30, 32, and 35)	400	49.76	49.89
4	3 BESS near RES (near buses 30, 32, and 35)	1000	49.75	49.88

D.3.2 RoCoF results for Line 13-14

		RoCoF for Control Area 1 (Hz/s)			**RoCoF for Control Area 2 (Hz/s)**			**Max. RoCoF Time in Control Area 1 (s)**			**Max. RoCoF Time in Control Area 2 (s)**		
Scenario no.	**S, BESS (MVA)**	**500 ms**	**250 ms**	**100 ms**	**500 ms**	**250 ms**	**100 ms**	**500 ms**	**250 ms**	**100 ms**	**500 ms**	**250 ms**	**100 ms**
Base case	-	1.36	2.236	2.52	0.293	0.492	0.715	6	6.5	6.5	5	5.25	5.1
1	100	1.36	2.213	2.48	0.293	0.491	0.721	6	6.5	6.4	5	5.25	5.1
2	300	1.32	2.13	2.43	0.293	0.488	0.719	6	6.5	6.4	5	5.25	5.1
3	400	1.32	2.11	2.44	0.294	0.488	0.725	6	6.5	6.4	5	5.25	5.1
4	1000	1.28	1.96	2.395	0.295	0.485	0.713	6	6.5	6.4	5	5.25	5.1

D.3.3 RoCoF reduction percentage for Line 13-14

Tested scenarios	SC power rating (MVA)	RoCoF variation for Control Area 1 (%)		
		500 ms	250 ms	100 ms
3 BESS near RES (near buses 30, 32, and 35)	100	0	-1.03	-1.59
3 BESS near RES (near buses 30, 32, and 35)	300	-2.94	-4.74	-3.57
3 BESS near RES (near buses 30, 32, and 35)	400	-2.94	-5.64	-3.17
3 BESS near RES (near buses 30, 32, and 35)	1000	-5.88	-12.34	-4.96

D.3.4 Nadir results for Line 2-25

Scenario no.	Scenarios	S, BESS (MVA)	Nadir 1	Nadir 2
Base case	Scenario 5	-	49.73	49.88
1	3 BESS near RES (near buses 30, 32, and 35)	100	49.73	49.85
2	3 BESS near RES (near buses 30, 32, and 35)	300	49.73	49.83
3	3 BESS near RES (near buses 30, 32, and 35)	400	49.73	49.83

D.3.5 RoCoF results for Line 2-25

Scenario no.	S, BESS (MVA)	RoCoF for Control Area 1 (Hz/s)			RoCoF for Control Area 2 (Hz/s)			Max. RoCoF Time in Control Area 1 (s)			Max. RoCoF Time in Control Area 2 (s)		
		500 ms	250 ms	100 ms	500 ms	250 ms	100 ms	500 ms	250 ms	100 ms	500 ms	250 ms	100 ms
Base case	-	1.59	1.77	2.27	0.352	0.57	0.832	6	6.5	6.5	5	5.25	5.1
1	100	1.59	1.76	2.26	0.352	0.57	0.84	6	6.5	6.4	5	5.25	5.1
2	300	1.58	1.75	2.26	0.351	0.57	0.838	6	6.5	6.4	5	5.25	5.1
3	400	1.58	1.75	2.26	0.351	0.57	0.838	6	6.5	6.4	5	5.25	5.1

D.3.6 RoCoF reduction percentage for Line 2-25

Tested scenarios	SC power rating (MVA)	RoCoF variation for Control Area 1 (%)		
		500 ms	250 ms	100 ms
3 BESS near RES (near buses 30, 32, and 35)	100	0	-0.56	-0.44
3 BESS near RES (near buses 30, 32, and 35)	300	-0.63	-1.13	-0.44
3 BESS near RES (near buses 30, 32, and 35)	400	-0.63	-1.13	-0.44

D.3.7 Nadir results for Line 13-14

Scenario no.	Scenarios	S, BESS (MVA)	Nadir 1	Nadir 2
Base case	Scenario 5	-	49.74	49.92
1	7 BESS near RES (buses 30, 32, 33, 34, 35, 36, 37)	100	49.74	49.91
2	7 BESS near RES (buses 30, 32, 33, 34, 35, 36, 37)	300	49.76	49.9
3	7 BESS near RES (buses 30, 32, 33, 34, 35, 36, 37)	400	49.76	49.87

D.3.8 RoCoF results for Line 13-14 (1 BESS per RES)

		RoCoF for Control Area 1 (Hz/s)			RoCoF for Control Area 2 (Hz/s)			Max. RoCoF Time in Control Area 1 (s)			Max. RoCoF Time in Control Area 2 (s)		
Scenario no.	**S, BESS (MVA)**	**500 ms**	**250 ms**	**100 ms**	**500 ms**	**250 ms**	**100 ms**	**500 ms**	**250 ms**	**100 ms**	**500 ms**	**250 ms**	**100 ms**
Base case	-	1.36	2.236	2.52	0.293	0.492	0.715	6	6.5	6.5	5	5.25	5.1
1	100	1.34	2.199	2.449	0.293	0.49	0.72	6	6.5	6.5	5	5.25	5.1
2	300	1.31	1.997	2.395	0.291	0.486	0.716	6	6.5	5.1	5	5.25	5.1
3	400	1.289	1.894	2.381	0.291	0.485	0.714	6	6.5	5.1	5	5.25	5.1

D.3.9 RoCoF results for Line 13-14 (1 BESS per RES)

		RoCoF variation for Control Area 1 (%)		
Scenario no.	**SC power rating (MVA)**	**500 ms**	**250 ms**	**100 ms**
1	100	-1.47	-1.65	-2.82
2	300	-3.68	-10.69	-4.96
3	400	-5.22	-15.3	-5.52

D.4 Installation of 3 synchronous condensers with 1000 MVA and 3 BESS near the RES

D.4.1 Nadir results for Line 13-14

Scenario no.	Scenarios	S, BESS (MVA)	Nadir 1	Nadir 2
Base case	7 renewables -25% inertia in the synchronous generators	-	49.74	49.92
1	3 SCs near the synchronous machines + 3 BESS near the RES (30, 32, 35)	100	49.84	49.95
2	3 SCs near the synchronous machines + 3 BESS near the RES (30, 32, 35)	300	49.86	49.93
3	3 SCs near the synchronous machines + 3 BESS near the RES (30, 32, 35)	400	49.86	49.92
4	3 SCs near the synchronous machines + 3 BESS near the RES (30, 32, 35)	1000	49.88	49.9

D.4.2 RoCoF results for Line 13-14

		RoCoF for Control Area 1 (Hz/s)			RoCoF for Control Area 2 (Hz/s)			Max. RoCoF Time in Control Area 1 (s)			Max. RoCoF Time in Control Area 2 (s)		
Scenario no.	**S, BESS (MVA)**	**500 ms**	**250 ms**	**100 ms**	**500 ms**	**250 ms**	**100 ms**	**500 ms**	**250 ms**	**100 ms**	**500 ms**	**250 ms**	**100 ms**
Base case	-	1.36	2.236	2.52	0.293	0.492	0.715	6	6.5	6.5	5	5.25	5.1
1	100	0.815	0.872	0.998	0.224	0.412	0.622	7	7	6.7	5	5.25	5.1
2	300	0.722	0.76	0.87	0.209	0.395	0.608	7	6.75	6.8	5	5.25	5.1
3	400	0.7	0.74	0.847	0.212	0.397	0.608	7	7	6.8	5	5.25	5.1
4	1000	0.609	0.666	0.73	0.232	0.405	0.603	7	6.75	6.7	5	5.25	5.1

D.4.3 RoCoF percentual reduction for Line 13-14

		RoCoF variation for Control Area 1 (%)		
Tested scenarios	**SC power rating (MVA)**	**500 ms**	**250 ms**	**100 ms**
1	100	-40.07	-61	-60.4
2	300	-46.91	-66.01	-65.48
3	400	-48.53	-66.91	-66.39
4	1000	-55.22	-70.21	-71.03

D.5 Installation of 3 BESS near the synchronous machines

D.5.1 Nadir results for Line 13-14

Scenario no.	Scenarios for the integration of BESS	S, BESS (MVA)	Nadir 1	Nadir 2
Base Case	Scenario 5	-	49.74	49.92
1	3 BESS near the synchronous machines	100	49.76	49.91
2	3 BESS near the synchronous machines	300	49.77	49.91
3	3 BESS near the synchronous machines	400	49.77	49.91
4	3 BESS near the synchronous machines	1000	49.77	49.91

D.5.2 RoCoF results for Line 13-14

		RoCoF for Control Area 1 (Hz/s)			RoCoF for Control Area 2 (Hz/s)			Max. RoCoF Time in Control Area 1 (s)			Max. RoCoF Time in Control Area 2 (s)		
Scenario no.	**S, BESS (MVA)**	**500 ms**	**250 ms**	**100 ms**	**500 ms**	**250 ms**	**100 ms**	**500 ms**	**250 ms**	**100 ms**	**500 ms**	**250 ms**	**100 ms**
Base Case	-	1.36	2.236	2.52	0.293	0.492	0.715	6	6.5	6.5	5	5.25	5.1
1	100	1.32	2.056	2.44	0.289	0.49	0.721	6	6.5	6.4	5	5.25	5.1
2	300	1.236	1.686	2.432	0.281	0.486	0.721	6	6.5	5.1	5	5.25	5.1
3	400	1.194	1.54	2.43	0.277	0.484	0.721	6	6	5.1	5	5.25	5.1
4	1000	0.989	1.555	2.41	0.255	0.471	0.719	6	5.5	5.1	5	5.25	5.1

D.5.3 RoCoF percentual reduction for Line 13-14

		RoCoF variation for Control Area 1 (%)		
Tested scenarios	**SC power rating (MVA)**	**500 ms**	**250 ms**	**100 ms**
3 BESS near the synchronous machines	100	-2.94	-8.05	-3.17
3 BESS near the synchronous machines	300	-9.12	-24.6	-3.49
3 BESS near the synchronous machines	400	-12.21	-31.13	-3.57
3 BESS near the synchronous machines	1000	-27.28	-30.46	-4.37

D.6 Combining synchronous condensers with BESS near the loads

D.6.1 Nadir results for Line 13-14

Scenario no.	Scenarios for the integration of BESS	S, BESS (MVA)	Nadir 1	Nadir 2
Base Case	7 renewables -25% inertia in the synchronous generators	-	49.74	49.92
1	3 Synchronous condensers near SM + 1 BESS at bus 16 + 1 BESS at bus 8	100	49.86	49.96
2	4 Synchronous condensers near SM + 1 BESS at bus 16 + 1 BESS at bus 8	300	49.87	49.97
3	5 Synchronous condensers near SM + 1 BESS at bus 16 + 1 BESS at bus 8	400	49.88	49.98
4	6 Synchronous condensers near SM + 1 BESS at bus 16 + 1 BESS at bus 8	1000	49.91	49.99

D.6.2 RoCoF results for Line 13-14

		RoCoF for Control Area 1 (Hz/s)			RoCoF for Control Area 2 (Hz/s)			Max. RoCoF Time in Control Area 1 (s)			Max. RoCoF Time in Control Area 2 (s)		
Scenario no.	S, BESS (MVA)	500 ms	250 ms	100 ms	500 ms	250 ms	100 ms	500 ms	250 ms	100 ms	500 ms	250 ms	100 ms
Base Case	-	1.36	2.236	2.52	0.293	0.492	0.715	6	6.5	6.5	5	5.25	5.1
1	100	0.774	0.881	0.949	0.208	0.394	0.61	7	6.75	6.8	5	5.25	5.1
2	300	0.76	0.876	0.942	0.207	0.392	0.609	7	6.75	6.7	5	5.25	5.1
3	400	0.753	0.872	0.937	0.207	0.392	0.608	7	6.75	6.7	5	5.25	5.1
4	1000	0.705	0.833	0.899	0.204	0.388	0.605	7	6.75	6.8	5	5.25	5.1

D.6.3 RoCoF percentual reduction for Line 13-14

		RoCoF variation for Control Area 1 (%)		
Tested scenarios	SC power rating (MVA)	500 ms	250 ms	100 ms
3 Synchronous condensers near SM + 1 BESS at bus 16 + 1 BESS at bus 8	100	-43.09	-60.6	-62.34
4 Synchronous condensers near SM + 1 BESS at bus 16 + 1 BESS at bus 8	300	-44.12	-60.82	-62.62
5 Synchronous condensers near SM + 1 BESS at bus 16 + 1 BESS at bus 8	400	-44.63	-61	-62.82
6 Synchronous condensers near SM + 1 BESS at bus 16 + 1 BESS at bus 8	1000	-48.16	-62.75	-64.33

D.7 Combining synchronous condensers with BESS near the synchronous machines

D.7.1 Nadir results for Line 13-14

Scenario no.	Scenarios for the integration of BESS	S, BESS (MVA)	Nadir 1	Nadir 2
Base Case	7 renewables -25% inertia in the synchronous generators	-	49.74	49.92
1	3 SCs+3 BESS near the synchronous machines	100	49.87	49.95
2	3 SCs+3 BESS near the synchronous machines	300	49.9	49.94
3	3 SCs+3 BESS near the synchronous machines	400	49.91	49.94
4	3 SCs+3 BESS near the synchronous machines	1000	49.94	49.95

D.7.2 RoCoF results for Line 13-14

		RoCoF for Control Area 1 (Hz/s)			RoCoF for Control Area 2 (Hz/s)			Max. RoCoF Time in Control Area 1 (s)			Max. RoCoF Time in Control Area 2 (s)		
Scenario no.	S, BESS (MVA)	500 ms	250 ms	100 ms	500 ms	250 ms	100 ms	500 ms	250 ms	100 ms	500 ms	250 ms	100 ms
Base Case	-	1.36	2.236	2.52	0.293	0.492	0.715	6	6.5	6.5	5	5.25	5.1
1	100	0.7	0.793	0.854	0.206	0.393	0.611	7	6.75	6.8	5	5.25	5.1
2	300	0.567	0.645	0.71	0.199	0.389	0.611	7	6.75	6.8	5	5.25	5.1
3	400	0.512	0.584	0.71	0.196	0.388	0.611	7	6.75	5.1	5	5.25	5.1
4	1000	0.294	0.337	0.717	0.179	0.377	0.61	7	5.5	5.1	5	5.25	5.1

D.7.3 RoCoF percentual reduction for Line 13-14

		RoCoF variation for Control Area 1 (%)		
Tested scenarios	SC power rating (MVA)	500 ms	250 ms	100 ms
3 SCs+3 BESS near the synchronous machines	100	-48.53	-64.53	-66.11
3 SCs+3 BESS near the synchronous machines	300	-58.31	-71.15	-71.83
3 SCs+3 BESS near the synchronous machines	400	-62.35	-73.88	-71.83
3 SCs+3 BESS near the synchronous machines	1000	-78.38	-84.93	-71.55

References

[1] XFLEX HYDRO. "This is the future of Hydro Power". Online. [Available]: https://www.xflexhydro.com/ (Accessed at 7/01/2023).

[2] ENTSO-E. "TYNDP 2020: Scenario Report". 2020. Online. [Available] : https://eepublicdownloads.azureedge.net/tyndp-documents/TYNDP_2020_Joint_Scenario_Report_ENTSOG_ENTSOE_200629_Final.pdf

[3] Zero- Associação Sistema Terrestre Sustentável, *"Março 100% Renovável: Primeiro mês com consumo de eletricidade assegurado por fontes renováveis é recorde de enorme relevância"*. Online. [Available] : https://zero.ong/marco-100-renovavel-primeiro-mes-com-consumo-de-eletricidade-assegurado-por-fontes-renovaveis-e-recorde-de-enorme-relevancia/

[4] ENTSO-E. "High Penetration of Power Electronic Interfaced Power Sources and the Potential Contribution of Grid Forming Converters". European Network of Transmission System Operators for Electricity: ENTSO-E Technical Group on High Penetration of Power Electronic Interfaced Power Sources." [Online]. Available: www.entsoe.eu

[5] A. Oulis Rousis et al., "State-of-the-Art Literature Review of System Scarcities at High Levels of Renewable Generation," Apr. 2018. [Online]. Available: https://eu-sysflex.com/documents/

[6] Francisco Sousa Fernandes, João Peças Lopes. "Assessment of frequency stability behaviour regarding inertia reduction due to high renewable integration in the Iberian system". IREP 2022. Banff, Canada. 2022. Online. [Available]: https://84e2630e-4427-4242-9907-5a501978e910.usrfiles.com/ugd/84e263_6e8d305c7a7040869343b7fa51df4dac.pdf

[7] Jovica Milanovitch. 14-19 November 2022. "Changing Nature of Power/Energy Systems and Associated Challenges". Presented at Graduate-Level Short Course: Dynamics of Low Carbon Power Systems. Melbourne, Australia.

[8] Michel Rezkalla., Michael Pertl., Mattia. Marinelli (2018). “Electric power system inertia: requirements, challenges and solutions. In *Electrical Engineering*, *100*(4), 2677–2693. August 2018. Springer-Verlag GmbH Germany. [Online]. Available: https://doi.org/10.1007/s00202-018-0739-z

[9] Dragozis, R., & Ernst, D. “Dynamics and control of low inertia power networks with high penetration of renewable energy sources*”*, MsC Dissertation, Electrical Engineering, Faculty of Applied Sciences, Université of Liège, France, 2020. [Online]. Available: http://hdl.handle.net/2268.2/9051

[10] Pieter Tielens, Dirk van Hertem, Ronnie Belmans. “Operation and Control of Power Systems with low synchronous inertia”. November 2017. Faculty of Engineering Science. Leuven, Belgium. [Online]. Available: https://limo.libis.be/primo-explore/fulldisplay?docid=LIRIAS1731471&context=L&vid=Lirias&search_scope=Lirias&tab=default_tab&fromSitemap=1

[11] Rodrigo da Cunha Afonso, João Peças Lopes. “Assessment of Demand Response Impact on the Frequency Stability of Low-Inertia Power Systems”, MsC Dissertation, Electrical and Computer Engineering, Faculdade de Engenharia da Universidade do Porto, Portugal, 2022. [Online]. Available: https://hdl.handle.net/10216/141866

[12] Fernando Maciel Barbosa. 2017. “*Estabilidade de Sistemas Elétricos de Energia”,* Faculdade de Engenharia da Universidade do Porto. [Online]. Available : https://paginas.fe.up.pt/~fmb/wp-content/uploads/2018/07/Estabilidade-SEE-setembro-2017.pdf

[13] Kamala Sarojini Ratnam, K. Palanisamy, Guangya Yang. “Future low-inertia power systems: Requirements, issues, and solutions – A review”. In *Renewable and Sustainable Energy Reviews* (Vol. 124). 2020. Elsevier Ltd. [Online]. Available: https://doi.org/10.1016/j.rser.2020.109773

[14] R. Bründlinger, T. Schaupp, G. Arnold, N. Schäfer, G. Graditi, and G. Adinolfi, "Implementation of the European Network Code on Requirements for Generators on the European national level Implementation of the European Network Code on Requirements for Generators on the European national level Current Status-Trends and Challenges". 2018. [Online]. Available: https://www.researchgate.net/publication/329124454

[15] ENTSO-E. 2012. "Network Code for Requirements for Grid Connection Applicable to All Generators – Requirements in Context of Present Practices" [Online]. Available : https://www.acer.europa.eu/Media/News/Documents/120626%20-%20NC%20RfG%20-%20Requirements%20in%20the%20context%20of%20present%20practices.pdf

[16] Hansen, Anca Daniela, Kaushik Das, Poul Sørensen, Pukhraj Singh, and Andrea Gavrilovic. 2021. "European and Indian Grid Codes for Utility Scale Hybrid Power Plants" *Energies* 14, no. 14: 4335. https://doi.org/10.3390/en14144335

[17] Taul, M. G., Wang, X., Davari, P., & Blaabjerg, F. 2019. "An Overview of Assessment Methods for Synchronization Stability of Grid-Connected Converters under Severe Symmetrical Grid Faults". *IEEE Transactions on Power Electronics*, *34*(10), 9655–9670. [Online]. Available: https://doi.org/10.1109/TPEL.2019.2892142

[18] Ministério do Ambiente e da Ação Climática. Portaria nº 73/2020. March 2020. [Online]. Available: https://dre.pt/dre/detalhe/portaria/73-2020-130273580

[19] ENTSO-E. "ENTSO-E Network Code for Requirements for Grid Connection Applicable to all Generators". 2013. [Online]. Available: https://eepublicdownloads.entsoe.eu/clean-documents/pre2015/resources/RfG/130308_Final_Version_NC_RfG.pdf

[20] Ana Sofia Carvalho da Silva, Carlos Coelho Leal Monteiro Moreira, "Comportamento dinâmico de sistemas de transmissão com inércia reduzida", MsC Dissertation, Electrical and Computer Engineering, Faculdade de Engenharia da Universidade do Porto, Porto, Portugal, 2022. [Online]. Available: https://paginas.fe.up.pt/~up201607775/wp-content/uploads/2022/07/up201607775_AnaSilva_MEEC.pdf

[21] Tamrakar, U., Shrestha, D., Maharjan, M., Bhattarai, B. P., Hansen, T. M., & Tonkoski, R. 2017. "Virtual inertia: Current trends and future directions". In *Applied Sciences (Switzerland)*, Vol. 7, Issue 7, MDPI AG. [Online]. Available: https://doi.org/10.3390/app7070654

[22] Frederico Milano, Florian Dörfler, Gabriela Hug, David J. Hill, Gregor Verbic. 2018. "Foundations and Challenges of Low-Inertia Systems". Energy Systems Integration Partnership Programme (ESIPP). [Online]. Available: https://www.researchgate.net/publication/326111831

[23] Kroposki, B., Johnson, B., Zhang, Y., Gevorgian, V., Denholm, P., Hodge, B. M., & Hannegan, B. 2017. "Achieving a 100% Renewable Grid: Operating Electric Power Systems with Extremely High Levels of Variable Renewable Energy". *IEEE Power and Energy Magazine*, *15*(2), 61–73. https://doi.org/10.1109/MPE.2016.2637122

[24] Mukund R. Patel, Omid Beik, "Wind and Solar Power Systems: Design, Analysis, and Operation", CRC Press, 3rd Edition, 2021.

[25] Abdulhamed Hwas, Reza Katebi. "Wind Turbine Control Using PI Pitch Angle Controller". IFAC Proceedings Volumes, 45(3):241–246, 2012. [Online]. Available: https://doi.org/10.3182/20120328-3-IT-3014.00041, doi:10.3182/20120328-3-IT-3014.00041.

[26] IEEE Press, "Power Electronics for Renewable Energy Systems, Transportation and Industrial Applications", 3rd edition, edited by Haitham Abu-Rub, Mariusz Malinowski, & Kamal Al-Haddad, United Kingdom, John Wiley & Sons, 2014.

[27] Francisco de Sousa Fernandes, João Peças Lopes, Carlos Moreira, and Bernardo Silva, "Assessment of frequency stability behaviour regarding inertia reduction due to high renewable integration in the Iberian system", MsC Dissertation, Electrical and Computer Engineering, Faculdade de Engenharia da Universidade do Porto, Porto, Portugal, 22nd July 2021. [Online]. Available: https://repositorio-aberto.up.pt/bitstream/10216/135232/2/485765.pdf

[28] M. Dreidy, H. Mokhlis, and S. Mekhilef, "Inertia response and frequency control techniques for renewable energy sources: A review". *Renewable and Sustainable Energy Reviews, 69,* 144–155. 2017. [Online]. Available: https://doi.org/10.1016/j.rser.2016.11.170

[29] Information Trust Institute: Grainger College of Engineering, "Illinois Center for a Smarter Electric Grid (ICSEG): IEEE 39-Bus System". [Online]. Available: https://icseg.iti.illinois.edu/ieee-39-bus-system/ (Accessed on 3/1/2023).

[30] Siemens Industry Inc., Siemens Power Technologies International, “Program Application Guide Volume 2 PSS/E 34.8.0”, September 2020.

[31] Siemens Industry Inc., Siemens Power Technologies International, “Model Library PSS/E 34.5.1”, November 2018. [Online]. Available: https://1drv.ms/b/s!AkW1rIbmmV2uiYcfj2tsMthxaHdsRA?e=W2bvvD

[32] ESIG: Energy Systems Integration Group, “Generic Models (WPPs)”. [Online]. Available: https://www.esig.energy/wiki-main-page/generic-models-wpps/ (Accessed on 8/2/2023).

[33] EPRI Project Manager, P. Pourbeik, “Model User Guide for Generic Renewable Energy System Models”, Electric Power Research Institute, California, June 2015. [Online]. Available: https://transmission.bpa.gov/Business/Operations/GridModeling/Model%20User%20Guide%20for%20Generic%20Renewable%20Energy%20System%20Models.pdf

[34] HUAWEI, “Informe de validación Modelo SUN2000-185KTL-H1 para España (PO9 & PO9 SENP)”, Spain, 30th October 2020.

[35] ENTSO-E. “Inertia and Rate of Change of Frequency”, 2020. [Online]. Available: https://eepublicdownloads.azureedge.net/

[36] I. D. Pasiopoulou, E. O. Kontis., T. A. Papadopoulos, G. K. Papagiannis. “Effect of load modeling on power system stability studies”. 2022. *Electric Power Systems Research*, *207*. [Online]. Available: https://doi.org/10.1016/j.epsr.2022.107846

[37] Pedro Rafael Araújo, “Dynamic Simulations in Realistic-Size Networks”, MsC Dissertation, Instituto Superior Técnico, Universidade Técnica de Lisboa, Portugal, 2010.

[38] Prabha Kundur. “Power System Stability and Control”, McGraw-Hill, 1st edition, 1994.

[39] Carmelo Mosca, Francesco Arrigo, Andrea Mazza, Ettore Bompard, Enrico Carpaneto, Gianfranco Chicco, Paolo Cuccia. “Mitigation of frequency stability issues in low inertia power systems using synchronous compensators and battery energy storage systems”. In *IET Generation, Transmission and Distribution*, *13*(17), 3951–3959. 2022. [Online]. Available: https://doi.org/10.1049/iet-gtd.2018.7008

[40] M. Nuhic and G. Yang, "A Hybrid System Consisting of Synchronous Condenser and Battery - Enhanced Services for Weak Systems," *2019 IEEE PES Innovative Smart Grid Technologies Europe (ISGT-Europe)*, Bucharest, Romania, 2019, pp. 1-5, doi: 10.1109/ISGTEurope.2019.8905459.